FACET

Facilities for Accelerator Science and
Experimental Test Beams at SLAC

A Proposal for a Multi-Purpose Experimental Research Facility using Electron and Positron Beams at SLAC

November 12, 2007

FACET Study Group

R. Arnold, K. Bane, L. Bentson, S. DeBarger, R. Erickson, T. Fieguth, M. Hogan, J. Jaros, N. Li, D.B. MacFarlane, Y. Nosochkov, J. Seeman, T. Raubenheimer, D. Walz, and M. Woods
Stanford Linear Accelerator Center

Contributors to the discussion of the scientific case

Principal scientific contacts are underlined

Advanced Accelerator Research
H. Badakov[2], I. Blumenfeld[1], C. E. Clayton[2], A. Cook[2], F.-J. Decker[1], M.J. Hogan[1], C. Huang[2], R. Ischebeck[1], R.H. Iverson[1], C. Joshi[2], A. Kanareykin[3], T. Katsouleas[7], N. Kirby[1], W. Lu[2], K. A. Marsh[2], W. B. Mori[2], P. Muggli[7], J.B. Rosenzweig[2], R.H. Siemann[1], M.C. Thompson[4], R. Tikhoplav[2], G. Travish[2], D. Walz[1], X. Wang[7], and M. Zhou[2]

Instrumentation and Detector Development
M. Breidenbach[1], C. Field[1], C. Hast[1], J. Jaros[1], L. Keller[1], D. Leith[1], D.B. MacFarlane[1], T. Markiewicz[1], T. Nelson[1], T. Raubenheimer[1], J. Va'vra[1], and M. Woods[1]

THz Radiation and Basic Energy Sciences
Y. Acremann[5], A. Dobin[6], S.J. Gamble[8], A.M. Lindenberg[5,9], A.Nilsson[10], H. Ogasawara[1], H.C. Siegmann[5], and J. Stohr[1]

[1]Stanford Linear Accelerator Center
[2]University of California at Los Angeles
[3]Euclid TechLabs, LLC
[4]Lawrence Livermore National Laboratory
[5]Photon Ultrafast Laser Science and Engineering Center (PULSE), SLAC and Stanford University
[6]Seagate Technologies
[7]University of Southern California
[8]Department of Applied Physics, Stanford University
[9]Department of Materials Science, Stanford University
[10]X-ray Laboratory for Advanced Materials (XLAM), SLAC and Stanford University

Table of Contents

1 Project Overview

The FACET project is a proposed relocation, refurbishment, and upgrading of accelerator components at SLAC, which will provide a combination of high-power beams for accelerator and instrumentation research at a new Accelerator Science Facility (ASF) in Sector 20 of the SLAC linac, plus test beams for detector development and large-scale instrumentation tests in End Station A (ESA). These new facilities will allow a continuation of the rich spectrum of advanced accelerator and particle physics R&D programs that have been conducted in the past at the Final-Focus Test Beam (FFTB) and ESA facilities by the U.S. and international HEP communities.

The high energy electron and positron beams from the SLAC linear accelerator have served as the backbone for the operating high energy physics program and as tools for advanced accelerator, instrumentation, and detector research and development. SLAC is the only place in the world with the high peak current, high energy electron and positron beams that make possible advanced accelerator R&D with plasma wakefield and dielectric wakefield techniques.

The FFTB and ESA have been the main facilities supporting this broad range of R&D activities over the past decade. The FFTB was initially constructed to demonstrate the demagnification required for the ILC final focus, as well as to verify beam optics codes and tuning procedures. Later, when combined with new bunch compression techniques, the FFTB also opened up many new and exciting areas of research in beam and plasma physics, ultra-short-pulse x-ray generation, advanced accelerator techniques, specialized diagnostic techniques, solid state physics, and high energy density science.

With the decommissioning of the FFTB in 2006, much of the work on developing ILC instrumentation and studying beam dynamics shifted to ESA where a 28.5 GeV beam was provided in a mode parasitic to PEP-II operation. The ESA programs addressed a variety of physics and R&D questions and included a suite of ILC instrumentation experiments involving prototype energy spectrometers, prototype RF beam position monitors, and studies of collimator wakefields, ILC interaction point backgrounds, and bunch length diagnostics.

FACET includes two new facilities to support the future evolution of the advanced accelerator and ILC development programs, both of which are of central importance to the long-term health of the national and international HEP programs. With FACET, the SLAC linac will continue to support these unique research programs by providing electron and positron beams with parameters unmatched anywhere else.

1.1 FACET Facilities

The FACET proposal involves modifications to the beam transport systems at SLAC to support a wide range of scientific research programs. It will replace and extend the functions of the Final Focus Test Beam (FFTB), which was dismantled as part of the Linac Coherent Light Source (LCLS) construction project, and support experiments requiring electron or positron beams with extraordinary peak power. It will also provide the means to deliver primary electron beams and secondary hadron beams to End Station A in the LCLS era to support ILC development work and a variety of programs, including upgrades to the LHC experiments, requiring large and easily accessible facilities for staging and operating experimental equipment. Both facilities will share the upstream end of the present linac complex as an injection system, allowing flexible, efficient and cost-effective scheduling of operations in support of a broad scientific community. The envisioned scientific activities include advanced accelerator R&D, small-scale ILC

instrumentation development and beam dynamics studies at the linac Sector 20 ASF facility, as well as ILC detector research and development, calibration, and performance characterization of large-scale components for the ILC or other future programs will be possible in the ESA facility. Additional unique science opportunities also exist in Basic Energy Sciences with terahertz radiation and intense electric fields.

The first part of the proposed FACET project will consist of a new experimental area, the Accelerator Science Facility (ASF), at Sector 20 in the existing linac tunnel, upstream of the LCLS injector. At this point along the linac, the beam has an energy of 24 GeV, and the emittance is very small. By installing a new focusing system at Sector 20, the beam can be focused and compressed in length to sizes appropriate for advanced accelerator research and other experiments requiring very high power densities. Comparable power densities for positron beams will be provided with the addition of an upstream positron bunch compressor. A shielding wall at the end of Sector 20 will allow access to the upstream portion of the linac during LCLS operations.

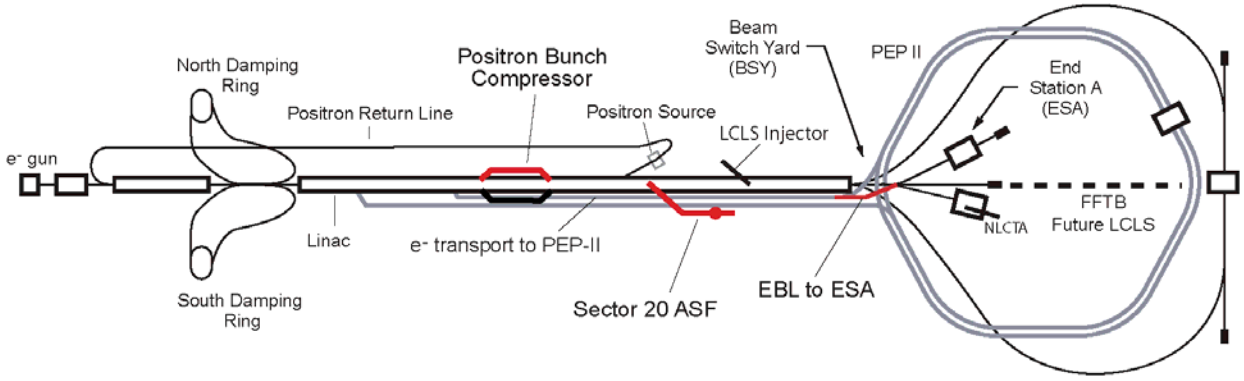

Figure 1-1. Schematic of the SLAC site with proposed FACET modifications to the beam delivery systems.

The second part of FACET will provide beams to End Station A (ESA), taking advantage of an existing beam line which is now used to transport electrons from the one-third point of the linac to the High Energy Ring (HER) of PEP-II. This beam line, which turns sharply north at the end of the linac tunnel and sends electrons down the north injection transfer (NIT) tunnel to PEP-II, would be extended for about 100 m into the Beam Switch Yard (BSY) to connect to the A-Line leading to ESA. The existing path from the end of the linac to the A-Line will be preserved, allowing for the delivery of LCLS electrons to ESA as well. With the FACET extension, beams with energies up to 12 GeV will be delivered to ESA. This system will provide electron beams with parameters suitable for most instrumentation and detector development tests of the kind envisioned for the ILC and for a wide range of other particle and particle astrophysics development programs.

The new Sector 20 beam and the beam to ESA will operate independently of the LCLS, except for sharing a section of beamline in the BSY. In addition, the Sector 20 beam and the ESA beam could be operated simultaneously on alternating pulses. The flexibility of operating these beams together or separately offers opportunities for sharing operating costs among programs and maximizing efficiency.

1.1.1 Accelerator Science Facility (ASF) at Sector 20

The Accelerator Science Facility (ASF) will consist of a final focus system and an experimental area that has been designed to fit in the existing linac tunnel in Sector 20. The new beam line equipment will start downstream of the positron production extraction point (where electrons are directed to the e^+ production target) and extend to a new beam dump near the end of Sector 20, a few meters upstream of the point where the LCLS injector line enters the linac tunnel. The length of the tunnel between these two points is about 120 m.

The Sector 20 system will consist of a dogleg trajectory to compress the beam longitudinally and offset it from the linac axis, followed by an arrangement of quadrupoles to focus the beam to an interaction point near the middle of the sector. The dipole magnets for the dogleg and most of the quadrupole magnets for the focusing system will be salvaged from the SLC final focus system. The quadrupole magnets for the final doublet were salvaged when the FFTB was decommissioned. Tracking programs that include second-order effects have been used to compute the ASF beam parameters summarized in Table 1-1.

Table 1-1. ASF beam parameters

Energy	Adjustable up to 30 GeV without compression; and up to about 23 GeV with full compression and maximum peak current.
Charge per pulse	2 x 10^{10} (3 nC) e^- or e^+ per pulse with full compression; 3.5 x 10^{10} e^- or e^+ per pulse without full compression.
Pulse length at IP (σ_z)	15.5 μm with 4 % fw momentum spread; 30 μm with 1.5 % fw momentum spread.
Spot size at IP ($\sigma_{x,y}$)	10 μm nominal (7.9 x 8.7 μm achieved in computer simulations).
Momentum spread	4 % full width with full compression; (3% FWHM); < 0.5 % full width without compression.
Momentum dispersion at IP (η and η')	0
Drift space available for experimental apparatus	2 m from last quadrupole to focal point; approximately 23 m from the focal point to the beam dump.
Transverse space available for experimental apparatus	3 x 3 m

The space available for experimental equipment in the linac housing is more restricted than that in the ESA facility, but it is sufficient for the advanced accelerator R&D and ILC instrumentation and beam dynamics experiments that require high power-density beams. The linac tunnel cross section is approximately ten feet by ten feet, while there is about 25 meters of longitudinal space between the last beamline quadrupole and the beam dump. The floor and beamline pitch downward at an angle of approximately 0.25 degrees. The experimental region is approximately 10 m below ground in the linac tunnel, where it is well shielded by earth and concrete so that the full beam power can be absorbed safely. This is a significant advantage over the former FFTB facility, in which radiation safety considerations imposed limitations on beam power for several important research programs.

A new controlled entry point in the existing Sector 19 equipment shaft will provide users with convenient stairway access to this experimental region, enabling them to set up and work on experimental apparatus without interfering with LCLS operations. A counting house will be located adjacent to the Klystron Gallery to support experiments in the linac tunnel.

1.1.2 End Station A Facility

The PEP-II HER bypass line was built to transport electrons in the range 9 to 12 GeV from the Sector 10 extraction point to the BSY (and on to PEP-II), a distance of 2000 m, thereby "bypassing" the downstream two-thirds of the linac. For the new ESA application, the transport line will continue to be used in the same way to bypass the LCLS portion of the linac. No modifications are needed to bring the beam most of the way to the BSY.

Table 1-2. ESA beam parameters with the EBL

Energy	Adjustable up to 12 GeV nominal; 24 GeV achievable as a future upgrade by moving the extraction point to Sector 18.
Charge per pulse	0.1 to 3.5 x 10^{10} (3 nC) e^- in the single-bucket mode; up to 3 x 10^{11} e^- in the undamped long-pulse mode.
Pulse length at IP (σ_z)	1 mm nominal with 1 % fw momentum spread; pulse trains up to 360 ns without damping ring.
Spot size at IP ($\sigma_{x,y}$)	< 1 mm nominal
Momentum spread	<1% full width
Momentum dispersion at IP (η and η')	0
Drift space available for experimental apparatus	60 m
Transverse space available for experimental apparatus	5 x 5 m

To deliver the electron beam to ESA, a new section of beam transport line will be needed to connect the existing PEP-II bypass line to the A-Line. This new section is hereafter referred to as the Electron Bypass Line (EBL). A geometrically acceptable layout has been found in which the beam from the bypass line will be deflected downward through Sectors 29 and 30 to the elevation of the linac and then deflected inward (northward from the south side of the linac) to match the original A-line trajectory. A major cost savings for this arrangement, compared to earlier SABER design studies [1], accrues from the use of the existing bypass line and accepting the 12 GeV limit on the beam energy to ESA.

ESA is a large experimental hall, 60 meters in length, with 15- and 50-ton overhead cranes and well developed utilities, cable plant, and data acquisition systems. This facility is well suited for detector development and testing large-scale prototypes or complete systems. The A-line that transports the beam from the linac to ESA provides precise (0.1%) momentum-analysis and provisions for a secondary hadron beam. A future energy upgrade to 24 GeV will also be possible.

1.2 Summary of Science Opportunities

The full-intensity, high-energy electron and positron beams available at SLAC, capable of being compressed longitudinally and transversely to the level of 10's of microns, are a unique resource for understanding advanced acceleration mechanisms in plasmas and dielectric waveguides, and, by virtue of their similarity to the beams at the ILC, provide a one-of-a-kind test laboratory for developing ILC beam instrumentation, diagnostic equipment, and detector prototypes. The facility will also support development and calibration studies for the upgrades of the LHC experiments. A broad array of science opportunities will also be possible based on the short intense electric and magnetic fields from the precision electron beams, which create terahertz radiation for the exploration of materials science, condensed matter physics and chemistry.

1.2.1 Advanced Accelerator Development

A major challenge for high energy physics and the accelerator science community is the development of new concepts for future energy-frontier accelerators that will be able to provide the tools needed for high energy physics within reasonable cost limits [2]. Meeting this challenge requires the formation of broad collaborations across a wide variety of areas in science and technology, as well as state-of-the-art facilities. Breadth of expertise is necessary because the needed advances call for new, perhaps even radical, approaches to acceleration that will come from scientists and engineers who can bring new perspectives. New concepts must be explored experimentally. Appropriate facilities are critically important for this work.

The SLAC FFTB was a superb facility for experiments requiring beams with high energy, high peak current, and low emittance. These are exactly the beams needed for studying dielectric wakefields and plasma wakefields. The electron and positron beams available at the FFTB were unique in the world because of the capabilities of the SLAC linac and the special optical properties of the FFTB. The opportunities at the FFTB attracted many university scientists and led to collaborations with the necessary breadth of expertise. The experiments performed there could not have been performed anywhere else, and the results have received worldwide interest.

As part of this proposal, the FFTB, which has been removed to make way for the LCLS, will be replaced with a new facility in Sector 20, designated the Accelerator Science Facility (ASF). The SLAC linac, together with FACET/ASF, will provide high energy, high peak current, low transverse emittance electron and positron beams and the infrastructure needed to carry out the experimental program. The primary focus of the ASF will be research into and development of dielectric and plasma wakefield accelerators, although there will be other science opportunities making use of these beams as well.

Significant dielectric wakefield results were obtained during a short run in the FFTB; the breakdown threshold for 200 μm inner diameter dielectric tubes was measured to be greater than 1.5 GeV/m accelerating field. Future experiments will need to study a variety of materials, dependence of accelerating gradient and breakdown on the dielectric cross section, and the feasibility of long (~1 m) dielectric accelerator tubes [3]. If these experiments are successful, they could lead to a substantially larger effort to develop a high-energy collider based on dielectric wakefields.

In the past seven years, plasma wakefield accelerators (PWFA) have emerged as a promising approach to advanced accelerators, thanks to progress on a number of fronts [4]. The SLAC/UCLA/USC E-162/164/167 collaboration has been the leading group pioneering this research. These experiments, conducted at the FFTB facility at SLAC, have shown that plasmas

can accelerate and focus both electron and positron high energy beams. In addition, they have demonstrated a variety of new effects, such as the collective refraction of a charged particle beam at a plasma-neutral vapor interface, the generation of betatron x-rays from a few keV to tens of MeV energy, and the acceleration of electrons from the plasma itself with extremely high acceleration gradients. Striking results have come from experiments using a short ($\sigma_z \sim 15$ μm), high peak-current electron beam that field-ionizes a neutral lithium vapor to produce the plasma. Accelerating wakefields in excess of 50 GeV/m have been sustained in an 85 cm-long plasma. This gradient is roughly 3,000 times that in the SLAC linac; the ~1 m-long plasma accelerated some electrons in a 42 GeV beam to energies approaching 100 GeV.

A vigorous and scientifically compelling PWFA research program at FACET/ASF will pursue the further development of these ideas, including generating 50 GeV range beams with a narrow energy spread and a small emittance, reasonable energy extraction efficiency from the plasma wake (beam loading) without severe degradation of either the energy spread or the emittance, plasma focusing of high energy beams to nanometer sizes, and high gradient acceleration and focusing of positrons. There will be critical issues, such as betatron radiation loss, possible hosing instability of both the drive beam and the beam load, emittance growth due to plasma ion motion, and multiple Coulomb scattering and beam head erosion limiting the energy transfer efficiency from the drive beam to the wake, which will have to be scrutinized and mitigated. It is precisely because these issues are so scientifically compelling that the PWFA attracts some of the brightest students in the field of beam physics. Good science, strong collaborations between university and laboratory groups, and forefront facilities are the key ingredients to a successful advanced accelerator research program. The plasma wakefield accelerator is one of the most promising approaches to advancing the energy frontier, and FACET/ASF is the only facility worldwide that will allow continued development of these areas of advanced accelerator research.

1.2.2 Instrumentation and Detector Development for ILC and HEP

The International Linear Collider (ILC) has taken center stage in recent years as the next major initiative in particle physics, and it has garnered broad and enthusiastic international support. Both the ILC accelerator and the detectors used to study its physics will challenge the current state-of-the-art for accelerator instrumentation and collider detector technology. Testing ILC instrumentation will require ILC-like beams, while testing new detector technologies will require more traditional particle test beams, ideally with ILC timing properties. FACET will provide both. The FACET test beams will support the full spectrum of ILC instrumentation and detector development work, ranging from proof-of-principle studies, large-scale prototyping, production and calibration testing, to system integration studies. FACET will also be a valuable resource to the broader community for detector development and testing. A good example is the near-term hardware development work anticipated for the LHC detector upgrades.

Many ILC beam instrumentation tests have been conducted in recent years with the 28 GeV electron beam in ESA. These studies will evolve to testing system components that will eventually be committed to the ILC. These instrumentation studies include RF beam-position monitors (BPMs), bunch length diagnostics, collimators, and BPM and synchrotron stripe energy spectrometers. The Sector 20 experimental area will also be a good location for small-scale tests requiring high-power beams, such as for BPMs and bunch length diagnostics, or material damage tests for ILC collimators, spoilers and beam dumps. Other examples of ILC beam instrumentation work will exploit synchrotron radiation and optical transition and diffraction

radiation. The infrastructure developed in ESA with many RF BPM stations spanning 60 meters along the beam provides an excellent tool for measuring and demonstrating the required micron-level tolerances for BPM and quadrupole mechanical stability needed for the ILC linac. A beam-based measurement of the stability of the cold quadrupole's magnetic center will be possible, which will address one of the critical issues in the ILC beam dynamics. Beam tests of large-scale mockups for the interaction region components will also be possible, motivated by the need to validate the stringent requirements on vibration and stability.

The ILC detector community has been working to define the test beam needs for future detector development. The recent ILC Detector Test Beam Workshop, which was held at Fermilab in January 2007, produced a "Roadmap for ILC Detector R&D Test Beams" [5]. This document provides a summary of test beam facilities worldwide and the test beam needs of the ILC detector community. It is clear from recent experience with LHC detector development and construction that this demand will be substantial; four test beams at CERN have been fully occupied by the LHC detector development and testing over much of the last decade. An accounting of current and established ILC detector test beam needs totals nearly 200 weeks per year; *i.e.,* there already is a need for four beamlines operating year round. This demand far exceeds present test beam availability and is expected to increase.

ILC detectors will depend on real advances in detector technologies. New vertex detector technologies are essential at the ILC; present detectors are read out too slowly, consume too much power, and are too thick to reach the performance goals set by ILC physics. New technologies will need development and beam tests, preferably with moderate to high momentum beams. ILC calorimeter designs also go well beyond the current state of the art. A new paradigm, employing fully imaging calorimeters, promises the performance needed to distinguish W and Z (and top and Higgs) decays cleanly, event by event, which will be needed to reach the full potential of ILC physics. The current designs rely on new, but untried technologies to provide the high degree of transverse and longitudinal segmentation needed, and they are based on today's imperfect knowledge of hadron cascade development. The new technologies need extensive beam tests, new jet energy algorithms need full-scale calorimeter tests, and eventually large-scale prototypes and production modules will need thorough evaluation, calibration, and testing. The development of optimal ILC detector designs and other future forefront HEP projects will benefit enormously from the unique capabilities of FACET.

1.2.3 Terahertz Radiation and Science Opportunities in Basic Energy Sciences

In recent years there have been significant scientific advances in solid state physics and chemistry induced by terahertz radiation. Applications as diverse as semiconductor and high temperature superconductor characterization, tomographic imaging, label free genetic analysis, cellular level imaging and chemical and biological sensing have thrust terahertz research from relative obscurity into the limelight. Highly relativistic electron bunches are the most intense sources of terahertz radiation known today. Conventional laboratory sources are typically limited to peak electric fields of the order of 1 MV/m. In contrast, the fields surrounding relativistic electron beams exceed 1 GV/m. Such field strengths rival those experienced by valence electrons in materials (~1 V over the size of an atom) and their application can therefore create new states of matter previously not observable. As a result, FACET offers unique possibilities to undertake cutting edge research with terahertz radiation.

Terahertz radiation is now viewed for example as an ideal tool for the study of spin dynamics, which is essential for the basic understanding of magnetism and its technological

applications [6,7,8]. Ultrafast changes of the magnetization induced, *e.g.*, by a laser pulse, will lead to the emission of terahertz radiation that probes the time dependence of the spontaneous magnetization [8,9]. However, the last experiments conducted at the FFTB demonstrated that the terahertz radiation accompanying compressed highly relativistic electron bunches can also be used to create large electric and magnetic fields in metals at terahertz frequencies [10]. This technique holds considerable interest and future promise.

One important application will be exploration of magnetic storage and ultrafast magnetic switching. The development of faster, higher density, non-volatile storage mechanisms using ferroelectric materials depends on how small one can make a functional ferroelectric domain, and how fast it can be switched in an applied electric field, with corresponding ultrafast atomic-scale displacements within the unit cell. Intense femtosecond time-scale THz fields, as will be produced at FACET, enable control and characterization of the intrinsic dynamics associated with ferroelectric devices, and provides a new way of visualizing the processes that fundamentally determine the properties of real devices. The magnitude, direction and the pulse length of the applied field can be very accurately controlled by changing the compression of the electron bunch of the FACET beam. The field will be very uniform up to micrometer lengths; however it will be changing in magnitude and direction over larger areas, which would allow investigation of polarization dynamics as a function of field magnitude and direction in just one exposure.

The THz radiation from the electron beam is also an ideal tool to study electronic properties of materials on the femto- to pico-second time scale under extreme electrical fields. This combination makes the THz field unique to study materials for future electronic devices. We anticipate a program of THz scattering experiments with semiconductors and insulators. The THz field will modify the electronic structure of the materials and lead to self-modulation of the THz field. In addition, time resolved laser spectroscopy using a THz pump pulse will allow us to investigate carrier generation and dynamics caused by the electrical field of the THz pulse in the time domain. The THz field can be modified by lithographically defined micro antennas on the sample, leading to even stronger electromagnetic fields by concentrating the THz radiation to a small area. It will be extremely interesting to study the limits of electronic conduction in metals and semiconductors.

Another important science opportunity is the study of ultrafast processes in surface reactions. There are a vast number of economically important processes that rely on reactions at surfaces and interfaces, such as catalysis in chemical and energy production. The microscopic understanding of reactions at surfaces requires an in-depth knowledge of the dynamics of elementary processes on an ultrafast timescale. As a consequence, it has been extremely challenging to visualize the underlying reaction mechanism and dynamics of processes at surfaces. One approach to the study of an ultrafast excitation is to initiate a chemical reaction and then probe the progression of the reaction. Excitation of phonons, frustrated rotational and translational motions of molecular adsorbates plays an important role in processes at surfaces that are driven by kT, *i.e.*, temperature. The broad-band THz radiation from the ultra short electron bunches in FACET open up the opportunity to develop new methods for triggering the motion of nuclei. The highly directional nature of the strong electric field is also an important mechanism. We envision the use of electric field pulses with durations in the 100 fs – 1 ps range and field strengths $>1x10^9$ V/m (or >0.1 V/atom) can be used to drive chemical reactions [11]. FACET will therefore provide a unique tool for studying surface processes over a wide range of reactions that are of primary societal and economic interest.

1.3 References

[1] SABER White Paper (August 2006).

[2] "Report of the HEPAP Subpanel on the Assessment of Advanced Accelerator Research and Development" (August 2006).

[3] "Wakefield Acceleration in Dielectric Structures", proposal by H. Badakov *et al.* (E-169 Collaboration).

[4] C. Joshi and T. Katsouleas, Physics Today, **47** (June 2003).

[5] "Roadmap for ILC Detector R&D Test Beams," by the World Wide ILC Detector R&D Community (2007); available at http://www-hep.uta.edu/~yu/research/linear-collider/ilc-tb-roadmap-v6.1.pdf.

[6] J. Stöhr and H. C. Siegmann, "Magnetism: From Fundamentals to Nanoscale Dynamics", Springer Series in Solid-State Sciences **152**, (Springer, New York, 2006).

[7] D.J. Hilton *et al.*, Optics Lett. **29,** 1805 2004: "Terahertz emission via ultrashort excitation of magnetic metal films".

[8] E. Baurepaire *et al.*, Appl. Phys. Lett. **84**, 3465, 2004: "Coherent terahertz emission from ferromagnetic films excited by femtosecond laser pulses".

[9] J.B. Héroux *et al.*, Phys.Stat.Sol.(c) **3**, 4271 (2006): "Magnetization induced terahertz radiation from GaMnAs".

[10] S. J. Gamble, Mark H. Burkhardt, W. Harrison, H. C. Siegmann, J. Stöhr, A. Kashuba, Rolf Allenspach, and Stuart S. P. Parkin, to be published.

[11] H. Ogasawara, D. Nordlund, A. Nilsson, SLAC-PUB-11503 (2005).

[12] The Stanford Two Mile Accelerator, R.B. Neal, Editor (November 1968).

[13] SLC Design Handbook, R. Erickson, Editor (November 1984).

[14] P. Krejcik *et al.*, Commissioning of the SPPS Linac Bunch Compressor, PAC'03, Portland, OR, USA, SLAC-PUB-9858, (2003).

[15] LCLS Conceptual Design Report, SLAC-R-593 (2002).

[16] Proceedings of the SABER Workshop (2006) are available at http://www-conf.slac.stanford.edu/saber/

[17] R. Erickson *et al.*, SABER Optical Design, SLAC-PUB-11944 (2006).

[18] T. Fieguth, "The Optical Design of the PEP-II Injection Beamlines", Proceedings of 5th European Particle Accelerator Conf., 2471-3, (1996), SLAC-PUB-7171.

2 Opportunities in Advanced Accelerator Research

During the last century, particle accelerators have steadily increased their energy, leading to extraordinary discoveries about the structure of the universe while at the same time finding their way into many practical applications ranging from television tubes to medical diagnostics and treatment to industrial materials processing. Historically, the maximum particle energy has increased exponentially, rising by a factor of 10 every decade. While this trend apparently continues for proton machines with the startup of the LHC, the growth in electron/positron accelerator energy has begun to show signs of leveling off in the last decades. This has been attributed to the fact that the technology of accelerating these particles with radio frequency cavities is approaching its limits [1]. Various approaches have been proposed to extend the energy reach of electron/positron accelerators. They can be placed into one of five general categories:

- Extending RF technologies to higher frequencies,
- Powering dielectric accelerator structures with lasers,
- Accelerating particles with wakefields produced in dielectrics,
- Driving an accelerating wave in a plasma with high power lasers, and
- Accelerating particles with plasma wakefields driven by a particle beam.

The first three of these techniques use boundary conditions from materials to produce an accelerating mode (high frequency RF, laser powered dielectric structures, and dielectric wakefield accelerators), while the last two techniques based on plasmas (laser and particle beam driven plasma waves). Each of these areas presents significant unknowns and will require extensive programs of fundamental research to even reach the point where an assessment of future viability as a working technology can be made.

A major challenge for high energy physics and the accelerator science community is developing these new concepts for future energy frontier accelerators that will be able to provide the exploration tools needed for high energy physics within a feasible cost to society [2]. Meeting this challenge requires both the collaboration of individuals with a wide variety of expertise in science and technology and state-of-the-art facilities. Breadth of expertise is necessary because the needed advances call for new, perhaps even radical, approaches to acceleration that will come from scientists and engineers who can bring new perspectives. Examples are plasma, laser and materials scientists, researchers working at the forefront of advanced computing, and people who can develop new and novel instrumentation. In addition, conventional accelerator physicists put issues into the context of high energy physics and create, operate and optimize the facilities necessary for experiments.

Ultimately concepts must be explored experimentally and appropriate facilities are critically important. For the case of plasma-based accelerators, the correlation between state-of-the-art facilities and rapid experimental progress is clearly illustrated in Figure 2-1. In just fifteen years, laser-driven plasma accelerators have advanced from making 10 MeV beams with ~100% energy spread to GeV bunches with a few percent energy spread. The steady increase in maximum energy was enabled by the rise of multi-terawatt laser facilities around the world in Japan (KEK), Great Britain (RAL), France (LOA) and the United States (LLNL, U. of Michigan, U. of T. Austin and L'OASIS). The progress for beam-driven experiments has been even more remarkable with the maximum energy gained in the plasma increasing from a couple hundred MeV to over 40 GeV in just two years. In this case progress came entirely from the capability

with the SLAC linac to produce and deliver increasingly high intensity bunches to experiments in the Final Focus Test Beam (FFTB) Facility.

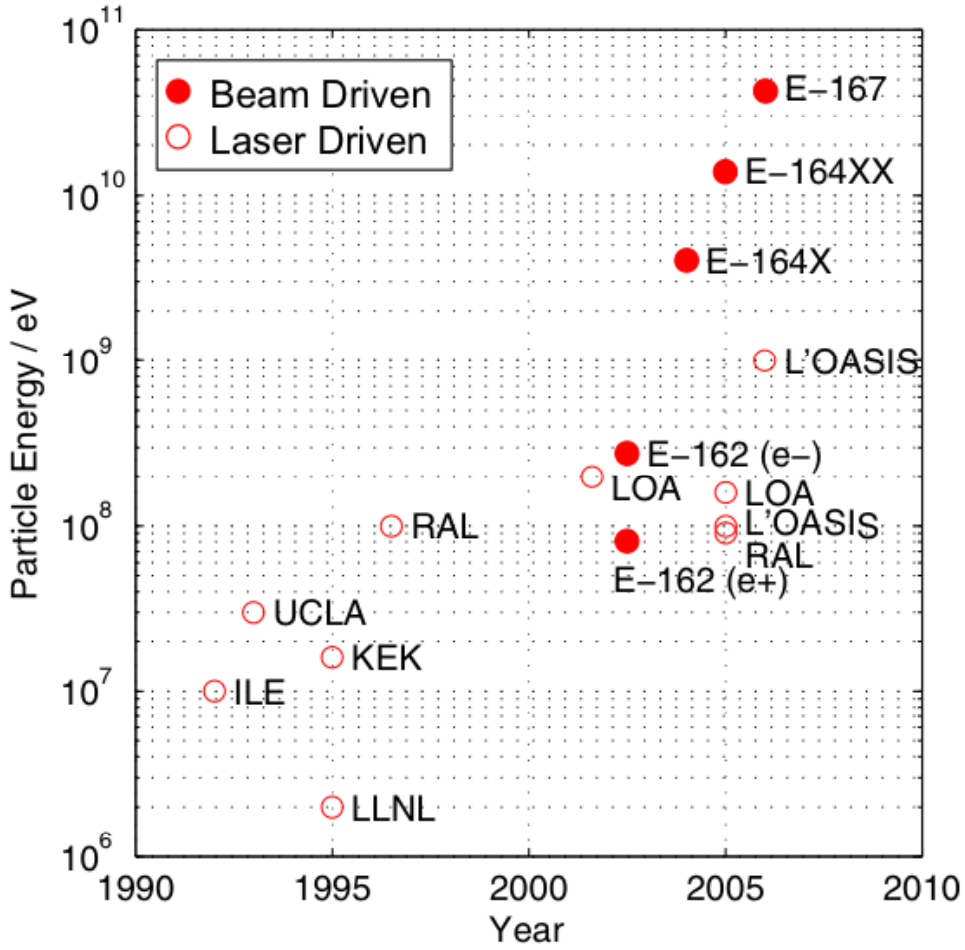

Figure 2-1. The maximum energy achieved by plasma-based accelerator experiments (laser and particle beam driven) versus time.

The SLAC FFTB was a superb facility for experiments requiring beams with high energy, high peak current, and low emittance. These are exactly the beams needed for studying dielectric wakefields and plasma wakefields. The electron and positron beams available at the FFTB were unique in the world because of the optics of the FFTB and, more importantly, the SLAC linac itself. The opportunities at the FFTB attracted university scientists and led to collaborations with the necessary breadth of expertise. The experiments performed there could not have been performed anywhere else, and the results have received worldwide interest.

The FFTB was decommissioned in 2006 for construction of the Linear Coherent Light Source (LCLS); we are proposing to replace it with a new high-quality facility, FACET/ASF. The SLAC linac together with ASF will provide high energy, high peak current, low transverse emittance electron and positron beams and the corresponding experimental infrastructure. The primary focus of FACET/ASF will be research into and development of dielectric and plasma wakefield accelerators, although there will be other important science opportunities making use of these beams as well.

Significant dielectric wakefield results were obtained during a short test beam run in the FFTB—the breakdown threshold for 200 μm inner diameter dielectric tubes was measured to be greater than 1.5 GeV/m accelerating field. Future experiments will need to study a variety of materials, dependence of accelerating gradient and breakdown on the dielectric cross section, and the critical issue of the feasibility of long, ~1 m, dielectric accelerator tubes [3]. If these experiments are successful, it will be natural to initiate a substantially larger effort to develop a high-energy collider based on dielectric wakefields.

Plasma wakefield experiments at the FFTB demonstrated that high gradients, ~50 GeV/m, can be sustained over meter-scale distances. The challenge now is to take the next steps to realize a plasma-based collider. Several configurations have been proposed [4,5] and should be scrutinized. We need to identify critical issues and perform corresponding research in order to make progress. Among the issues that must be addressed are:

- Efficient acceleration of mono-energetic beam bunches,
- Shaped single bunches and/or multiple bunches to increase the transformer ratio,
- Acceleration of positrons,
- High demagnification focusing of positrons and electrons, and
- Plasma ion motion.

All these areas of development can be directly addressed at a scientific level at FACET/ASF and will inform our ability to extrapolate the applicability of this approach to a future TeV class linear collider. The first stage of the plasma wakefield research at ASF has clear goals [6], would use much of the experimental apparatus and techniques developed at the FFTB, and could be ready to be resume as soon as the Sector 20 portion of FACET is completed. Longer term there is a substantial amount of work to be done, and it is important to engage additional scientists and groups. Our colleagues at UCLA and USC are planning to hold a workshop in the summer of 2008 to make others aware of the opportunities and to engage them in this research.

These two research programs described above hold the promise of extending the energy reach of electron/positron accelerators with accelerating gradients that are significantly above those realized today. The underlying physical mechanisms are very different, as are the resultant performances including achievable gradient and electron versus positron acceleration. They are also at different stages of development. The plasma acceleration results came from extensive experimentation from 1999 to 2006 in the FFTB while the dielectric wakefield results were obtained in a two day long run.

With the addition of FACET/ASF, SLAC will be uniquely positioned to support the further development of these promising advanced accelerator research directions. Reproducing the beams from the SLAC linac, and the ASF beamline and infrastructure would be prohibitively expensive anywhere else in the world. As a result, research and development of dielectric and plasma wakefield accelerators, two of the five fundamental concept approaches to extending the energy reach of electron/positron accelerators, depends critically on construction of FACET/ASF.

2.1 Plasma-Wakefield Acceleration and Beam-Plasma Physics

In the past seven years, plasma wakefield accelerators (PWFA) have emerged as a leading approach to advanced accelerators, thanks to progress on a number of fronts [7]. The SLAC/UCLA/USC E-162/164/167 collaboration has been the leading group pioneering this research (see Appendix A). These experiments, conducted at the FFTB facility at SLAC, have

shown that plasmas can accelerate and focus both electron and positron high energy beams. In addition, they have demonstrated a variety of new effects, such as the collective refraction of a charged particle beam at a plasma-neutral vapor interface, the generation of betatron x-rays from a few keV to tens of MeV energy, and the acceleration of electrons from the plasma itself with extremely high acceleration gradients. Striking results have come from experiments using a short ($\sigma_z \sim 15$ μm), high peak-current electron beam that field-ionizes a neutral lithium vapor to produce the plasma. Accelerating wakefields in excess of 50 GeV/m have been sustained in an 85 cm-long plasma. This gradient is roughly 3,000 times that in the SLAC linac and the ~1 m-long plasma accelerated some of the 42 GeV electrons to energies approaching 100 GeV.

These experiments have produced a number of rich new beam and plasma physics results, demonstrated the promise of beam-driven plasma accelerators and developed sophisticated laboratory apparatus and techniques for conducting beam and plasma experiments. We propose to relocate and further develop much of this experimental hardware to FACET/ASF to conduct the next generation of experiments.

FACET/ASF will be a unique resource for continuing research on new ideas for accelerating and focusing electron and positron beams at energies relevant to high-energy physics. As the FFTB experiments have shown, beam-plasma interactions are an extremely rich area of inquiry. Yet there is much to do before the potential of this method can be realized in useful technology. The goal of the second generation of research on PWFA is to address the critical issues for realizing a plasma-based accelerator at the energy frontier. Paraphrasing the Marx HEPAP subpanel, "the challenge is to undertake and sustain the difficult and complex R&D needed to enable a feasible, cost and energy effective technology on the several decade horizon. Achieving these goals will require creativity and the development of new accelerator approaches and technologies."

Such research cannot be carried out without the availability of a high-quality facility. The facility needed in this particular instance is a high-energy beam and beam line that are able to provide extremely bright pulses of both electrons and positrons. In this regard the Marx subpanel suggests, "OHEP should accept proposals from the laboratories to pursue longer term R&D that has the potential for significant impact and to invest in appropriate research and funding infrastructure."

A vigorous and scientifically compelling PWFA research program at FACET/ASF will include the following key topics: generating 50 GeV range beams with a narrow energy spread and a small emittance; reasonable energy extraction efficiency from the plasma wake (beam loading) without severe degradation of either the energy spread or the emittance; plasma focusing of high energy beams to nanometer sizes; and high gradient acceleration and focusing of positrons. There will be many critical issues, such as betatron radiation loss, possible hosing instability of both the drive beam and the beam load, emittance growth due to plasma ion motion, and multiple Coulomb scattering and beam head erosion limiting the energy transfer efficiency from the drive beam to the wake, that will have to be scrutinized and solutions will have to be found. It is precisely because these issues are so scientifically compelling that the PWFA attracts some of the brightest students in the field of beam physics. Good science, strong collaborations between university and laboratory groups and forefront facilities are the key ingredients to a successful advanced accelerator research program. The intention of second-generation research on PWFA is to bring these three elements together to significantly advance the field of plasma-based accelerators towards a practical technology.

2.1.1 The Plasma Wakefield Accelerator

The basic concept of the plasma wakefield accelerator involves the passage of an ultra-relativistic electron bunch through a stationary plasma [8]. The plasma can be formed by ionizing a gas with a laser [9] or through field-ionization by the Coulomb field of the relativistic electron bunch itself [10]. This second method allows the production of meter-long, dense (10^{16}-10^{17} cm^{-3}) plasmas suitable for the PWFA and greatly simplifies the experimental set-up. In single bunch experiments the head of the bunch creates the plasma and drives the wake. The wake produces a high-gradient accelerating field that in turn accelerates particles in the back of the bunch, as shown in Figure 2-2. The system effectively operates as a transformer, where the energy from the particles in the head is transferred to those in the back, through the plasma wake.

2.1.2 PWFA Principle

Experiments in the FFTB addressed the key question of the magnitude and sustainable length for the accelerating field in a beam-driven plasma. In the beam-driven PWFA, a short but high-current electron bunch, with beam density n_b larger than the plasma electron density n_p expels the plasma electrons as shown in Figure 2-2. The expelled plasma electrons rush back in and set-up a large plasma wakefield, which has a phase velocity equal to the beam velocity (≅ c). There are several accelerating buckets in the wakefield trailing the initial driving bunch. The FFTB experiments used only a single bunch to sample the entire wakefield. Ideally, one would instead place a separate "witness" bunch in one of these buckets, which would then be accelerated. Appropriate techniques to craft two bunches spaced in time by roughly one plasma period are an integral component to the second generation plasma experiments proposed for FACET.

Table 2-1. Legend of symbols used in this proposal

Physical Parameter	Symbol
Speed of light in vacuum	c
Charge of an electron	e
Classical electron radius	$r_e = e^2 / 4\pi\varepsilon_0 m_e c^2$
Accelerating gradient	eE
Plasma focusing gradient	$K=\omega_p/(2\gamma)^{1/2}c$
Plasma wavenumber	$k_p= \omega_p/c$
Plasma wavelength	$\lambda_p=2\pi/k_p$
Mass of an electron	m_e
Number of electrons per bunch	N
Drive beam density	$n_b=N/(2\pi)^{3/2}\sigma^2_r\sigma_z$
Plasma density	n_p
Drive beam transverse size	σ_r
Drive beam bunch length	σ_z
Beam plasma frequency	$\omega_{pb}=(n_b e^2/\varepsilon_o m_e)$
Electron plasma frequency	$\omega_p=(n_o e^2/\varepsilon_o m_e)$

Physical Parameter	Symbol
Beta function of the beam	$\beta=\gamma\sigma_r^2/\varepsilon_N$
Normalized emittance of the beam	$\varepsilon_N=\gamma\varepsilon$
Spot size of the beam in x, y	σ_x, σ_y
Focal length of the lens in x, y	f_x, f_y
Skin depth of plasma	c/ω_p

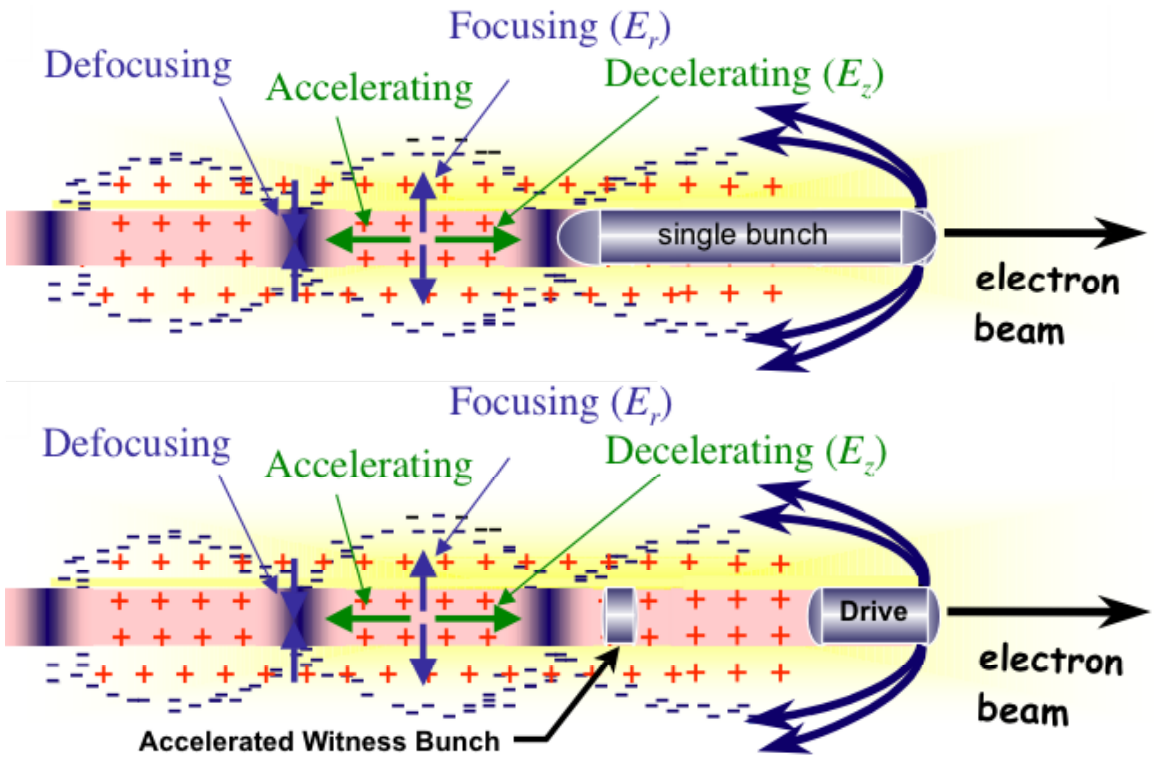

Figure 2-2. Physical mechanism of the Plasma Wakefield Accelerator for previous single bunch experiments in the FFTB (top) and the two bunch case proposed for FACET (bottom).

According to linear plasma theory for a single bunch, for small transverse beam sizes ($k_p\sigma_r << 1$), the accelerating field in the back of a single bunch is maximized for $k_p\sigma_z \approx \sqrt{2}$, *i.e.*, when the plasma electrons rush back on axis immediately behind the bunch. The maximum accelerating field has a value given by

$$eE_{linear} = 100\,GeV/m\left(\frac{N}{1.8\times10^{10}}\right)\left(\frac{20}{\sigma_z(\mu m)}\right)^2 \qquad (1)$$

where N is the number of particles in the electron bunch and σ_z is the bunch length.

Equation 1 indicates that generating large amplitude wakefields requires short, high-density electron bunches. When the wake is excited in the so called blow-out regime ($n_b > n_p$

and $k_p\sigma_r << 1$), all the plasma electrons are expelled from the beam volume, the wake excitation is highly nonlinear (spikey) and can reach a higher peak value $(eE)_{peak}$ of up to three to four times $(eE)_{linear}$. For the portion of the wake that can be used to effectively accelerate particles, the amplitude is somewhere in between the peak value and the absolute value given by linear theory $(eE)_{linear}$.

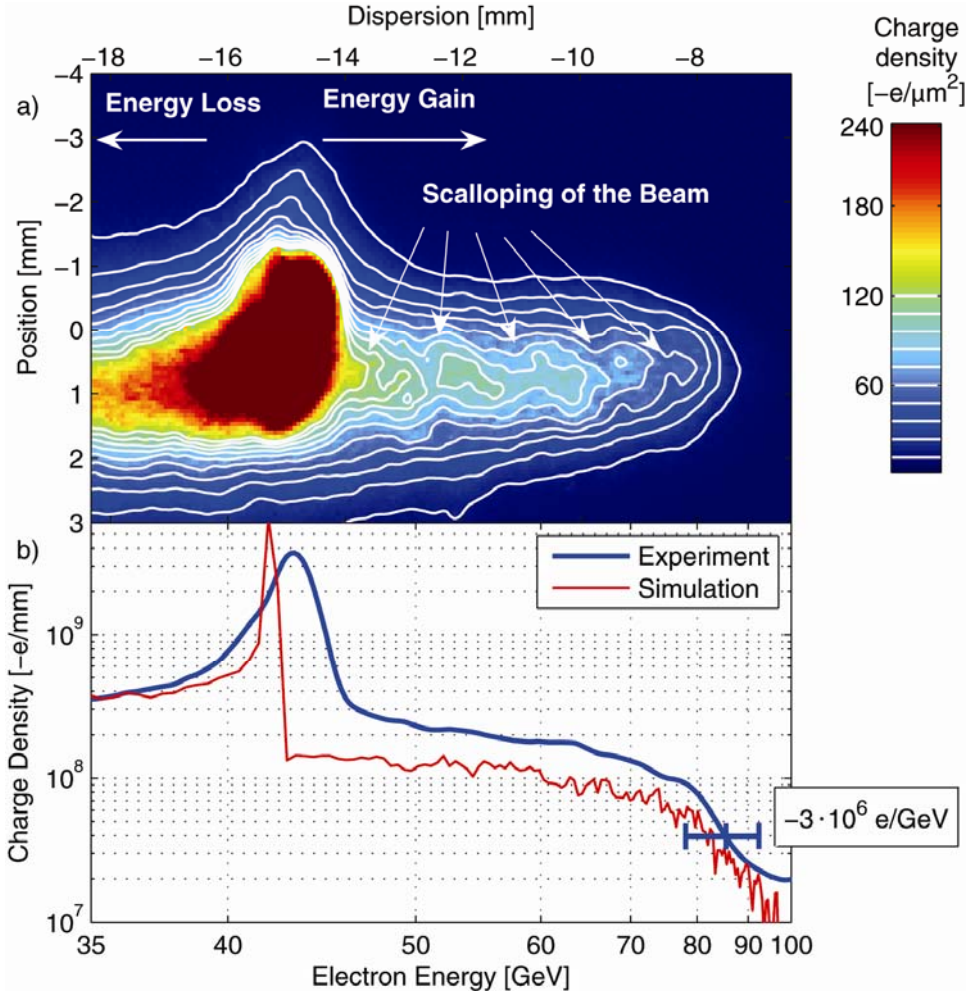

Figure 2-3. (a) Energy spectrum of the electrons in the 30-100 GeV. The head of the pulse, which is unaffected by the plasma, appears at −15 mm, equivalent to 43 GeV. The core of the pulse, which has lost energy driving the plasma wake, is dispersed partly out of the left field of view of the camera. Particles in the back of the bunch, which have reached energies up to 85 GeV, are visible to the right. The pulse envelope exits the plasma with an energy-dependent phase advance, which is consistent with the observed scalloping of the dispersed beam. (b) Projection of the image in (a), shown in blue. The simulated energy spectrum is shown in red. The differences between the measured and the simulated spectrum near 42 GeV are due to an initial correlated energy spread of 1.5 GeV not included in the simulations [11].

Experiments E-164X and E-167 operated in a new hybrid regime of PWFA where σ_r/σ_z is no longer much less than 1 and where $k_p\sigma_r \sim 1$ (recall $k_p = \sqrt{2}/\sigma_z$). In this case $n_b/n_0 \geq 1$ and the wakefield is weakly non-linear. Nevertheless, these experiments have demonstrated, as

shown in Figure 2-1 [11,12], the dramatic increase in accelerating gradients predicted for short bunches by Equation 1.

The ion column left behind the head of the bunch also provides a very large focusing force (strength ≈ 3MT/m for n_p=10^{17} cm^{-3}), which maintains the beam density and allows the beam to drive the wake over an extended distance. The combination of large focusing and accelerating gradient leads to the large energy gains observed in previous experiments. A result of these experiments is shown in Figure 2-3 some of the electrons doubled in energy, gaining 43 GeV in just 85 cm of plasma.

2.1.3 Computer Simulations

Current and proposed experiments operate in a regime where linear plasma theory is not valid. To help interpret the experimental data and design new experiments, our collaboration has developed extensive computer simulation capabilities that allow us to perform one-to-one modeling of the experiment in this non-linear regime. Two codes are used, OSIRIS [13] and QuickPIC [14]. OSIRIS is a 3-D, fully electromagnetic, relativistic, parallelized particle-in-cell (PIC) code that has been benchmarked against other codes and model problems that can be solved analytically. QuickPIC is a 3-D, parallel particle-in-cell code that uses a quasi-static approximation to decreases the computing time. OSIRIS and QuickPIC include the effects of field ionization and electron energy loss due to radiation from oscillations in the ion column. OSIRIS and QuickPIC are now the standard tools for simulating the beam plasma interactions in our experiments and have successfully described many of the observed phenomena in a quantitative manner [8,12,15].

2.1.4 Producing High-Intensity Drive Bunches

The dramatic increase in the maximum particle energy produced by beam-driven plasma wakefield accelerators (Figure 2-2) is a direct result of the advent of high-intensity drive bunches at SLAC. There are two factors involved in achieving the high intensities needed for large amplitude wakes—a high peak current and small transverse size.

The high peak current will be achieved in ASF by making use of a threefold compression process similar to that used for the FFTB experiments. Longitudinal compression is accomplished by manipulating the longitudinal phase space of the electron bunches, which is constant after the exit of the North Damping Ring (NDR). Achieving the short bunches necessary to drive large amplitude wakes (Eq. 1) requires raising the beam energy and energy spread. The nominal ASF compression process is described below and illustrated in Figure 2-4.

Longitudinal bunch compression is accomplished by creating a large energy spread correlated with position along the bunch and then providing an energy dependent path length that results in the bunch “tail” catching up with the “head”. Accelerating to higher energy then reduces the relative energy spread to a level acceptable for the final focus system. The maximum beam energy available is given by the amount of linac available. LCLS will operate the last kilometer of the SLAC linac with 14 GeV beams and the ASF beam energy is thus limited to the 25 GeV reached at Sector 20.

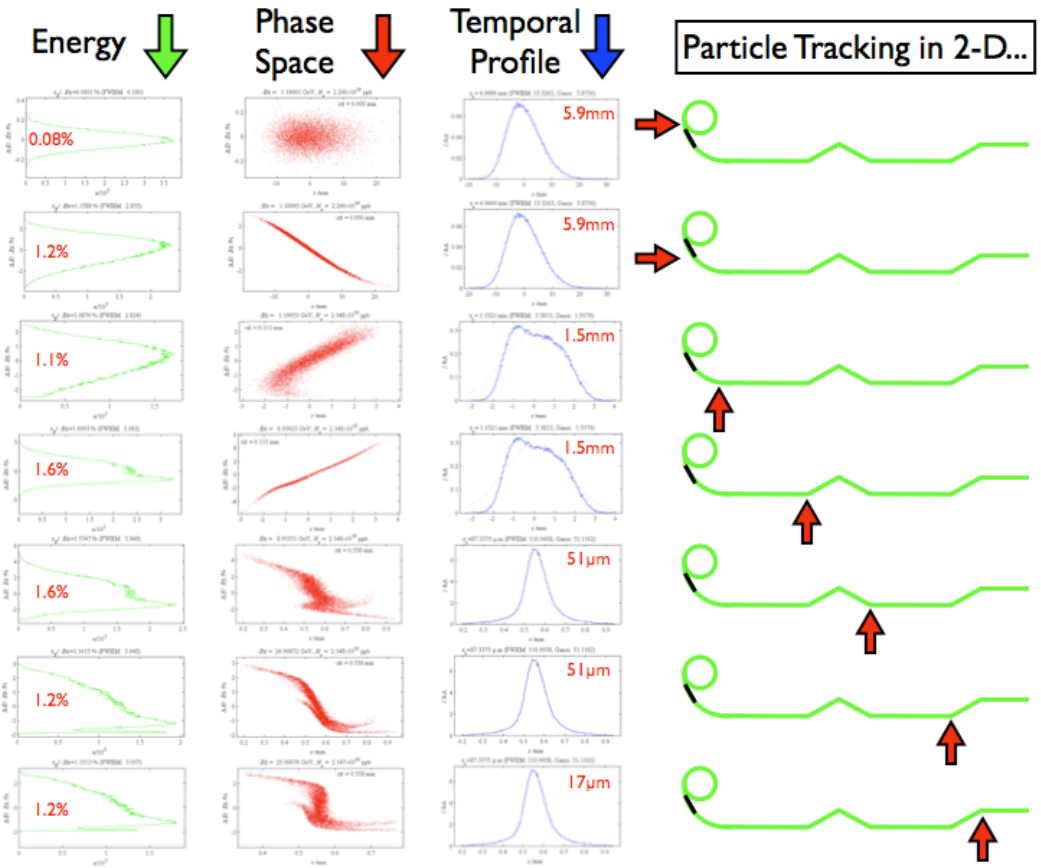

Figure 2-4. The evolution of longitudinal phase space of the compressed ASF beam illustrating the three stage compression process that yields a beam with a 17μm rms bunch length and a 22 kA peak current.

In the summer of 2002, a bunch compressor chicane was added at the 9 GeV point roughly one-third of the way down the 3 km SLAC linac. In a three stage process similar to that used for the FFTB, the bunches will be compressed to a predicted minimum of 17μm rms. A 6 mm-long bunch exits the North Damping Ring of the accelerator with an energy of 1.19 GeV and is given a correlated energy spread in an RF cavity run at the zero crossing phase, which leaves the mean energy unchanged. The resulting correlated energy spread, coupled with the non-zero momentum compaction of the ring-to-linac transport line, compresses the bunch to 1.2mm before it re-enters the main linac. The phase of the accelerating structures in the linac is set to add an additional energy correlation as the bunch is accelerated to 9 GeV. As a result, at the entrance of the chicane, the tail is more energetic than the head. The magnetic chicane then compresses the bunch to 50μm. Longitudinal wakefields in the remaining 1 km of linac impose an additional energy correlation, which is used to compress the bunch a third and final time to the minimum value of 17μm in FACET/ASF. The bunch length and current distribution will be adjusted by changing parameters in the main linac. A final focus system will then deliver beams with a transverse size similar to those available in the FFTB or about 5 μm rms. As indicated by Eq. 1, the resulting combination of high-energy, small transverse size, short bunch length and high peak current create a beam ideal for driving large amplitude wakes in a beam driven plasma wakefield accelerator.

2.1.5 Plasma Production by Field Ionization

Producing large amplitude wakefields requires short, high-density beams propagating through uniform high-density meter-long plasmas. When the current density of the electron bunch is high enough, the Coulomb field of the relativistic electron bunch can also create the plasma in a tube of vapor, in this case lithium vapor. With a sufficiently dense bunch, the ionization is accomplished by the leading particles of the bunch, so the majority of the bunch encounters a fully ionized plasma. Field ionization has several advantages over other techniques. Most notably it allows for the production of long, uniform, high-density plasmas with no timing or alignment issues. Plasma production by field ionization is the only known technique capable of producing the uniform high-density plasmas envisioned for future machines where the plasma length will be ten meters or more.

The lithium vapor is created in a heat pipe oven [9] where the neutral lithium vapor density and length are controlled through the pressure of the helium buffer gas, which confines the hot lithium at both ends, and the heating power. Lithium has a relatively low ionization potential for the first electron (5.4 eV), allowing ionization sufficient for wakefield generation over a broad range of beam parameters. The larger ionization potential of the second electron (75.6 eV) ensures that the plasma density does not evolve significantly along the bunch due to secondary ionization. In the experiments described here, the neutral lithium vapor is fully ionized by the large radial electric field at the front of the compressed electron bunches and the plasma density is then equal to the lithium vapor density.

This combination of short bunch length for multi-GeV/m gradients and the large beam density necessary to create the long high-density plasma is unavailable anywhere else in the world.

2.1.6 Two Bunch Experiments

Plasma wakefield accelerators have now demonstrated the ability to sustain very large gradients over meter scale distances. The large amplitude wakefield has been both created and sampled by a single bunch, resulting in a large continuous energy spread in the particles emerging from the plasma. To accelerate a separate witness bunch with finite energy spread requires crafting two distinct bunches separated by a fraction of a plasma wavelength (<100 μm). Until now, there has been no technique capable of both producing the short, high peak current drive bunches required to drive a large wake while simultaneously creating a following bunch to sample and load the accelerating portion of the wake.

For studies at the FACET/ASF, we propose to use a notch collimator installed in the Sector 10 bunch compressor chicane to create the two bunches needed for these next generation plasma experiments. The concept of a notch collimator is as follows. The electron bunch entering the bunch compressor chicane necessarily has an energy spread that is highly correlated with position along the bunch. In the middle of the magnetic bunch compressor chicane, the beam is dispersed in energy in the bend plane. Since it is dispersed in energy, the correlated energy spread dictates that it is also dispersed in time. Thus, collimating a different portion of the bunch energy spectrum, or position at this location, will collimate a different portion of the bunch in time. By placing a collimator of appropriate variable geometry at different locations along the bunch, a wide variety of drive/witness bunch configurations can be created. One example is shown in Figure 2-5.

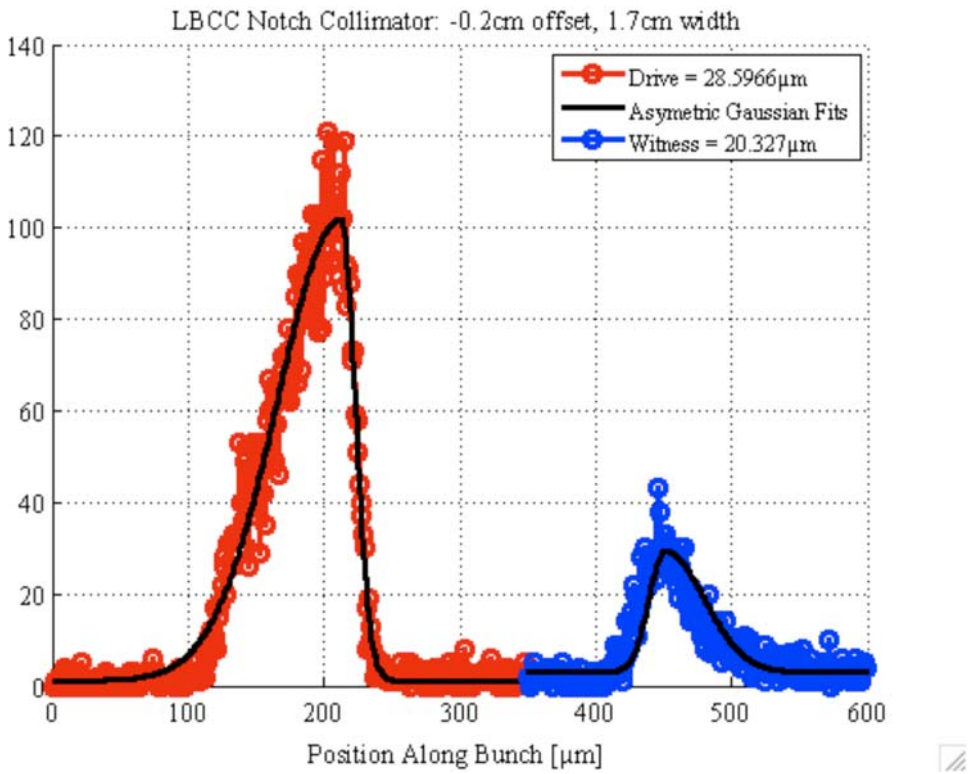

Figure 2-5. (a) Simulated drive and witness bunches created for FACET/ASF PWFA experiments after exiting the Linac Bunch Compressor Chicane (LBCC) in sector 10 and (b) the time profile of the same two bunches after propagation to the FACET/ASF focal point.

The collimation process is modeled in 6 dimensions (x, x', y, y', t, p) with a combination of tracking codes linked together by MATLAB. ELEGANT [16] is used to track the beam from the exit of the North Damping Ring to the middle of the Linac Bunch Compressor Chicane (LBCC) in Sector 10. The particles are then converted into an appropriate input for EGS4 [17] via the program SHOWER [18]. The notch collimator and the vacuum region around it are simulated with EGS4. The EGS4 output is then converted and loaded back into ELEGANT for tracking to the exit of the chicane and on to the FACET/ASF focal point. The notch collimator concept has the ability to craft several bunches from a single initial bunch and has been recently demonstrated experimentally [19].

2.1.7 Production of an Accelerated Bunch with Narrow Energy Spread

For plasmas to be useful in future colliders, they must provide not only high gradients, but also a high energy transfer efficiency and small energy spreads. We will take advantage of the two bunch capability to address these two issues for the first time. The two bunch capability will provide a number of particles to beam load the plasma wake sufficiently to make the wake amplitude constant over the witness bunch length, and minimize the bunch energy spread. Experiments at FACET/ASF will systematically study the physics of the beam loading of plasma wakes. We will vary the witness bunch delay and charge and measure the corresponding energy gain and energy spread. These two parameters will be optimized for the maximum energy gain with the minimum energy spread.

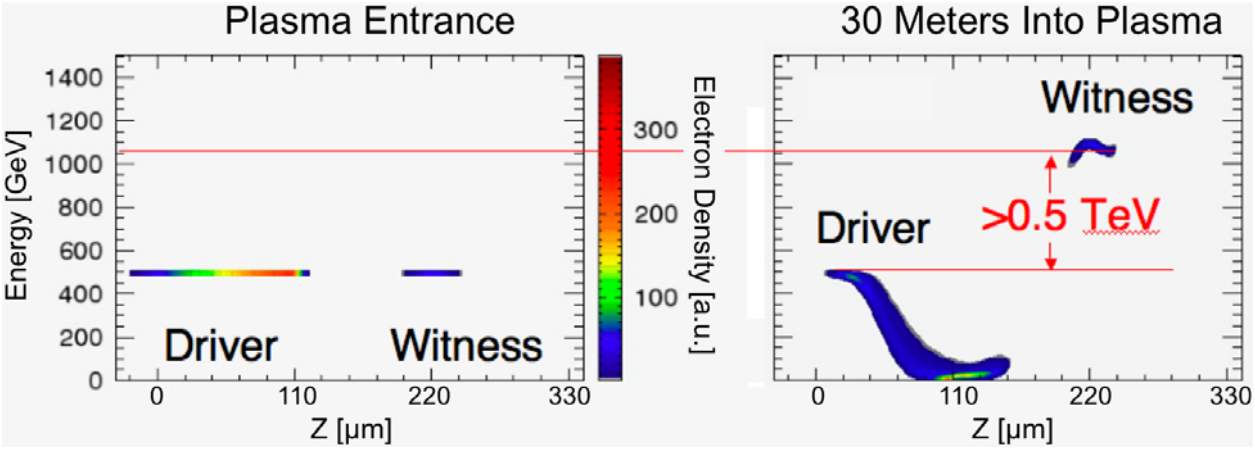

Figure 2-6. QuickPIC simulations showing a PWFA utilizing a drive/witness bunch configuration to produce a high energy witness bunch with a relatively narrow energy spread of a few %. The 3:1 ratio between drive to trailing particle beam number resulted in a loaded wake and a few percent energy spread with relatively high efficiency (~33% energy transfer). For these simulations the drive bunch length was 145μm, the witness bunch length was 10μm, the bunch separation was 100μm and the plasma density was 5.7 x 10^{16} e^-/cm^3.

QuickPIC simulations have shown that with appropriate combinations of drive/witness bunch charge, bunch length and separation, the PWFA mechanism can be used to double the energy of a trailing bunch with a final relative energy spread of a few percent (Figure 2-6).

2.1.8 Efficiency

Accelerating a second bunch with narrow energy spread will open the door to a set of measurements concerning the efficiency of the plasma wakefield accelerator. When the drive beam excites a wakefield in the plasma, if the wake is not sufficiently loaded by a second bunch, the wake will continue to oscillate behind the drive bunch. These additional oscillations correspond to energy left in the plasma that will eventually heat the plasma electrons. On the other hand, if the wake is fully loaded the plasma electron oscillation will last for only one-half of a period and terminate after the second bunch. Such a scenario would maximize the efficiency (~95%) at the expense of larger energy spread in the second (accelerated) bunch.

The efficiency can be separated in two parts: efficiency for the transfer of energy from the drive bunch to the plasma wake, and from the plasma wake to the witness bunch. The latter is optimized through beam loading. The former is optimized by maximizing the transformer ratio *R*, defined as the ratio between the peak accelerating field and the peak decelerating field of the wake (within the drive bunch). In the linear wakefield theory for bunches with a symmetric Gaussian current profile, the transformer ratio is equal to two. However, in the case of a Gaussian bunch various transverse slices of the drive bunch lose energy at different rates so that some slices will lose all their energy before the others. As an example, at the end of the simulation shown in Figure 2-6 some of the drive beam had almost stopped. However, much of the beam had not stopped since the decelerating field was not constant inside the bunch. The non-uniform energy loss in turn will lead to particles dephasing, possible loss of beam quality, and less than optimal energy transfer efficiency. This situation can be improved by using a bunch

with a longitudinal shape tailored such that all transverse slices lose energy at the same rate (except for the very first ones). This is accomplished by ramping up the current along the bunch, and the optimum longitudinal shape is triangular [20]. In that case, the peak loss wake field remains constant at a low value, while the peak accelerating field left behind the bunch keeps increasing with the bunch length. The transformer ratio then scales as π times the number of plasma wavelengths covered by the bunch, and can be much larger than two. More sophisticated bunch profiles can also lead to larger enhancements of R. We propose to investigate higher transformer ratios by manipulating the phase space of the bunch along the three compression stages of the linac. The compromise between optimum efficiency and beam quality will be studied and characterized.

2.1.9 Emittance Preservation

The high-gradient electron acceleration experiments are performed in what is known as the "blow-out" regime of the PWFA [21]. In this regime the beam density n_b is larger than the background plasma density n_p ($n_b>n_p$), and all the plasma electrons are expelled from the bunch volume. As a result, the focusing force of the pure ion column is linear with radius and constant along the bunch, and the peak accelerating gradient can exceed the value predicted by linear theory. However, because of the strong focusing force of the ion column, the beam may experience many betatron oscillations along the plasma [22,23]. For example, in the E-167 experiments, the betatron wavelength for the 42 GeV electrons is 1.3 cm in the $2.7\text{x}10^{17}$ cm^{-3} plasma, corresponding to about 65 beam betatron oscillations over the 85 cm plasma. Therefore, in a future PWFA collider application it will desirable to match the beam to the ion column in order to avoid large changes in the beam exit angle caused by possible small variations in plasma density or incoming beam parameters. The matching condition for a beam with a relativistic factor γ and normalized emittance ε_N focused to a transverse size σ_r is $\gamma n_p \sigma_r^4/\varepsilon_N^2=2\pi r_e$. Considering the normalized emittances envisaged for a future collider (of the order of 10,000/20 nm in the vertical and horizontal plane respectively), the transverse beam sizes matching the ion column focusing are of the order of 1 μm and 50 nm.

The density of the bunch with $2\text{x}10^{10}$ electrons now exceeds 10^{20} cm^{-3} ($n_b>>n_p$). When $n_b>n_p$. the massive plasma ions can be assumed to be at rest for a few plasma periods, while when n_b/n_p approaches $m_{ion}/m_{electron}$ this assumption is not valid anymore. In this case the drive or the witness bunch will impart such a large transverse momentum to the plasma ions that they will be focused onto the axis within one plasma wake period [24]. The focusing of the plasma ions will create non-linear focusing forces that will vary along the bunch, and will result in significant emittance growth of the accelerated bunch.

A number of methods have been proposed to try to mitigate the effect of plasma ion motion on the beam quality [25]. These include using atoms heavier than lithium for the plasma, *e.g.*, argon or xenon; using an input beam with phase-space correlation to compensate for the nonlinearity of the focusing force; using a plasma with a radial density gradient similar to that used to guide laser pulses. However, a solution has yet to be demonstrated. It is therefore important to find ways to minimize the effect of ion motion both with numerical simulations and in experiments. The effect of plasma ion motion could be tested, for example, in a plasma lens experiment where the beam charge and transverse size could be varied from $n_b>n_p$ to $n_b>>n_p$. Another possibility would be to repeat the betatron oscillation measurements that we performed with longer bunches [22], while varying the n_b/n_p ratio. These types of experiments are ideally performed with beams that will be available at FACET/ASF: with low emittance to be focused to

small transverse sizes, combined with very high charge to reach densities much larger than the plasma density.

The next significant result in electron PWFA research will be the demonstration of the acceleration of a particle bunch with a narrow energy spread and large efficiency. Computer simulations will aid in exploring the parameter space and narrowing it to a tractable number of cases, but in the end these cases must be investigated and proven in experiments. Optimizing the two bunch configuration to generate 50 GeV range beams with a narrow energy spread and small emittance with high efficiency will be the primary focus of the initial plasma research program at the ASF.

Issues such as betatron radiation loss, hosing instability of both the drive beam and the beam load, emittance growth due to plasma ion motion and multiple Coulomb scattering and beam head erosion limiting the energy transfer efficiency from the drive beam to the wake will have to be investigated and solutions will have to be developed and tested.

2.1.10 Positron Acceleration

The concept of a plasma afterburner for a linear collider [4] relies on the acceleration of both electrons and positrons in high-gradient plasma accelerator sections. We therefore propose to modify the compressor at Sector 10 to allow for the compression of positron bunches as well as electron bunches. The upgrade of the bunch compressor chicane will open up areas of beam-plasma interaction that are so far unexplored. Consequently, understanding the behavior of short, high peak current bunches of positrons in plasmas will be a major component of advanced accelerator research at the ASF.

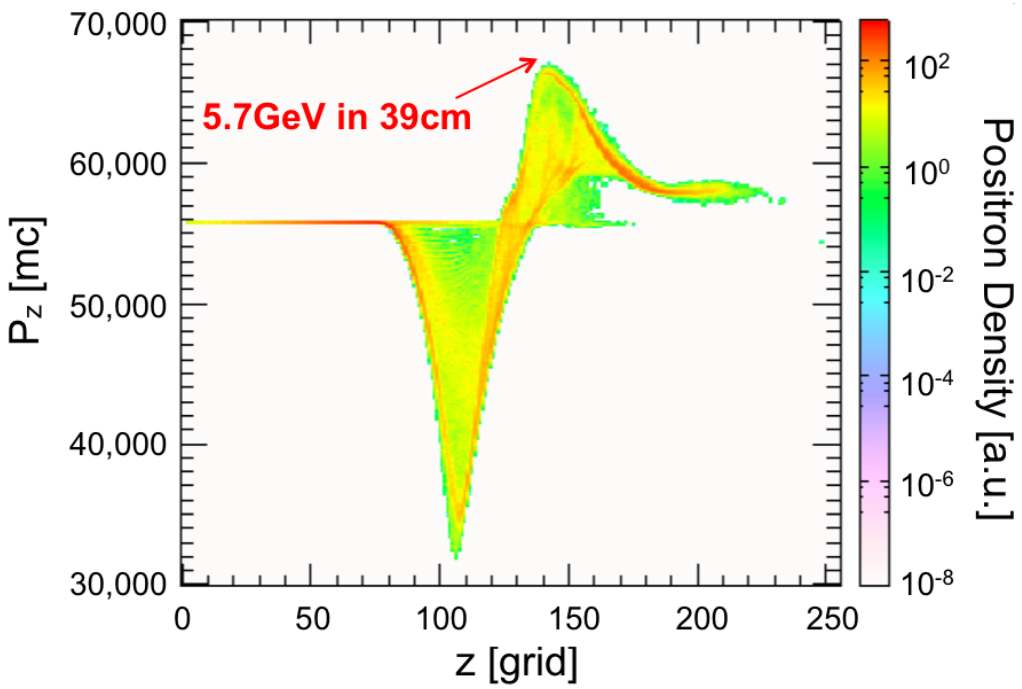

Figure 2-7. Simulated longitudinal phase space of a compressed positron beam after propagation through 39 cm of field-ionized plasma showing a maximum energy gain of 5.7 GeV.

In this regime non-linear and relativistic plasma effects are dominant. Positron and electron beams are fundamentally different, because plasma electrons are repelled by an electron beam but attracted by a positron beam. The plasma-positron beam interaction must be understood through experiments, and these experiments can only be performed at the ASF. The questions we will address specifically are: Can positron beams be accelerated at high-gradients in much the same way as electron beams have been in a self-ionized plasma, or will some specially crafted plasma structures, such as hollow plasma fibers, be needed? Can the positron beam emittance be preserved? Can energy doubling of a positron beam using a 25 GeV drive beam be demonstrated at the ASF?

Experiments in the FFTB demonstrated for the first time the acceleration of positrons in plasmas using the long positron bunches ($\sigma_z \approx 700$ μm) available at SLAC prior to 2003. However, the measured acceleration gradients were only of the order of 70 MV/m [26]. Numerical simulations suggest that short positron bunches with parameters similar to the electron bunches can excite wakefields with amplitudes of the order of 5 to 10 GV/m as shown in Figure 2-7.

2.1.11 Hollow Channels

Plasma wakefield acceleration in plasma channels has been a holy grail for plasma accelerators for some time now for several reasons. For laser wakefields the channel guides the laser overcoming diffraction limits. For particle beam-driven plasma wakefields, channels and particularly hollow channels, have been shown to offer potentially higher beam quality [27,28]. Numerical simulations show that plasma wakes generated by positron beams can be maximized by using a hollow plasma channel with a radius approximately equal to one plasma skin depth. The channel provides a timing mechanism for the "sucked-in" plasma electrons, preventing phase mixing that reduces the positron wake. Since there are no charges in the hollow plasma channel, the transverse oscillations are suppressed. The beam transverse size can be larger than would be necessary to match the beam to the plasma, allowing for a higher beam current, and for a tighter focusing of the beam after the plasma exit. Plasma channels may provide an opportunity to maximize both the center-of-mass energy and the luminosity of an electron-positron plasma-based collider. Creating hollow channel plasmas in the field-ionized regime is a challenge. Ideas exist to manipulate the neutral vapor radial profile [29,30], but these ideas are in their infancy and require a sustained program with the promise of eventual testing to be fully explored.

2.1.12 Positron Acceleration in Electron Driven Wakes

In addition to hollow channel plasmas, there are alternative techniques that may provide an ability to accelerate positrons in a high-gradient plasma wakefield excited by an electron beam. Testing this idea experimentally involves merging independent bunches of positrons and electrons produced and accelerated in the main linac. At the plasma entrance, the merged beams would need to be on the same transverse orbit, with the positron bunch trailing the electron bunch by roughly one plasma wavelength (~100 μm). Simpler ideas exist to generate positrons *in situ* within an electron beam driven plasma wake by focusing the electron beam into a small tungsten wire located right inside the plasma [31]. Here, the electron pulse generates an electromagnetic shower, consisting of secondary electrons, positrons and photons. If the wire is thin enough, the emittance of the primary electron beam is not seriously degraded, and it can still drive a non-linear plasma wake containing a blow-out region. Such a plasma wake includes a region where the electromagnetic fields are both focusing and accelerating for positively charged

particles. Simulations suggest that this region could be used to trap positrons from the shower, and accelerate them to relativistic energies. This idea is highly speculative and in the early stages of development, but if successful this setup would allow one class of positron acceleration experiments to proceed before the completion of the symmetric chicane in Sector 10.

2.1.13 High Demagnification Plasma Lens

Plasma lenses, with their extra-large focusing strength, are the natural complement to high-gradient, plasma-based accelerators. Beam focusing by plasmas has been demonstrated both for electrons [32] and positrons [33,34]. However, these experiments showed low demagnification ratios (<5) and relatively large focused transverse sizes (>1 μm at 28.5 GeV), while a high-demagnification leading to sub-micron sizes is required for collider applications.

There are a number of very interesting experimental topics to be studied with plasma lenses at FACET/ASF. First, in an under-dense lens with a beam density larger than the plasma density, the lens is formed by expelling the plasma electrons from the bunch volume, thereby creating a pure ion column with linear radial focusing strength (free of geometrical aberrations). The dynamics of the lens formation must be studied in detail. The same two bunch capability described in previous sections would provide a "drive" bunch to both create the plasma and expel its electrons, and a following witness bunch that is cleanly focused. Second, when in the focusing process the beam transverse size becomes comparable to the average distance between plasma particles (≈ plasma density$^{-1/3}$), the focusing field becomes random and may limit the ultimate transverse size achievable. Third, as the electron beam is focused its peak space charge field increases with its density and may become large enough to set the plasma ions into motion, thereby degrading the quality of the focused beam. Fourth, contrary to a magnetic lens, the focusing strength can be made to increase adiabatically along the lens itself [35] in order to reduce the lens length and beam final size, as well as to minimize the synchrotron radiation loss (Oide radiation). The combination of a well characterized high energy, high density electron beam, plasma source, specialized instrumentation and techniques developed for the plasma acceleration research are critical components to any plasma lens program and make ASF a natural facility for conducting this research.

2.1.14 Brightness Transformer

While probing new regimes in beam-plasma interaction, the possibility of discovering new and exciting phenomena remains high. As an example, it was observed in the SLAC PWFA experiments that plasma electrons are trapped and accelerated by accelerating gradients comparable to those experienced by the beam electrons when the plasma wake amplitude exceeds ≈30 GV/m [36]. Optical measurements show that those electrons emit coherently in the visible range, indicating that they have time structures at the visible time scale (≈1.3 fs for 500 nm radiation). Energy measurements show that these trapped electrons reach multi-GeV energies over the 85 cm-long plasma, with a spectrum that exhibits narrow energy spread features.

Numerical simulations of the experiment show that these trapped electrons originate from the very beginning of the plasma. The plasma source consists of a column of lithium contained in the hot region of a heat-pipe oven by a helium buffer gas at room temperature. As the electron beam is focused near the entrance of the lithium column it field-ionizes the lithium atoms. In the transition region where both helium and lithium coexist, helium is not directly ionized because its ionization potential (24.6 eV for the first electron) is much larger than that of lithium (5.4 eV).

However, the beam excites the plasma wake and is focused by the newly created lithium plasma, its peak space charge field increases, and can now exceed the threshold for ionization of helium electrons. The helium electrons are ionized inside the wake itself, where the beam pinches, and are therefore much more likely to be trapped by the ultra-relativistic wake than the lithium electrons ionized ahead of the wake itself. The trapping stops at the end of the transition region (≈10 cm), when the beam reaches the pure lithium region of the oven. Once ionized, the helium electrons quickly slip in phase, bunch near the peak of the wake field and are accelerated.

Simulation results confirm that the bunch of trapped particles has very interesting characteristics. The bunch length is of the order of 1-2 μm rms. The peak current can exceed 35 kA, more than twice the peak current of the linac drive bunch. At the same time the trapped bunch normalized emittance is smaller that that of the drive bunch and the trapped bunch brightness is two orders of magnitude larger than that of the drive bunch. The bunch reaches an energy of 12 GeV after 85 cm of plasma with an energy spread of about 4%. The combination of a high brightness beam (such as the FACET/ASF beam) and a PWFA can therefore be used to produce higher brightness beams than available today, beams with possible applications to uv and x-ray FELs.

The experimental results obtained so far are consistent with the trapped bunch properties obtained in numerical simulations. However, this brightness transformer scheme must be optimized both experimentally and numerically to produce the highest possible beam quality. The helium buffer gas can be replaced by an easier gas to ionize (such as argon) in order to increase the bunch current and therefore brightness. The drive beam parameters in the helium to lithium transition region can be optimized, and the transport of the high brightness bunch in the buffer gas region following the plasma must be adjusted in order to avoid further trapping in exit transition region of the plasma and preserve the bunch characteristics.

These experiments can only be performed with the type of beams that will be available at the ASF. No other beam can drive a wake with large enough amplitude to trap "plasma" electrons and produce these high brightness beams.

2.1.15 Experimental Timeline

The physics of the Plasma Wakefield Accelerator is critically dependent on almost every beam parameter: charge, transverse spot size, longitudinal pulse shape, orbit and incoming energy spread. Many of the diagnostics to measure these parameters on a single pulse were developed as part of the plasma program in the FFTB. When beams first become available in the ASF the first order of business will be to commission the diagnostics that are so critical to understanding the beam-plasma physics.

A timeline for how the experimental program may proceed is outlined in Table 2-2. For the case of electron acceleration the program will build upon the results of the FFTB and extend the large gradient acceleration from bunches with 100% energy spread to discrete bunches with much lower energy spread. Subsequent steps will study the utility of the plasma lens to produce sub-micron spot sizes while gaining insight into the possibly deleterious effects of ion motion. Positron acceleration will begin by studying high gradient acceleration for single bunches driving large amplitude wakes in a field-ionized plasma for the first time. The experiments will transition to more exotic plasma sources with hollow channels to increase the magnitude of the accelerating gradient while reducing the emittance growth from the highly non-uniform plasma column. The final phase of experiments will explore the possibility of accelerating positron bunches in electron beam driven wakes. It should be noted that these experiments often produce

startling and unexpected phenomena (e.g. trapped particles and the brightness transformer) that will necessitate fluidity in the predicted timeline.

Table 2-2. Experimental timeline for the ASF plasma wakefield accelerator research

Run	Plasma Wakefield Accelerator Program	
	Program	**Description**
	Electrons	
FY10	Commissioning	Commission profile monitors, bunch length diagnostics and energy spectrometers. Initiate first experiments.
FY11	Acceleration of witness bunch with narrow energy spread	Demonstrate creation of two bunches with notch collimator then accelerate a witness bunch with narrow energy spread.
FY12	Quantify efficiency & optimization	Optimize notch collimator & plasma density to quantify tradeoff between final energy spread and efficiency.
FY13	Quantify efficiency & optimization	Continuing from FY12.
FY14	Plasma lens	Demonstrate high demagnification plasma lens with sub-micron spot size.
FY15	Emittance preservation & Ion motion	Vary ratio of the beam/plasma density to quantify emittance growth due to ion motion.
	Positrons	
FY10		
FY11	High Gradient Acceleration	Study wake amplitude for single, short positron bunches in a field ionized plasma for the first time.
FY12	High Gradient Acceleration	Continuing from FY11.
FY13	Hollow Channel Plasmas	Use plasma sources with a hollow channel, density minimum on axis, to increase wake amplitude and minimize emittance growth.
FY14	Positrons in electron beam driven wakes	Create positrons within the electron wake using a conversion target within the plasma source.
FY15	Positrons in electron beam driven wakes	Re-configure ASF beamline to combine electrons & positrons from the main linac.

2.2 Dielectric Wakefield Accelerators

Future accelerators with ultra-high fields will not be based on conventional metallic resonant cavities, because the power necessary to excite such structures becomes excessive. This forces consideration of shorter wavelength linac structures. Existing linacs, which have tens of MV/m acceleration gradients in the 1 to 10 cm wavelength range, would be naturally scaled to mm and sub-mm wavelengths for GV/m operation. It would be advantageous to operate in the THz region, $\lambda \sim 0.3$ mm, but here the problem is the power source because no conventional sources exist with the power needed to achieve GV/m fields. Therefore, the emphasis has been on beam-driven wakefields to address the need for higher electromagnetic power at THz frequencies. In a dielectric wakefield accelerator electromagnetic power is radiated by an ultra-short, intense

"driving" electron bunch propagating in a high impedance environment formed by a hollow dielectric fiber. This power is then used to accelerate another "witness" bunch just as in the case of the plasma wakefield accelerator.

Sufficient available power for high gradients depends on having high peak currents, a small inner radius of the hollow dielectric fiber, and, therefore, a drive beam with small transverse emittance to propagate through the fiber. The required beam can only be provided by ASF making ASF unique for exploring dielectric wakefield acceleration.

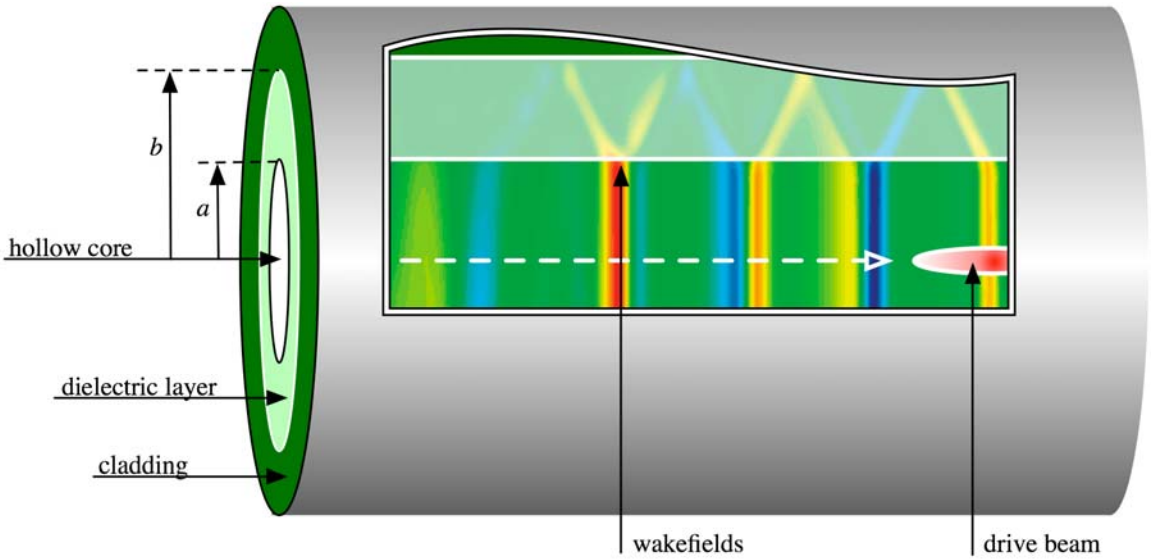

Figure 2-8. Conceptual drawing of the dielectric wakefield accelerator. A "drive" beam excites wakefields in the tube, while a subsequent "witness" beam (not shown) would be accelerated by the reflected wakefields (bands of color).

2.2.1 The Hollow Dielectric-Tube Dielectric Wakefield Accelerator

Wakefield-driven accelerating-schemes can offer high gradients and conceptually simple geometries. The Dielectric Wakefield Accelerator (DWA) based on a hollow dielectric tube is one such approach (Figure 2-8). A short (<1 ps) drive-bunch traversing the tube creates Cerenkov wakefields that propagate towards the dielectric boundary at the Cerenkov angle, and are reflected back towards the center axis, where a second bunch arrives and is accelerated [37]. The dielectric wakefield accelerator solves the THz-power problem by using radiated fields from short electron bunches, leveraging high-precision fabrication technology from developments in fiber optics, and provides a straightforward means of producing large on-axis accelerating fields. These fields may be used most straightforwardly by accelerating a trailing on-axis bunch, or by directing the radiated fields to an off-axis, higher impedance structure (step-up transformer [38]). Note that these mechanisms work equally well with electrons or positrons.

2.2.2 Work to Date

With the above considerations in mind, an experiment (T-481) carried out at the FFTB was designed to assess the survivability of dielectric tubes subjected to high fields generated by short electron-bunches. Tubes, produced from commercially available, hollow SiO_2 fiber-optics, were

cut, polished, baked to remove the cladding, and metallized on the outer surface. An array of 10 tubes, each 1 cm in length, was placed in a precision holder with multiple V-shaped grooves cut in parallel. The holder, which was optically pre-aligned to the nominal electron beam path, could be moved transversely to the beam path, allowing placement of any of the tubes along the beam axis. A vacuum chamber housed the holder and various beam diagnostics. Tubes of both 100 μm and 200 μm ID were exposed to a number of beam shots, with the induced wakefield tuned by variation of bunch length. CCD array cameras were placed to observe the tube-end from the top and side (relative to the beam path). The side camera image was digitized and recorded, along with a relevant electron beam parameters, for offline analysis.

The main results of the T-481 collaboration include [39]:

- Demonstration of beam control (trajectory, bunch length, etc.) adequate for a dielectric wakefield accelerator;
- Generation of surface fields in excess of 20 GV/m; and,
- Measurement of breakdown fields in excess of 1 GV/m.

These results were obtained in a 2-day long run in the FFTB, and it would have been impossible to obtain them without the expertise and instrumentation developed in the plasma wakefield research. To extend these studies further, it is necessary to provide more direct experimental measures of the electromagnetic wake properties.

2.2.3 Next Steps

Following on the success of T-481, the next round of experiments would involve three phases of development based on the FACET/ASF beams [3]. The first phase would be a detailed breakdown study including exploration of a large range of design parameter space, materials, and cladding designs; and, quantifying of the fields by measurement of the coherent Cerenkov radiation. The second phase would attempt to directly observe acceleration and deceleration of particles in 10 cm length fibers. The third phase—once ASF is well characterized and fully operational—would involve significant acceleration, building on the results and expertise gained in the initial two phases, by using tubes around one meter in length.

The specific goals of the proposed dielectric wakefield accelerator studies at ASF can be listed:

- **Coherent Cerenkov Radiation (CCR) measurements**: Investigations of coherent Cerenkov radiation in the THz spectral range will serve as a measure of the fields in the dielectric, and as a bunch length diagnostic.
- **Materials**: In T-481, only fused silica tubes were tested; additional materials including CVD-fabricated diamond [40] will be explored.
- **Coating**: The thin metallic coating used on the tubes in T-481 proved inadequate to withstand ohmic heating due to induced currents. Use of dielectric cladding will be explored at FACET/ASF.
- **Varying tube diameters**: T-481 used off-the-shelf fused silica tubes which were available in 100 μm and 200 μm IDs, and fixed 350 μm OD. We plan to have several custom diameters fabricated, allowing the breakdown limit to be explored at fixed beam parameters.

- **Varying tube length**: Short, 1 cm tubes were used in T-481. The ASF experiments will use lengths from 1 to 10 cm with the ultimate goal of pursuing a 1 m long dielectric wakefield accelerator module. They will also allow the dependence of breakdown on time of exposure to high gradient wakefields.
- **Direct observation of beam changes:** Longer fibers will allow for the direct measurement of momentum change to the beam due to wakefield acceleration and deceleration, and may also produce notable changes in the transverse centroid due to transverse wakes.
- **Preparation**: Alternative fiber preparation techniques will be considered and tested. Different methods of cladding removal and tips polishing (*e.g.* diamond cleaving) to eliminate debris contamination in the tube bore will be employed.

The study of the coherent Cerenkov radiation emitted from fused silica fibers is a central part of this experimental work, as it directly probes the wakefield excitation process, giving an independent measurement of the wakefield strength. The coherent Cerenkov radiation measurements would be one of the first efforts undertaken at ASF. The total energy lost to emission of coherent Cerenkov radiation may be estimated as

$$U_{\bar{C}} \cong Q_b E_{z,dec} L_d / 2$$

where *Ld* is the length of the tube. For L_d =1 cm, Q_b = 3 nC, and $E_{z,\,de}c$ = 2 GV/m, we estimate that 30 mJ of coherent Cerenkov radiation will be emitted. The radiation emitted at the downstream fiber end will use metallic cones (*e.g.* horns) as a means of impedance matching to free space, and directing the radiation in a forward cone.

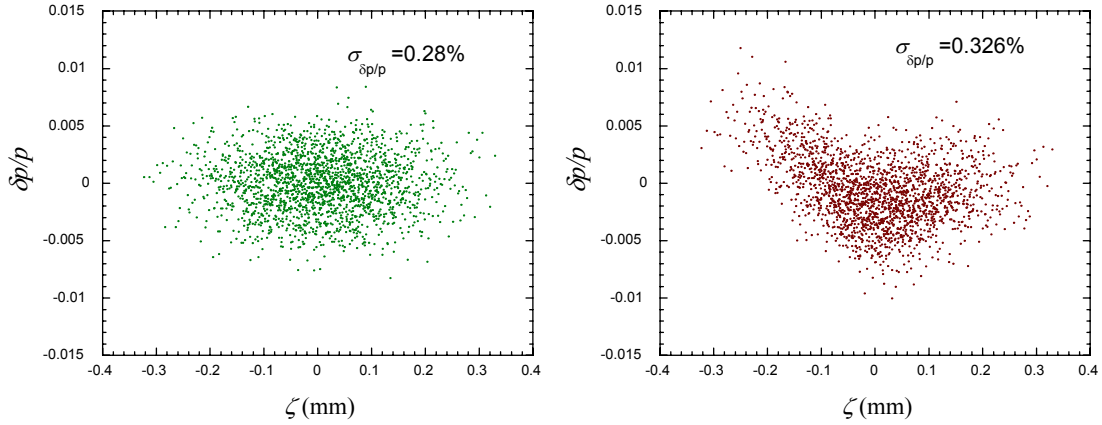

Figure 2-9. Longitudinal phase spaces 10 cm dielectric tube (a=75 μm, b=175 μm, ε=3). The initial phase space for the Q_b=3 nC, σ_z = 110 μm beam is shown at left, the final state after 10 cm propagation is shown at right, with the trailing edge of the beam displaying easily resolvable acceleration.

The first measurements of wakefield acceleration would be made with relatively long bunches that would have a low energy spread. Simulations confirm that acceleration could be observed. In Figure 2-9, we display the results of propagation through 10 cm with a Q_b=3 nC, σ_z = 110 μm beam, and compare the initial and final longitudinal phase spaces. It can be seen that the tail of the beam shows resolvable acceleration, while the beam core is notably decelerated. Even without a time resolved diagnostic, one may still observe the energy changes in the beam

through the increase in the overall momentum spread. One could also observe transverse wake effects. An initial 20 μm (~4σ) offset in the beam centroid may produce, in diamond tubes, a transverse wake force of 200 MeV/m, or an integrated transverse kick over 10 cm of 20 MeV. This corresponds to an angle of 80 μrad, which is a bit smaller than the angles due to emittance (140 μrad for β^*=5 cm).

Successful energy gain measurements with a 10 cm tube would lead to the next stage of this research—using meter-long dielectric tubes with a permanent magnet focusing channel to confine the beam transversely. The results should include gradients in excess of 1 GV/m and energy gains of a GeV or more.

2.2.4 Theory and Limitations

Acceleration methods relying on material boundaries, including the dielectric wakefield accelerator and conventional metallic cavities, are ultimately limited in their gradient by material breakdown. Breakdown has been well studied in a number of scenarios. For metallic cavities, where Fowler-Nordheim [41] emission can lead to break-down, all breakdown phenomena are typically empirically represented by a Kilpatrick-like limit on the achievable gradient [42]. In laser driven structures breakdown has been experimentally studied for both short and long timescales [43]. In optical-IR structures, laser-induced breakdown, which generally occurs at higher fields than metallic structures, has also examined in detail [44]. Prior to the T-481 work, field gradients producible by beams in dielectrics were low (tens of MV/m) and on a longer wavelength scale [45], in the 10 GHz range, due to relatively long (many ps) beams used. The unprecedented combination of high charge, short bunch duration, and small spot-size available at SLAC's Final Focus Test Beam (FFTB) enabled the GV/m fields of the T-481 experiment to be achieved [39]. This combination of beam attributes was obtained through both magnetic compression, to obtain <100 fs bunch lengths, and high energy, which gave small beam sizes naturally through adiabatic damping of the emittance.

The criticality of these beam parameters for driving ultra-high field wakes in a dielectric wakefield accelerator can be deduced from the following approximate expression for the decelerating field:

$$eE_{z,\mathrm{dec}} \cong -\frac{4N_b r_e m_e c^2}{a\left(\sqrt{\frac{8\pi}{\varepsilon-1}}\varepsilon\sigma_z + a\right)} \qquad (1)$$

where a is the inner radius of the hollow dielectric tube, σ_z is the rms bunch length, N_b is the number of beam particles, r_e and mc^2 are the classical radius and the rest energy of the electron, respectively, and ε is the relative permittivity of the dielectric. FACET/ASF beam parameters will be $\sigma_z \geq$20 μm, with transverse beam size σ_r ~10 μm, and bunch population $N_b = 2\times10^{10}$. Thus, with such small beam dimensions, and the choice of a as small as 100 μm, fields as high as 8 GV/m could be produced during experiments. For breakdown studies, the radial electric field at the dielectric surface,

$$E_{r,\mathrm{surface}} \cong -\frac{4N_b r_e m_e c^2 \varepsilon}{a\left(\sqrt{8\pi}\sigma_z\varepsilon + a\sqrt{\varepsilon-1}\right)} \qquad (2)$$

is also of primary interest. In the T-481 experiments, radial surface fields as high as 22 GV/m were present, and comparable fields would be achievable in ASF.

With the availability of both high power laser and microwave sources, dielectric breakdown has been studied in detail in the optical and cm-wavelength spectral regions. For the very short pulse times explored in the present THz studies, however, one may refer only to laser induced breakdown for comparison. The fundamental mechanism in laser driven breakdown in the short pulse regime is avalanche ionization, in which quantum absorption of a single photon or multiple photons produces a free electron that initiates an avalanche of subsequent ionization [44], thus producing damage in this situation. The situation differs for the beam driven, relatively long wavelength wakefields found in the dielectric wakefield accelerator. In this case the Keldysh parameter [46] is small, and conducting electrons are created by tunneling ionization, not by photon absorption. This mechanism yields a lower threshold for creation of conducting electrons than from optical excitation.

It should be noted that optical to UV photons are created via incoherent Cerenkov excitation in the dielectric wakefield accelerator, but this flux is too low to be important for initiating breakdown. More importantly, in a high energy electron beam environment, breakdown inducing ionization may arise from stray electrons or X-rays. Finally, laser driven dielectric breakdown studies have shown lower field thresholds at longer exposure times. In our case, the exposure time in the downstream end of a 1 cm long dielectric wakefield accelerator is ~100 ps, due to group velocity effects and will be proportionately longer for longer dielectric structures.

2.2.5 Modeling and Simulations

Simple analytic models bolstered by particle in cell codes serve to predict the outcome of the FACET/ASF experiments. Adjustment of the bunch length is both the mechanism for achieving high wakefields and for parametrizing the experiments. As shown by Eq. 1, fields greater than 10 GV/m can be produced during these experiments (Figure 2-10).

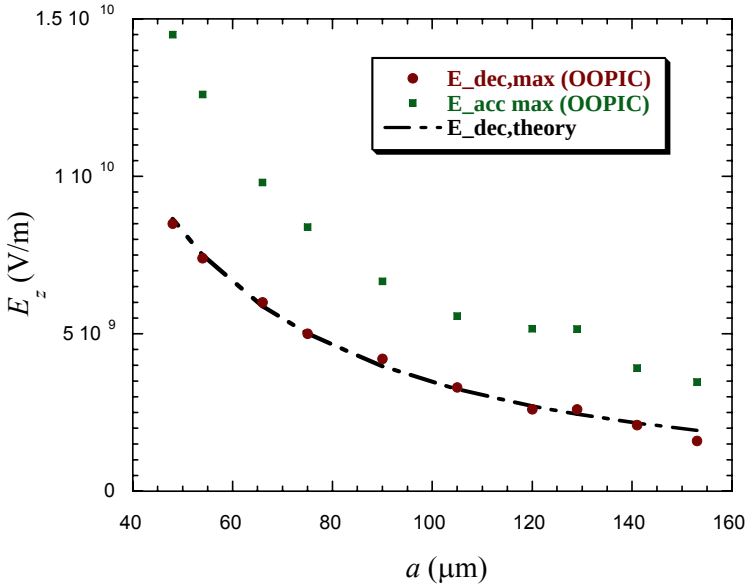

Figure 2-10. Dependence of longitudinal fields on a, the inner radius of the dielectric tube, in OOPIC Cerenkov wake simulations, with b/a=3, ε=3, and beam parameters N_b=1.9×10^{10}, σ_z=20 μm, σ_r = 10 μm, beam energy 30 GeV, with predictions of Eq. 1.

OOPIC [47] simulations verify the predictions of Eq. 1 concerning the maximum decelerating field. This figure also illustrates that, as is typical of wakefields driven by symmetric drive beams, the peak accelerating field behind the beam is less than or equal to two times the decelerating field.

2.2.6 Future Research

The measurements from these initial ASF experiments would significantly advance the state of knowledge on dielectric wakefield accelerators. By having characterized the breakdown threshold for multiple materials, having measured the coherent Cerenkov emission, and having shown direct energy exchange with the beam, these experiments would prove the viability of dielectric-tube wakefield accelerators with GV/m accelerating gradients.

The next phase measurements would increase the dielectric accelerator length to the meter scale and demonstrate substantial, high-gradient acceleration of beams. The β*'s are significantly less than a meter, and it will be necessary to focus the beam transversely. Small bore permanent magnet quadrupoles can have high enough gradient for building a FODO array that will extend over the length of the fiber and confine the beam. Acceleration of 1 GeV or more would be measured with the dielectric fiber contained in such a FODO channel. This would open the possibility of colliders and compact, high energy machines based on dielectric-tube wakefield structures.

2.3 Conclusions

In this section, we have summarized the past progress in plasma wakefield accelerators and described the next steps needed to develop this concept into an accelerator for high energy physics. Recent experiments have successfully answered questions regarding the magnitude and sustainable length of the accelerating field in a plasma wakefield accelerator. Due to the high quality and unique characteristics of the beam that was available at the FFTB, this approach has demonstrated capabilities applicable to high-energy accelerators by accelerating electrons with a gradient of 50 GeV/m for almost a meter. The ultimate utility of a plasma wakefield accelerator must be further studied at FACET/ASF. Second generation experiments performed at the ASF will harness these large gradients to study efficient acceleration of mono-energetic electron bunches with preserved emittance. Previous experiments have studied the highly non-linear nature of positron focusing in long plasmas and low gradient acceleration. Experiments at FACET/ASF will probe the virtually unexplored territory of high-gradient positron acceleration in plasmas.

These are critical experiments that that must be performed to move the plasma accelerator toward a useful technology for high-energy accelerators. The ASF beam line, offering ultra-short, high-energy and high-charge electron and positron beams, will be the only facility in the world where these experiments can be performed. With FACET/ASF, it will be possible to engage a larger community in the development of the plasma wakefield accelerator while performing the needed experiments. The success of research at the FFTB has shown that collaborations including a national laboratory and a strong contingent of university faculty, staff, and students are a vital component of a successful program in advanced accelerator R&D. FACET/ASF will be the only facility worldwide that will allow continued development of these areas of advanced accelerator research.

2.4 References

[1] M. Tigner, Accelerator R&D. Eur. Phys. J. C **33**, s01, s146–s148 (2004), http://dx.doi.org/10.1140/epjcd/s2003-03-017-5.

[2] "Report of the HEPAP Subpanel on the Assessment of Advanced Accelerator Research and Development" (August 2006).

[3] "Wakefield Acceleration in Dielectric Structures", proposal by H. Badakov *et al.* (E-169 Collaboration).

[4] S. Lee *et al.*, Phys. Rev. STAB **5**, 01 1001 (2002).

[5] V. Yakimenko and R. Ischebeck, Proceedings of the 12th Advanced Accelerator Concepts Workshop (AAC 2006), Lake Geneva, Wisconsin.

[6] "Multi-GeV Plasma Wakefield Acceleration Experiments", M. Berry *et al.* (E-168 Collaboration).

[7] C. Joshi and T. Katsouleas, Physics Today, **47** (June 2003).

[8] P. Chen *et al.*, Phys. Rev. Lett. **56**, 1252 (1986); T. Katsouleas *et al.*, Phys. Rev A **33**, 2056 (1986); J. Rosenzweig *et al.*, Phys. Rev. Lett. **61**, 98 (1998); and R. Ruth *et al.*, Particle Accelerators **17**, 171 (1985).

[9] P. Muggli *et al.*, IEEE Trans. Plasma Sci. **27**, 791 (1999).

[10] C.L. O'Connell *et al*, Phys. Rev. STAB **9**, 101301 (2006).

[11] I. Blumenfeld *et al.*, Nature **445**, 741-744 (2007).

[12] M. J. Hogan *et al.,* Phys. Rev. Lett. **95**, 054802 (2005).

[13] R. Hemker *et al.*, Phys. Rev. STA*B* **3**, 061301 (2000).

[14] C. Huang *et al.*, Proceedings, 18th Annual Review of Progress in Computational Electromagnetics, P 557 (2002).

[15] P. Muggli, *et al*., Nature **411**, 43-43 (03 May 2001).

[16] M. Borland, Advanced Photon Source LS-287 (2000).

[17] W. R. Nelson *et al.*, SLAC-R-265 (1985).

[18] M. Borland, *et al.*, proceedings of the PAC 03 conference, p. 3461 (2003).

[19] P. Muggli, *et al.*, proceedings of the PAC 07 conference, p. 3079 (2007).

[20] K.L. Bane *et al.*, IEEE Trans. Nucl. Sci. **32**, 3524 (1985).

[21] J.B. Rosenzweig Phys. Rev. Lett. **58**, 555 (1987).

[22] C. E. Clayton, *et al,* Phys. Rev. Lett. **88**, 154801 (2002).

[23] P. Muggli *et al*, Phys. Rev. Lett. **93**, 014802 (2004).

[24] J.B. Rosenzweig *et al.*, Phys. Rev. Lett. **95**, 195002 (2005).

[25] R. Gholizadeh *et al.*, proceedings of the PAC 07 conference, p. 3067 (2007), and AAC 07 Proceedings, AIP Conference Proceedings Volume 877, 504 (2006).

[26] C. E Clayton, *et al*., Phys. Rev. Lett. **88**, 154801 (2002).

[27] B. Blue *et al*, Physical Review Letters **90**, 214801 (2003).

[28] T. C. Chiou and T. Katsouleas, "High Beam Quality and Efficiency in Plasma Accelerators," Phys. Rev. Lett. **81** (16), 3411 (1998).

[29] S. Lee *et al.* , Phys. Rev. E **64**, 045501 (2001).

[30] M. J. Hogan, Private Communication (2007).

[31] C.M. Fauser, Masters Thesis, University of Texas at Austin (1997).

[32] X. Wang *et al.*, AAC07 Proceedings, AIP Vol. 877, 568 (2007) and Proceedings of the PAC'07 Conference, 3082 (2007).

[33] G. Harapetian, *et al.*, Phys. Rev. Lett. **72**, 2403 (1994).

[34] J. S. T. Ng *et al.*, Phys. Rev. Lett. **87**, 244801 (2001).

[35] M. J. Hogan *et al*., Phys. Rev. Lett. **90**, 205002 (2003).
[36] P. Chen *et al.*, Phys. Rev. Lett. **64**, 1231 (1990).
[37] E. Oz *et al.,* Phys. Rev. Lett. **98**, 084801 (2007).
[38] W. Gai *et al.,* Phys. Rev. Lett. **61**, 2756 (1988).
[39] M. E. Conde *et al*, Advanced Accelerator Concepts, AIP Conf. Proc. 472, 626 (1999).
[40] M. C. Thompson *et al*, "Gigavolt per Meter Breakdown Limits on Wakefields Driven by Electron Beams in Dielectric Structures", submitted to Physical Review Letters.
[41] A. Kanareykin *et al*, Proc. AAC-2006, 320 (2006).
[42] R.H. Fowler, L. Nordheim, Proc. Roy. Soc., v. 119, n. A781, 173 (1928).
[43] W. D. Kilpatrick, Rev. Sci. Instrum. **28**, 824 (1957).
[44] B.C. Stuart *et al*, J.Opt.Soc.Am. B **13**, 459 (1996).
[45] D. Du *et al*, Appl. Phys. Lett, **64**, 3071 (1994).
[46] M.E. Conde *et al*, Proceedings of 2005 Particle Accelerator Conference, 1485 (2005).
[47] V. Keldysh, Sov. Phys. JETP 20, 1307 (1965).
[48] D. L. Bruhwiler *et al*, Phys. Rev. ST Accel. Beams **4**, 101302 (2001).

3 Opportunities for Instrumentation and Detector Development

The International Linear Collider has taken center stage as the next major initiative in particle physics, and it has garnered broad and enthusiastic international support. There is consensus that the ILC, through clean and precise measurements, will uncover the physics behind the discoveries expected at the LHC and will complement the LHC's capabilities. The ILC is expected to elucidate Nature's mechanism for mass generation, discover and study the particles responsible for the universal dark matter, and search for the effects of new symmetries, quantum gravity, and extra dimensions. Further, by way of precision measurements, it will probe otherwise inaccessible energy scales by searching for virtual effects in Standard Model processes. This ambitious program challenges the current state of the art of both collider detector technologies [1] and accelerator instrumentation. Developing a new generation of detectors will require extensive beam testing, first of candidate detector technologies, then of full scale detector prototypes, and finally of production modules for commissioning and calibration. Developing the instrumentation needed for ILC's precision beam position measurements, beam energy measurements, bunch length monitoring, and precision collimation requires ongoing experiments with ILC-like beams, proof of principle demonstrations, and eventual production module tests.

Table 3-1. Summary of currently known ILC detector R&D group test beam needs [2]

Subdetector system	Number of groups	Particle species	P (GeV/c)	B (T)	N weeks/ year	ILC time structure	Note
Beam Instrumentation & Machine-Detector Interface	16	e	<100	-	64	-	Mostly low energy electrons
Vertex	10	e, π, p, μ	<100	3–6	40	Yes	
Tracker	3 TPC+2Si	e, π, p, μ	<100	3–6	20	Yes	
Calorimeter	5 ECALs 3 DHCALs 5 AHCALs	e, n, π, K, p, μ	1–120	Some needed	30–60	Yes	
Muon/ TCMT	3	e, π, μ	1–120	-	12	-	

There is an acute shortage of high energy particle test beams for detector development in the US today. Many of the beams which do exist, in the US and around the world, are not well-suited to current detector R&D—momenta are too low, or hadrons are not available, or timing properties are mismatched to future detector needs. The "Roadmap for ILC Detector R&D Test Beams" [2], the output from an ILC Detector Test Beam Workshop in January 2007, documents the availability of test beams worldwide and the needs of the ILC detector community. Only Fermilab, LBNL, and SLAC are currently providing test beams in the US, and the beams at LBNL are of such low energies (< 2 GeV) that they have limited utility for ILC detector development. Fermilab has recently upgraded its test beam facility in the M-Test beamline, and is considering developing an additional beamline.

Table 3-1 summarizes currently known ILC detector test beam needs that emerged from the January 2007 workshop. Since current demand addresses only early development and proof-of-

principle tests over the next few years, ultimately, ILC test beam needs will be substantially greater. However, even at this early stage, the workshop study establishes that four test beamlines operating year round are required. This number is commensurate with the test beam activity that has occurred at CERN in response to developing the LHC detectors. CERN has four test beamlines at the PS and four at the SPS; in 2007 there were requests from 47 groups representing about 1500 users, roughly half of which were LHC related. FACET can help satisfy the need for more US test beams.

The situation regarding beams suitable for ILC accelerator instrumentation studies is particularly problematic. To quote from the Roadmap Report: "SLAC's End Station A facility, with its unique capability for a high energy primary electron beam that matches many of the ILC beam parameters, is an important facility for Beam Instrumentation (BI) and Machine Detector Interface (MDI) R&D activities. Shutting down this facility after FY08 limits the BI & MDI group activities to KEK's ATF which has to be shared with other accelerator R&D efforts."

FACET beams in the ASF and ESA will provide a valuable and often unique resource for ILC accelerator and beam instrumentation R&D, and for ILC detector development and testing. Other programs requiring detector R&D and test beams will benefit as well. The ATLAS and CMS Collaborations are in the early stages of planning for major detector upgrades to be pursued on the timescale of the middle of the next decade. These upgrades projects will place significant demand on US test beam resources. Advanced detector development for future high energy physics experiments will profit from the continued availability of test beams at SLAC. The particle astrophysics community, which has used SLAC for novel tests of Cherenkov shower detection, Nitrogen Scintillation, and detector calibration, can be expected to put FACET beams to good use. Important radiation physics and material damage studies can be carried out as well.

3.1 ILC Accelerator and Beam Instrumentation R&D

A high energy test beam facility at SLAC will be a vital test bed for the ILC project. The Final Focus Test Beam (FFTB) at SLAC was such a facility; it demonstrated the demagnification required for the ILC and verified the beam optics codes and tuning procedures. The small spot sizes achieved there also enabled important material damage studies and spurred development of novel beam instrumentation such as the Shintake interferometric spot size monitor and optical transition radiation (OTR) profile monitors. The FFTB was decommissioned in 2006, but ILC tests are continuing in End Station A in 2006-08 using a 28.5 GeV beam, parasitic with PEP-II operation. Synchrotron radiation in the 24.5-degree A-line bend and the existing A-line optics limit the spot sizes achievable in ESA, but a wide variety of ILC tests not requiring micron-sized beams are possible. FACET beam to ESA provides a high energy beam in a large, accessible experimental hall; this enables critical ILC tests that are not possible elsewhere. With the new ASF experimental region at Sector 20 in the linac tunnel, small spot sizes will be achievable enabling material damage and other ILC experimental tests to be conducted there.

Current ILC tests in ESA are described below, many of which will need to continue through the ILC's engineering design and construction phases. Additional ILC tests are described that will be important and can be carried out at ASF or ESA. The FACET beam capabilities in the ASF and ESA experimental areas are summarized in Tables 1-1 and 1-2.

3.1.1 ILC Tests in ESA in 2006-2008

Current ILC beam tests are for a variety of accelerator physics, machine-detector interface (MDI), and beam instrumentation studies [3, 4]. Approximately 50 users from 18 institutions

participate in the ILC test beam program. ESA beam tests run parasitically with PEP-II, using a 28.5 GeV primary electron beam at 10 Hz repetition rate.

The SLAC linac delivers to ESA a high-energy test beam with bunch charge, bunch length and bunch energy spread comparable to those for the ILC. Five weeks of beam tests have been carried out in each of 2006 and 2007 and an additional 3-4 weeks are expected in 2008. Beam tests carried out during these runs include prototype energy spectrometers [5, 6], prototype RF beam position monitors (BPMs) for the ILC linac [7], studies of collimator wakefields [8], background studies for the ILC IP (Interaction Point) Feedback BPMs [9], bunch length diagnostics using Smith-Purcell radiation [10] bunch length studies using transverse RF cavities and high frequency diode and pyroelectric detectors [11], and studies of beam-induced electro-magnetic interference (EMI) [12]. The largest efforts are for the prototype energy spectrometer studies and for collimator wakefield studies.

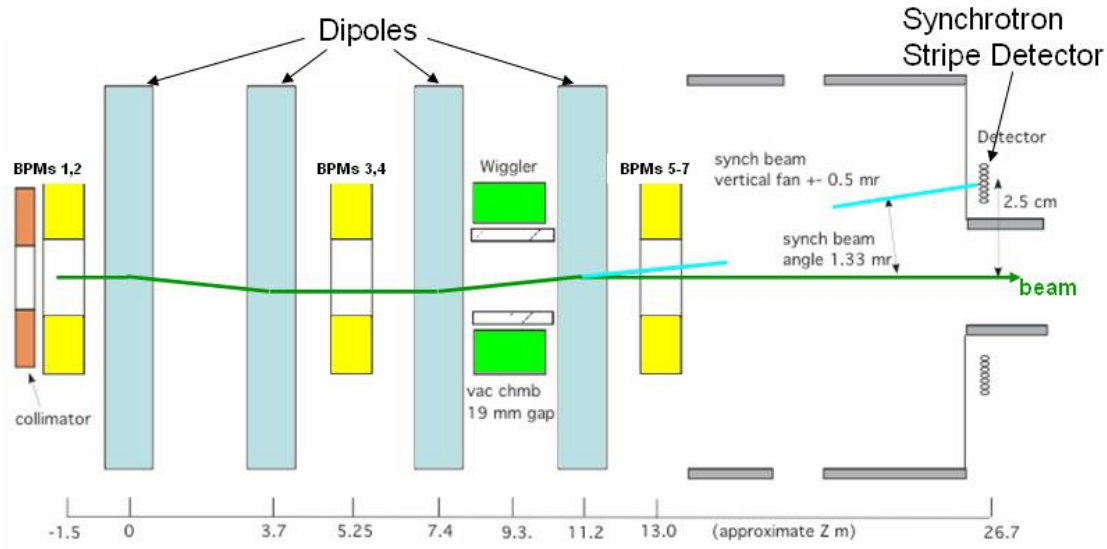

Figure 3-1. Plan view of 4-dipole chicane with vertical wiggler magnet for energy spectrometer studies. Two additional BPM doublets are 10 meters and 50 meters upstream of BPMs1, 2 respectively. Not shown is an interferometer system measuring horizontal offsets and stability of BPMs 1-4.

At the ILC, beam energy measurements with an accuracy of 100-200 parts per million (ppm) are needed for the determination of particle masses, including the top quark and Higgs boson. The energy of a linear collider, in contrast to that of a storage ring, is not known with any precision without a dedicated measurement. Prototype BPM (T-474) and Synchrotron Stripe (T-475) energy spectrometers have been constructed with a common 4-magnet chicane in ESA as shown in Figure 3-1. For T-474, three prototype RF BPMs for the ILC linac were built and commissioned; the other BPMs are existing SLAC RF BPMs, and one new RF BPM was built in the UK specifically for the ILC energy spectrometer. T-474 is studying mechanical and electrical stability for a total of eleven RF BPMs at five BPM stations distributed over ~60 meters at the end of the A-line and in ESA. T-475 measures hard x-ray synchrotron radiation from a Wiggler magnet in the third leg of the chicane with a quartz fiber array read out by a multi-anode photomultiplier tube. T-474 and T-475 are comparing energy measurements and sensitivity to environmental factors (magnetic fields, temperature, mechanical motion monitored by an

interferometer system) and changes in the beam parameters: bunch length, bunch charge, beam energy, beam trajectory. Other applications of the data gathered in T-474 include micron-level monitoring of the stability of BPM and quadrupole offsets over time scales of a day or more and over extended lever arms of tens of meters. This stability data is very relevant for ILC linac quadrupoles and BPMs, as well as other future projects requiring high quality beams.

Precise collimation of the beam halo is required in the ILC to prevent beam losses near the Interaction Region that could cause unacceptable backgrounds for the detector. The tight apertures of the collimators, however, cause wakefields that can result in beam deflections and increased emittance. The goal of T-480 is to verify analytic calculations and simulation codes for calculating wakefields and to determine the optimal material and geometry for the ILC collimators. This work directly impacts achieving ILC design luminosity goals. A "Wakefield Box" containing a sandwich holding four collimator insertions is installed in ESA about 8 meters upstream of the first BPM doublet shown in Figure 3-1. The T-474 BPMs are used to measure the wakefield kick angles. A total of 15 sets of collimators with differing geometry and material have been studied in 2006 and 2007. The beam is set up with a small ~100-micron vertical waist at the Wakefield Box for these studies. The vertical half-gap in the collimators is 1.4 mm and beam deflection angles (due to wakefield kicks) are measured as the collimator is moved vertically over ±1.2 mm.

3.1.2 ILC Tests in 2010-15

Many ILC tests underway in ESA will evolve to test system components that will eventually be committed to the ILC. This will include RF BPMs, bunch length diagnostics, collimators, and BPM and synchrotron stripe energy spectrometers. ESA provides easy access, adequate space and excellent infrastructure for these tests. The ASF experimental area will also be a good location for small-scale tests such as for BPMs and bunch length diagnostics, which do not require a lot of space. In addition, the ASF will be an important test area for experiments requiring small spot sizes, such as for material damage tests important for ILC collimators, spoilers and beam dumps.

Additional ILC beam instrumentation can be developed and system tests performed, for example using synchrotron radiation and optical transition and diffraction radiation. Beam halo monitors will be needed for ILC and can be developed with input from tests in ESA. The infrastructure developed in ESA with many RF BPM stations spanning 60 meters along the beam provides an excellent tool for measuring and demonstrating the required micron-level tolerances for BPM and quadrupole mechanical stability needed for the ILC linac. A beam-based measurement of the stability of the (cold) quadrupole's magnetic center will also be possible.

Beam tests of large scale mockups of Interaction Region (IR) system components may be required and ESA provides an ideal location for this. In particular, this may be important for developing and testing EMI standards for IR accelerator and detector components, to demonstrate that IR systems are both robust against EMI and that the EMI they generate is tolerable. IR magnets have exacting vibration and stability requirements; beam jitter and stability measurements in ESA could validate that the IR magnets meet these requirements.

3.2 ILC Detector Development

The ILC Global Design Effort is in the process of developing an engineering design for the ILC accelerator by 2010. The ILC physics and detector community has come to the realization that engineering designs for full ILC detectors are needed on the same time scale, and this has provided a significant impetus and urgency to ILC detector design, and to the detector R&D on which it is based. A call for the nascent detector concepts to submit Letters of Intent by Fall 2008 has recently been issued by the International Linear Collider Steering Committee and its new Research Director. Evaluation of the LOI's is expected to lead to two complementary and contrasting detector designs, possibly amalgamations of the current concepts, and the proponents will be charged to develop Engineering Design Reports ready for submission on the GDE's time table. Test beams are needed to support detector development for the engineering designs, as well as eventually to test prototype sub-detectors and to commission and calibrate detector modules.

ILC detectors depend on real advances in sub-detector technologies, both because detector performance must be advanced to meet ILC physics requirements, and because the comparatively benign ILC environment allows a much broader range of technical solutions than was possible at the LHC. Of course, the ILC environment poses some challenges of its own, and these must also be addressed.

New vertex detector technologies are needed at the ILC; present detectors are read out too slowly, consume too much power, and are too thick to reach the performance goals set by ILC physics. Many technologies are under development, including CCDs with fast readout, Depfets, CMOS detectors, and 3-D devices. All these developments need beam testing, preferably with moderate to high momentum hadron beams, so resolution effects are not obscured by multiple coulomb scattering, and so the shower debris accompanying electron beams doesn't obscure the analysis process.

Table 3-2. Summary of desired test beam features for ILC detector development and ESA capabilities.

Parameters	Test Beam Requirements	ESA
Energy	(0.1–100) GeV	(0.1–12) GeV e, (0.1–8) GeV π; up to 24 GeV e and 16 GeV π possible with energy upgrade
Charge per bunch	$0.2–10^5$	$0.5–10^{10}$ e, (0.1–10) π, ~0.1 K and p
Particle type	e, π, K, p	e, π, K, p
Bunch repetition rate (Hz)	10 Hz or higher	30 Hz
Precise beam trigger	Needed for time-of-flight measurements and TOF R&D	Yes
Spill length/pulse	Single RF bucket ideal; pseudo-ILC train useful for ILC electronics power pulsing	Single RF bucket; 2 bunches separated by 300 ns
Multiple particles/rf bucket possible?	Useful for some linearity tests; useful for vertex detector track confusion studies	Yes, with electrons or mix of electrons and pions
rms x, y spot size	<1cm; <1mm useful	5 mm ok; reduced rate at 1 mm
Momentum analysis ?	Yes; for some tests to 0.1%	Yes; 0.1% for electrons
x,y,z space available	1–4 m, 1–4 m, 1–3 m	5 m, 5 m, 15 m
Instrumentation	Trigger counters; Halo veto counters; High resolution beam hodoscope; Particle ID (Cherenkov, TOF, shower counter); Small, high field solenoid; sturdy support table with remote movers	Good availability for these capabilities, including plenty of space and time available for installation and commissioning
Crane	(0-10) tons	15- and 50-ton cranes available

ILC calorimeter designs will significantly extend beyond the current state of the art. A whole new paradigm, called Particle Flow Calorimetry, which employs fully imaging calorimeters, promises the performance needed to distinguish W and Z (and top and Higgs) decays cleanly, event by event, as needed to reach the full potential of ILC physics. The new designs rely on technologies which can provide the high degree of transverse and longitudinal segmentation needed, but which are unproven as calorimeters. In fact, the very idea behind Particle Flow Calorimetry needs demonstration, and current beam tests are underway at CERN, and planned for Fermilab, to begin addressing this need. The new technologies, including glass RPCs, micromegas and GEMs, and scintillating tiles read out individually with silicon photomultipliers, need extensive beam tests; new jet energy algorithms need full scale calorimeter demonstrations; and eventually detector prototypes and ultimately production modules will need thorough evaluation, calibration, and testing. Fundamental studies of hadron

shower development are also needed. These beam tests will require both electrons and charged pions, over the full momentum range, but especially at the low momenta (1 – 20 GeV/c) which dominate most jets. Tests with kaons and neutral hadrons are also desirable.

The "BeamCAL" detector will measure energy deposited into the very forward region (5-30 mrad polar angle) just outside the beams at the ILC, to monitor bunch-by-bunch beam conditions, and serve as a veto to backgrounds in new physics searches. Beamstrahlung and beamstrahlung-produced pairs flood the BeamCAL, depositing nearly 100 TeV per bunch crossing, and requiring high segmentation and readout between bunches separated by 300 ns. Finding a detector which is sufficiently radiation hard, segmented, and fast is proving to be a challenge. Testing BeamCAL in a realistic environment will require depositing an energetic pulse of electromagnetic radiation to simulate the beamstrahlung pairs, which is well-matched to the capabilities of the ESA test beam. In the presence of this large background of low energy pairs, BeamCAL is required to have 99.9% efficiency for identifying high energy electrons to allow rejection of 2-photon backgrounds in SUSY searches. Demonstrating this efficiency and studying fluctuations in electromagnetic showers will require careful test beam studies, for which the ESA facility using beams from FACET is ideal.

ILC detectors will be readout by electronics tailored to the ILC environment. At the ILC, the beams will collide at well-defined crossing times, spaced roughly 300 ns apart, for whole pulse trains of about 3000 crossings. This roughly 1 ms worth of collisions is followed by a 199 ms period when the beams are off. ILC detector electronics will take advantage of this time structure, to gate on at known times, and to cycle off during the periods between bunches to reduce power consumption and ambient heating. The ESA beam is well-suited to providing beam particles at known time and allowing ILC-like "power pulsing." This makes ESA ideal as a test laboratory for realistic ILC detector/readout designs.

The test beam requirements for ILC detector development and the capabilities of the End Station A facility are given in Table 3-2. In general, there is a very good match, especially when FACET is upgraded to provide incident electron energy of 24 GeV.

3.3 Advanced Detector Development

Future colliders, like the SLHC and the Super *B* Factory, need advances in detector development to improve upon current performance and to deal with the high rates and high radiation fields of the proposed colliders. SLAC test beams have played a critical role in developing the detectors presently in use in *BABAR*. Further developments, aimed at improving particle identification for future flavor-physics studies, are already underway in ESA tests and are described briefly below. FACET provides a facility for bringing these studies to completion, and one that can address future detector developments needed for future high energy physics experiments. FACET test beams could also be of great use in prototyping and testing detectors for the LHC detector upgrades, as well as components for the LHC accelerator complex, both of which involve SLAC and LHC user community.

Advanced detector R&D for a novel particle identification detector (PID) called Focusing DIRC is currently being tested in ESA with 10 GeV secondary electrons [13,14]. This work benefits from the recent introduction of new fast vacuum-based photon detectors with rms transit time distributions of ~30-150 ps, which provide the capability to tag photon color by timing and to correct the chromatic error. The prototype's concept is based on the *BABAR* DIRC with several important improvements: (a) ten times faster photon detectors, (b) highly pixilated photon detectors based on Burle MCP-PMT and Hamamatsu MaPMT, (c) mirror allowing to make the

photon detector smaller and less sensitive to background in future applications, (d) electronics providing single photon rms timing resolution better than ~100-200 ps. This is the first time the chromatic error was corrected by this method. Together with a high level of pixilization, this results in substantial (~30%) improvement in particle identification capability. This program is also testing a new detector concept for a time-of-flight (TOF) application that could reach sub-ten picosecond resolution, which could be used for Forward PID at a future flavor-physics factory, or for forward TOF at ALICE.

3.4 Radiation Physics and Material Damage Tests

These experiments are needed by radiation physicists for measuring radiation yields and activation of materials. Such experiments are also needed for materials damage tests. Two recent beam dump experiments took place in ESA in 2007. T-489 measured the residual activation and dose rates of materials due to irradiation in the vicinity of a beam dump to compare with simulation codes such as MARS and FLUKA. T-493 studied demagnetization. Spare permanent magnet pieces from the LCLS undulators were strategically arranged around a copper beam dump to receive an amount of radiation similar to what the magnets would be exposed to in the undulators if the beam went astray. The amount of demagnetization will be determined so that adequate measures (development of appropriate beam loss monitors) can be taken to protect these magnets during 20 years of operation.

3.5 Particle Astrophysics Detectors and Techniques

FACET will be an important facility to support future detector R&D for the particle astrophysics community. The combination of FACET beam capabilities and the excellent infrastructure and space availability at ESA provide a unique environment. Experiments to test and calibrate cosmic ray observational techniques have been carried out previously at the FFTB and ESA facilities, and future experiments are expected. Recent examples include:

- **T-429 and T-436:** GLAST LAT calibration. The GLAST experiment used secondary beams of positrons, hadrons and tagged photons in ESA to perform calibration and systems integration studies for an LAT Tower containing an anti-coincidence detector, a silicon tracker and a calorimeter [15].
- **T-461 and E-165:** The FLASH experiment in the FFTB helped calibrate detectors studying the energy spectra of ultra-high energy cosmic rays (10^{19} – 10^{20} eV) by making precision measurements of air fluorescence yields in electromagnetic showers under various conditions [16].
- **T-460:** This FFTB experiment demonstrated the principle of a novel detection technique for ultra-high-energy cosmic neutrinos based on a radio Cherenkov signal produced by the Askaryan effect [17].
- **T-486:** This ESA experiment calibrated the entire ANITA balloon flight antenna array and made the first observation of the Askaryan effect in ice [18]. A primary beam of 10^9 electrons/bunch was incident on a 7-ton, 5-meter long refrigerated ice block to simulate high energy neutrino showers in Antarctic ice. The ANITA antenna array was suspended from the ESA crane at the end of ESA to observe coherent microwave radiation at ~(0.2-1) GHz at the Cherenkov angle of ~40 degrees. Figure 3-2 shows the experimental setup and illustrates the unique capabilities in ESA that enabled this test.

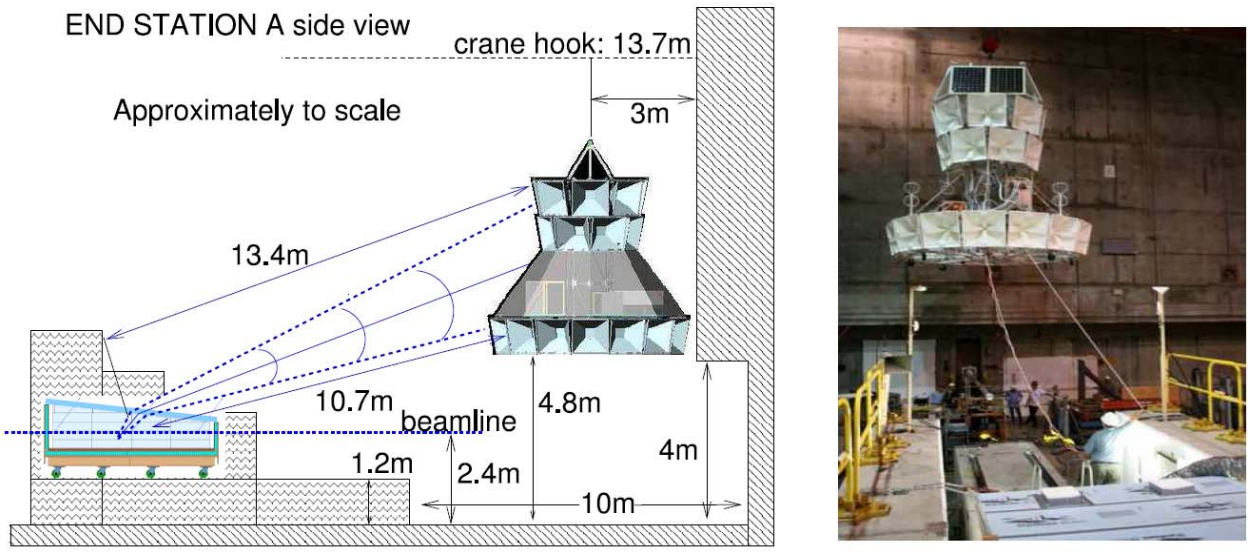

Figure 3-2. The ANITA payload and ice target in ESA (picture taken from Ref. [19]).

3.6 References

[1] ILC Reference Design Report, Volume 4 (Detectors) 2007.

[2] "Roadmap for ILC Detector R&D Test Beams", by the World Wide ILC Detector R&D Community, 2007; available at http://www-hep.uta.edu/~yu/linear-collider/ilc-tb-roadmap-v6.1.pdf.

[3] ILC-SLAC ESA website, http://www-project.slac.stanford.edu/ilc/testfac/ESA/esa.html.

[4] "Test Beam Studies at SLAC End Station A, for the International Linear Collider", M. Woods *et al.*, SLAC-PUB-11988, EUROTEV-REPORT-2006-060, 2006.

[5] T-474/T-491 Prototype BPM Energy Spectrometer for ILC. Related publications: "A prototype energy spectrometer for the ILC at End Station A in SLAC", A. Lyapin *et al.*, SLAC-PUB-12787, EUROTEV-REPORT-2007-039, 2007 and "Magnetic Measurements and Simulations of a 4-Magnet Dipole Chicane for the International Linear Collider", S. Kostromin *et al.*, paper THPMS038 contributed to PAC 07, 2007.

[6] T-475 Prototype Synchrotron Stripe Energy Spectrometer for ILC.

[7] "ILC Linac R&D at SLAC", C. Adolphsen, SLAC-PUB-12046.

[8] T-480 Collimator Wakefield Studies and related publications: "Measurements of the Transverse Wakefields Due to Varying Collimator Characteristics", S. Molloy *et al.*, SLAC-PUB-12597, EUROTEV-REPORT-2007-044, 2007 and "GdfidL Simulations of Non-Linear Tapers for ILC Collimators", J.D.A. Smith, paper TUPMS092 contributed to PAC 07, 2007; "Computations of Wakefields in the ILC Collimators", J. D.A. Smith and C.J. Glasman, paper TUPMS093 contributed to PAC 07, 2007; "Direct Measurement of Geometric and Resistive Wakefields in Tapered Collimators for the International Linear Collider", N.K. Watson *et al.*, SLAC-PUB-12029, EUROTEV-REPORT-2006-059, 2006, http://www.slac.stanford.edu/pubs/slacpubs/12000/slac-pub-12029.html; and "Direct Measurement of the Transverse Wakefields of Tapered Collimators", P. Tenenbaum *et al.,* SLAC-PUB-12086, Phys.Rev.ST Accel.Beams 10:034401,2007.

[9] T-488 Background Studies for ILC IP BPMs. Related publications: "Electromagnetic background tests for the ILC interaction-point feedback system", P.N. Burrows, *et al.*, SLAC-PUB-12758, EUROTEV-REPORT-2007-031, 2007; "Simulation of ILC feedback BPM signals in an intense background environment", A. Hartin *et al.*, SLAC-PUB-12760, EUROTEV-REPORT-2007-041, 2007; and "The Electromagnetic Background Environment for the Interaction-Point Beam Feedback System at the International Linear Collider", G. Christian *et al.*, paper THPCH089 presented at EPAC06.

[10] T-487 ILC Longitudinal Profile Diagnostics using Smith-Purcell Radiation.

[11] "Picosecond Bunch length and Energy-z correlation measurements at SLAC's A-Line and End Station A", S. Molloy *et al.*, SLAC-PUB-12598, contributed to PAC 07, 2007.

[12] "Disruption of Particle Detector Electronics by Beam Generated EMI", G. Bower *et al.*, SLAC-PUB-12613, contributed to PAC 07, 2007.

[13] "Development of a Focusing DIRC", J. Benitez et al., SLAC-PUB-12236, 2006.

[14] "The Focusing DIRC–the first RICH detector to correct the chromatic error by timing, and the development of a new TOF detector concept", J. Va'vra *et al.*, SLAC-PUB-12803, 2007.

[15] "Results from the Beam Test of the Engineering Model of the GLAST Large Area Telescope", E. do Couto e Silva *et al.,* SLAC-PUB-8682, Nucl.Instrum.Meth A **474**:19-37, 2001.

[16] Publications from the FLASH experiment: "Measurement of pressure dependent fluorescence yield of air: Calibration factor for UHECR detectors", FLASH Collaboration (J.W. Belz *et al.*), SLAC-PUB-11254, published in Astropart.Phys. **25**:129-139, 2006; "Comparison of air fluorescence and ionization measurements of E.M. shower depth profiles: test of a UHECR detector technique", J. Belz *et al.*, SLAC-PUB-11513, submitted to Astropart.Phys; and "Air fluorescence measurements in the spectral range 300-420 nm using a 28.5-GeV electron beam", R. Abbasi *et al.*, SLAC-PUB-12764, submitted to Astropart.Phys.

[17] T-460 publications: "Accelerator measurements of the Askaryan effect in rock salt: A Roadmap toward teraton underground neutrino detectors", P.W. Gorham *et al.*, SLAC-PUB-10912, Phys.Rev. **D72**:023002, 2005 and "Observation of the Askaryan effect: Coherent microwave Cherenkov emission from charge asymmetry in high-energy particle cascades", D, Saltzberg *et al.*, SLAC-PUB-8768, published in Phys.Rev.Lett. **86**:2802-2805, 2001.

[18] "Observations of the Askaryan effect in ice", by ANITA Collaboration (P.W. Gorham *et al.*), SLAC-PUB-12286, 2006; submitted to Phys.Rev.Lett.

4 THz Radiation and Science Opportunities in Basic Energy Science

In addition to the unique capability of FACET beams for accelerator R&D, and HEP instrumentation and detector development, the facility will also enable a much broader science opportunity through the high intensity electric and magnetic fields associated with the high quality beams. In this section, we present the case for the importance of FACET for problems in basic energy science, in particular, materials science, condensed matter physics and chemistry.

One would naively suspect that because of their high energy density, relativistic electron beams with an energy of about 30 GeV, a charge about 1 nC and a beam diameter of microns, would simply blow up any material put in its path. Surprisingly, this is not the case! In fact, quite the opposite is observed for the shortest electron bunches (about 100 fs), which are accompanied by extreme electric and magnetic fields. Such beams traverse a thin film sample without damage. When the sample is a magnetic film, the beam simply leaves behind a characteristic magnetic pattern, proving that it indeed traversed the sample. The electric and magnetic fields surrounding a relativistic electron bunch in fact have a close resemblance with half-cycle terahertz (THz) electromagnetic waves, but orders of magnitude stronger than those created by laboratory tabletop sources.

In recent years there have been significant scientific advances in solid state physics and chemistry induced by terahertz radiation. Applications as diverse as semiconductor and high temperature superconductor characterization, tomographic imaging, label free genetic analysis, cellular level imaging and chemical and biological sensing have thrust terahertz research from relative obscurity into the limelight. Highly relativistic electron bunches are the most intense sources of terahertz radiation known today. As a result, FACET offers unique possibilities to undertake cutting edge research with terahertz radiation.

Conventional laboratory sources are typically limited to peak electric fields of the order of 1 MV/m. In contrast, the fields surrounding relativistic electron beams exceed 1 GV/m. Such field strengths rival those experienced by valence electrons in materials (~1 V over the size of an atom) and their application can therefore create new states of matter previously not observable. Because the pulse length around 1 ps is considerably longer than the Bohr precession time of a valence electron (about 1 fs) in the atomic field, THz fields act like DC fields on the electron cloud and may thus distort the atomic electron cloud and even cause atomic motions which may be used to initiate chemical reactions.

We see exciting opportunities for new advances with the capabilities of the FACET beams. Examples of these applications are discussed in the sections below, after we review the nature of the fields associated with relativistic electron beams.

4.1 Relativistic Electron Beams as a Source for THz Radiation

The fields surrounding a relativistic electron bunch are shown schematically in Figure 4-1. Each electron carries electric and magnetic fields that, due to relativity, are confined to a plane perpendicular to the electron motion. The total fields surrounding an electron bunch are the sums of the individual contributions, which can be divided into two regimes corresponding to coherent and incoherent superposition.

In the coherent superposition regime the total field is the sum of individual contributions from single charges, so that E and B are proportional to Nq, where N is the number of electrons and $q = -e$ the electron charge. The associated fields are very large, as shown at the bottom of Figure 4-1.

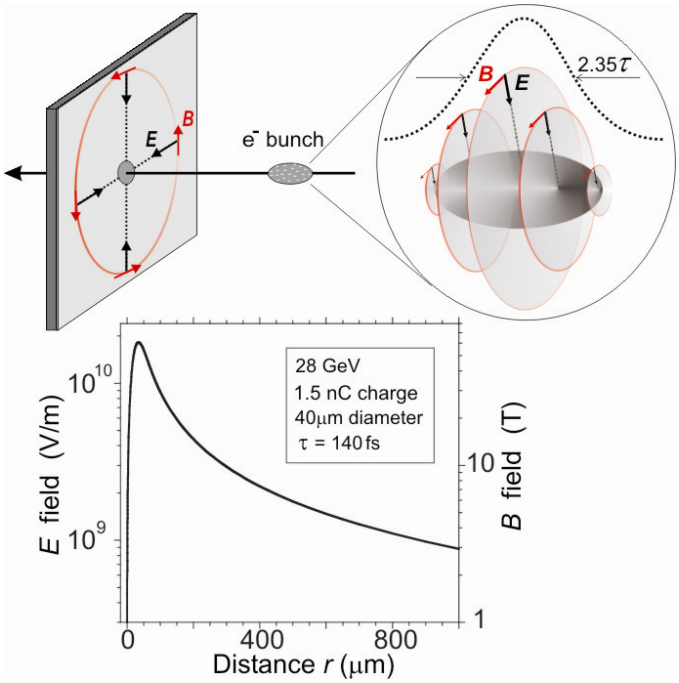

Figure 4-1. Experimental geometry and illustration of the spatial and temporal nature of the fields and their amplitudes surrounding a relativistic electron bunch incident on a stationary sample.

The frequency spectrum of the macro-bunch pulse of width (one standard deviation) τ is simply the Fourier transform of the pulse and the spectrum extends in frequency to a cut-off value $1/\tau$. Thus, qualitatively we expect a picosecond ($\tau = 10^{-12}$ s) field pulse to lead to a frequency spectrum extending to 1 THz (energy of 4.14 meV and wavelength of 300 μm). When the frequency spectrum of the electron beam pulse is compared to that of a half-cycle photon pulse of the same temporal width, so-called THz radiation, the two are virtually identical as shown in Figure 4-2. The difference at zero frequency comes from the fact that a true THz photon field is a propagating wave (true electromagnetic radiation) and therefore has a positive as well as negative cycle with no zero frequency component, while the e-beam field pulse is a Coulomb or velocity field attached to the electron bunch, and has a zero frequency component. In practice, there is little difference between a THz photon and e-beam field pulse. Also, the THz field pulse of an electron bunch may be separated from the electron bunch as an electromagnetic wave by either bending the electron beam in a magnetic field or sending it through a foil, where the absorbed fields will be re-radiated as true photons.

A relativistic electron beam also contains an incoherent field component. This is confined within the bunch, where the fields of the individual electrons may be out of phase. The calculation of the coherent and incoherent fields may be accomplished by the Weizsäcker-Williams methods, which describes an electron beam in terms of virtual photons. The idea is that the velocity fields accompanying the relativistic charge may be thought of as a cloud of virtual

photons carried by the charge. This cloud may be liberated and exchanged through interactions of the charge with its environment. For example, synchrotron radiation consists of the virtual photons liberated by the interaction of the electron bunch with a magnetic field. The virtual photon spectrum of a typical SLAC electron bunch, calculated by the Weizsäcker-Williams method, is shown in Figure 4-3. The incoherent virtual photons appear as x-rays, but with a much reduced field (E proportional to $\sqrt{N}$) and intensity (proportional to $E^2 \sim N$) compared to the THz component with intensity $\sim E^2 \sim N^2$.

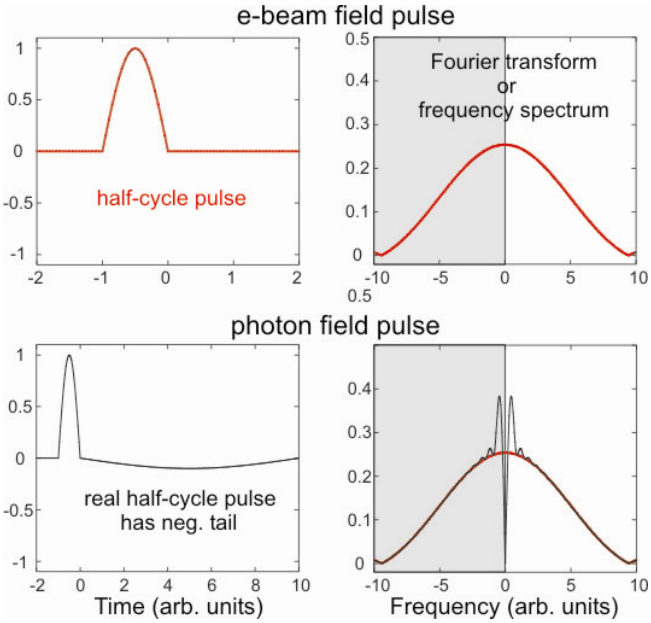

Figure 4-2. Comparison of two types of THz pulses of 1 ps width. A true half-cycle pulse (typically of Gaussian shape) produced by a passing electron beam (top) versus that produced from a nearly half-cycle electromagnetic wave (bottom). The frequency spectra differ only near zero. Note that only positive frequencies exist.

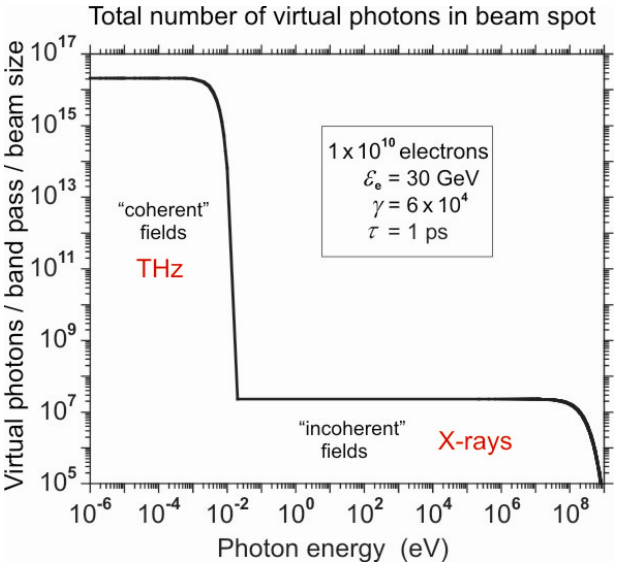

Figure 4-3. The total virtual photon spectrum within a Gaussian beam radius of a 30 GeV electron beam with τ = 1 ps and bunch charge of $N = 10^{10}$ electrons.

4.2 Terahertz Radiation and Magnetism

Very recently, it has been recognized that terahertz radiation is an ideal tool for the study of spin dynamics, which is essential for the basic understanding of magnetism as well as for its technological applications [1, 2, 3]. Ultrafast changes of the magnetization induced, *e.g.*, by a laser pulse, will lead to the emission of terahertz radiation that probes the time dependence of the spontaneous magnetization [3, 4]. However, the last experiments conducted at the FFTB have also demonstrated that the terahertz radiation accompanying compressed highly relativistic electron bunches can also be used to create very large electric and magnetic fields in metals [5]. This technique holds considerable interest and future promise.

The principle of the FFTB experiment is shown in Figure 4-4. A powerful electric and magnetic field pulse is created in a thin film of magnetic metal by a relativistic electron beam traversing the sample. As discussed above, such electromagnetic field pulses of 100 fs – 2 ps duration are very similar to half-cycle pulses of terahertz photons [1]. The electric field of the bunch generates a magnetic anisotropy, and the resulting anisotropy field leads to a spin precession (in addition to the one introduced by the magnetic field alone), which can be detected in the magnetic switching pattern.

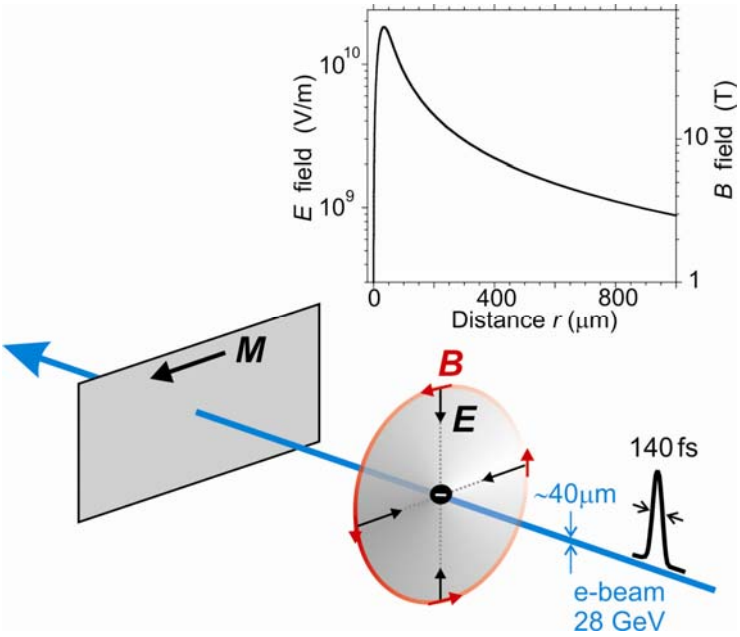

Figure 4-4. Injecting an electric field into a metal: An 28 GeV electron bunch traverses a thin metallic ferromagnetic film perpendicular to the surface. The magnetization *M* is initially uniformly as shown. The electron bunch of Gaussian half width duration of τ = 70 fs in the laboratory frame. The electric field *E* and the magnetic field *B* are perpendicular to each other and are confined to a flat disk perpendicular to the beam as shown. The inset shows the *E*- and *B*-field strengths versus distance from the beam center using the longitudinal, τ = 70 fs, and transverse, σ_r = 20 μm, Gaussian standard deviations corresponding to the conditions of the experiment.

The pattern is recorded in the film and we read it out long after the bunch has passed with a magnetic imaging technique. This stunningly simple experiment yields the first clear evidence of a new type of magnetic anisotropy, generated by an ***E***-field induced distortion of the valence states. Applications of magnetic materials are based on the control of magnetic anisotropies, in particular the creation of suitable atomic arrangements to manipulate the magnetic anisotropy energy. Generally, the electromagnetic fields lead to multiple ultrafast switching of the magnetization and moreover modify the electronic structure. It is safe to predict that in future applications pulses from terahertz lasers can replace the relativistic electron bunches and thus terahertz radiation will be one of the primary tools for the study and application of ultrafast magnetization switching and spin dynamics.

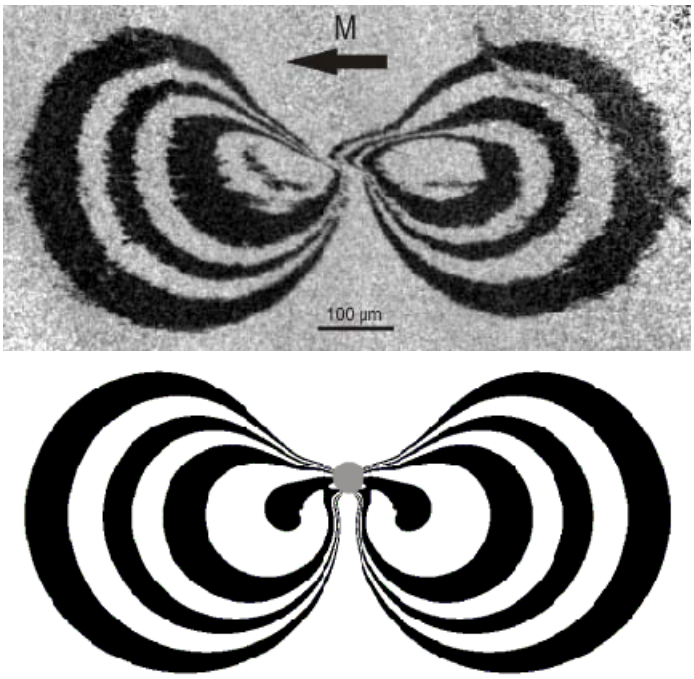

Figure 4-5. Experimental (top) and calculated (bottom) magnetic patterns for a single compressed electron bunch of τ = 70 fs that traverses a thin film sample along the surface normal. The experimental pattern was recorded by spin sensitive scanning electron microscopy (SEMPA). In the light grey regions, *M* points into the preset direction as shown, while in the dark regions *M* has switched into the opposite direction. The lower pattern is calculated with the Landau-Lifshitz-Gilbert (LLG) equation including the torque generated by the induced anisotropy field due to the *E*-field of the bunch. This pattern reveals the characteristic flattening of the upper switching boundaries, created by the presence of the *E*-field inside the metallic sample. Without a penetrating electric field, this feature would be absent. The location of beam impact and width of the bunch is indicated in grey**.**

4.2.1 Giant Magnetic Anisotropy in a Ferromagnet During an Electric Field Pulse

An electric field rivaling the field acting on the valence electrons can be generated in a 3d metal by the passage of a compressed highly relativistic electron bunch. The ***E***-field penetrates into the metal because relativistic contraction has forced the field into a flat disk parallel to the surface, as shown in Figure 4-4. Using spin precession as a diagnostic tool, we observe the generation of a large new type of magneto-electronic anisotropy in a ferromagnetic thin film subjected to such ultra-fast (70 fs) and ultra-strong ($\geq 10^9$ V/m) electric field pulses, as shown in Figure 4-5. The ***E***-field induced anisotropy can lead to switching of the magnetization in a thin film. This yet unpublished example illustrates the truly unique possibilities opened up in the study of solid materials with the advent of strong terahertz radiation from relativistic electron bunches.

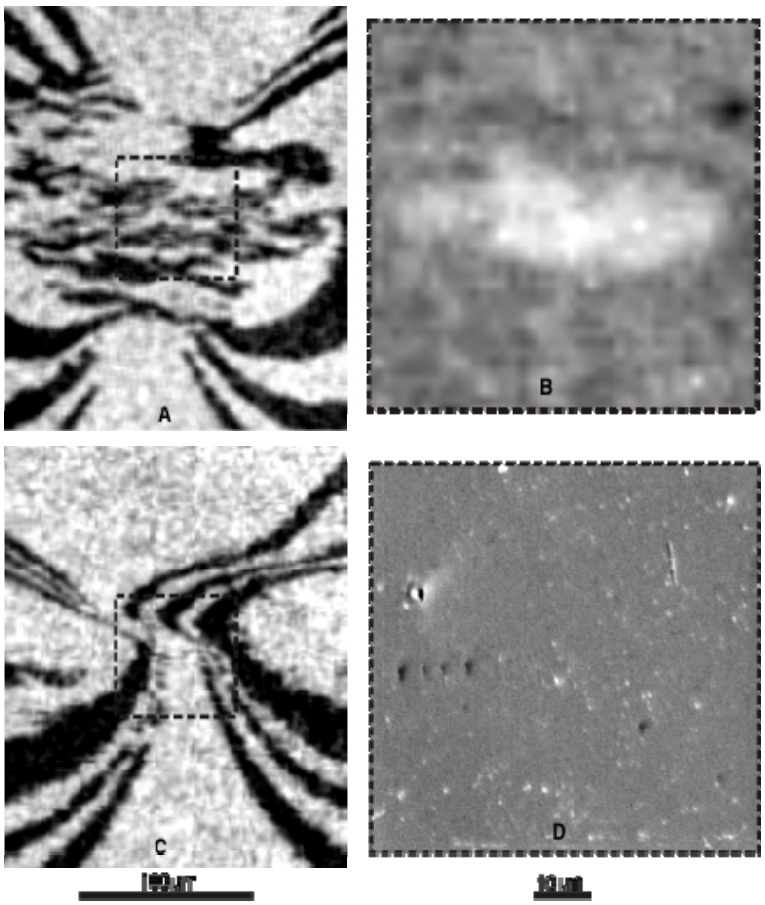

Figure 4-6. Magnetic (A, C) and magnified topographic (B, D) images of the sample close to the beam impact point for longer τ_1 (A, B) and shorter τ_2 (C, D) electron bunches. The images are taken with a scanning electron microscope with spin polarization analysis (SEMPA), which can be operated for magnetic or topographic contrast. With the τ_1 electron bunch, irregular magnetic domains indicate that the sample has been heated to $T \geq T_C$ (where T_C is the Curie temperature) in a region within 200 μm at the point of beam impact, and the topographic image reveals ablation of the sample within the beam impact area. With the τ_2 bunch (C, D), no random domains indicative of heating are observed, and there is no topographic modification of the sample. The topographic images (B, D) cover the marked region of the magnetic images.

4.2.2 Ultrafast Transformation of the Electronic Structure of a Metal by Electric Fields

Ultrafast manipulation of the electronic and magnetic structure of a metal by electric field pulses has also been observed. An analysis of the magnetic and topographic images of exposed samples reveal the absence of heating in a ferromagnetic thin film subjected to the ultrafast and ultra-strong electric fields. For this experiment two different temporal pulse lengths were used: τ_1 = 2.3 ps and τ_2 = 70 fs. The pattern produced by the longer pulse clearly heats and damages the sample as shown in parts A and B of Figure 4-6, while the pattern produced by the shorter pulse leaves the sample remarkably damage free as shown in parts C and D of Figure 4-6. The heating in the case of the longer τ_1 bunch is due to electron-phonon collisions, while the absence of

heating with the τ_2 bunch must be due to the lack of energy transfer from the electron gas to the lattice due to the short duration of the electric field pulse compared to the electron-lattice equilibration time.

4.3 Investigation of Ferroelectric Switching Dynamics with FACET

The development of faster, higher density, non-volatile storage mechanisms using ferroelectric materials depends on how small one can make a functional ferroelectric domain, and how fast it can be switched in an applied electric field, with corresponding ultrafast atomic-scale displacements within the unit cell. Intense femtosecond time-scale THz fields, as will be produced at FACET, will enable control and characterization of the intrinsic dynamics associated with ferroelectric devices, and provide a new way of visualizing the processes that fundamentally determine the properties of real devices.

Ferroelectrics are materials with a dipole moment within each unit cell that is correlated across the entire crystal, giving rise to a net polarization that can be reoriented by an applied field. These are important as storage devices, as infrared sensors, and as micro-electromechanical systems. The most technologically relevant ferroelectric materials, characterized by a switchable macroscopic polarization, involve the perovskite oxide structures, for example $BaTiO_3$ or $PbTiO_3$. Figure 4-7 shows the low and high temperature phases of the perovskite oxides which, on cooling below the Curie temperature (e.g. 493 ^oC for $PbTiO_3$), undergo a tetragonal distortion leading to the development of a spontaneous polarization. The phase transition is driven by a phonon softening of optical phonon modes (which may be directly driven under THz excitation), and has been studied using a variety of Raman, x-ray and inelastic neutron scattering techniques [6,7,8].

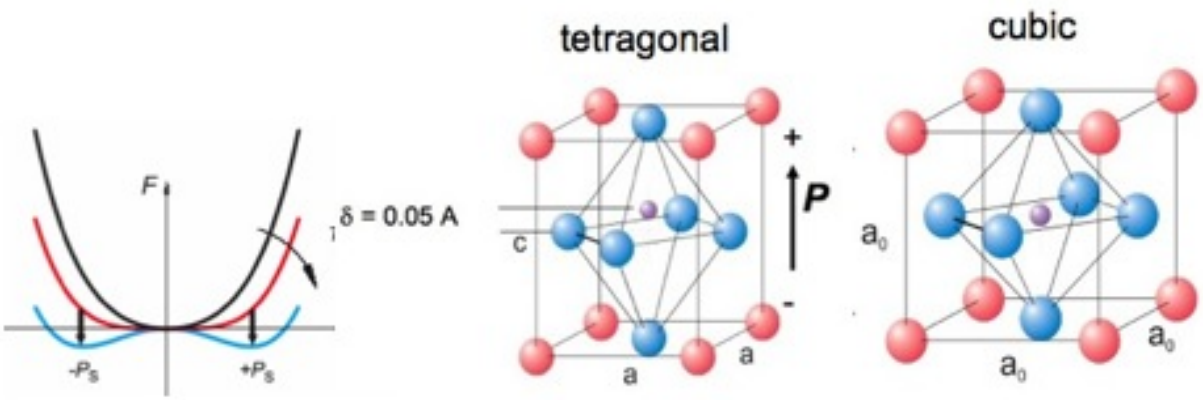

Figure 4-7. (left) Model free energy changes as the temperature is reduced towards the Curie temperature. (right) Unit cell structural changes associated with the development of the ferroelectric state.

The shortest time scale ferroelectric domain dynamics were observed in experiments that utilized photoconductive Auston switches (very common in the magneto-dynamic experiments as well) to create short electric pulses applied to the ferroelectric capacitors $Pt/La_{0.5}Sr_{0.5}CoO_3$ $/Pb(Nb_{0.04}Zr_{0.28}Ti_{0.68})O_3$ $/La_{0.5}Sr_{0.5}CoO_3$ /Pt with a thickness of 200 nm [9]. The shortest field rise time achieved in these experiments is ~70 ps with the field amplitude of 25 MV/m. The displacement current through the ferroelectric capacitor was measured with time resolution of 20 ps, from which polarization dynamics were inferred. The minimum switching time of this ferroelectric device was found to be ~220 ps, and it is considered the state-of-the-art switching

speed at the moment. The data was fitted to a Merz-Ishibashi expression for the switched polarization fraction $f(t)$ as a function of time t and applied field E:

$$f(t) = 1 - \exp\left\{-\exp\left[-E_0/E\right]\cdot\left(t/t_0\right)^3\right\},$$

resulting in the activation field value of $E_0 = 50$ MV/m and the characteristic switching time $t_0 = 70$ ps. Note that the expression above is obtained in the domain-wall-limited switching regime with inhomogeneous nucleation. In this regime the polarization kinetics is governed by the domains' coalescence as well as domain wall creep in the pinning potential, with E_0 being the pinning field.

The main disadvantage of this method is the need to have macroscopic contacts to apply the electric pulses and measure the response. It was found that the RC-characteristics of the contacts affect strongly the dynamic response of the ferroelectric at the shortest times. Accurate determination of the intrinsic switching time t_0 would require reducing the pulse rise time well below 70 ps (not possible with the current photoconductive switches) as well as reducing the capacitor planar dimensions (down from 5 x 5 μm) to avoid RC effects. Another disadvantage of this method is that the measured response is averaged over the ferroelectric volume inside the capacitor and does not allow spatially resolved investigation of domain nucleation and propagation.

The AFM/PFM method can be used to study spatially resolved ferroelectric domain wall dynamics [10]**.** Polar ferroelectric domains were written by applying short pulses of electric fields to the AFM tip above thin (29-130 nm) epitaxial PZT films grown on top of a conductive $Nb:SrTiO_3$ substrate. Field pulses can be as short as 5 ns with field amplitude up to 20 MV/m. The ferroelectric domains that appeared after exposure to these field pulses are then imaged by piezoresponse force microscopy (PFM). Measuring the domains sizes as a function of the electric field strength and duration provides ample information about polarization dynamics. Domain size decreases as the electric pulses are shortened, saturating at ~20 nm for pulses shorter than 20 μs down to 5ns. This minimum size is most likely related to the size of the AFM tip which serves as an electrode, therefore this experiment does not allow one to probe the inherent polarization dynamics at short time scales. The experimental data was found to fit better to the domain "wall creep in a random potential" model rather than the "periodic potential pinning model."

The main disadvantage of this experiment is poor control of the electric field pulses. Because the interaction of the tip with the sample is very complex, the field is only known with an order of magnitude accuracy. The field is spatially highly non-uniform, which affects the size of the smallest domains and prevents investigations of the characteristic nucleus size. The minimum pulse length of 5 ns is much longer than the characteristic switching time of less than $t_0 \approx 70$ ps (as measured in the first experiment described above) which does not allow studying the polarization dynamics in the nucleation limited regime.

Using the FACET electron beam resolves many difficulties and limitations encountered in the experiments described above. The experiments would be somewhat similar to the second experiment described above: the electric field is applied for a short time, and then the resulting domain pattern is imaged. Note that imaging will have to be done ex-situ, but since even the smallest domains (~20 nm) have been found stable for weeks after exposure in [10] it should not pose a problem. The magnitude, direction and the pulse length of the applied field can be very accurately controlled with the FACET beam. The field will be very uniform up to micrometer

lengths; however it will be changing in magnitude and direction over larger areas, which would allow investigation of polarization dynamics as a function of field magnitude and direction in just one exposure. The dependence of polarization dynamics on pulse length from 100 ps down to 100 fs can be studied by changing the compression of the electron bunch.

We can anticipate the following distinct regimes of ferroelectric switching that can be probed in an experiment with FACET e-beams:

1. Domain wall creep limited regime–for fields well below the pinning field $E \le E_0 \sim 50$ MV/m and pulse lengths longer than the characteristic switching time $t \ge t_0 \sim 70\,\text{ps}$. Studying the domain size as a function of field magnitude and pulse length will allow an accurate measurement of the pinning field and switching time avoiding the difficulties associated with electrodes in [9]. These parameters are extremely important for predicting the dynamic response in current applications such as ferroelectric memories.
2. Nucleation limited regime – for fields larger than the pinning field $E \ge E_0 \sim 50$ MV/m and pulse lengths shorter than the characteristic switching time $t \le t_0 \sim 70\,\text{ps}$. This regime cannot be accessed by any of the currently existing experimental techniques. In this regime the propagation of the domain wall will be "ballistic" and limited by the energy dissipation rate. Important parameters such as nuclei size distribution and average nucleation time as a function of applied field magnitude and orientation can be extracted.
3. Intrinsic switching regime–for fields much larger than the pinning field $E >> E_0 \sim 50$ MV/m and pulse lengths much shorter than the characteristic switching time $t << t_0 \sim 70\,\text{ps}$. In this regime polarization switching is not limited by extrinsic (impurities, defects etc) domain nucleation mechanisms, but occurs through a coherent (homogeneous) single-domain reorientation, similar to the well-known switching of single-domain magnetic particles. Very little is known about this interesting regime in ferroelectrics. It has been claimed that intrinsic switching has been observed in Langmuir–Blodgett ferroelectric films [11], but this claim is based not on the dynamic switching measurements, but instead on comparison of the measured switching field with that calculated from the Landau-Ginzburg theory. The molecular dynamics simulations of intrinsic switching in $KNbO_3$ were performed in [12] and yielded a very short switching time of 10-20 ps with applied field of 50 MV/m which can easily be accessed in the FACET e-beam experiments. These experiments will determine the ultimate switching speed of ferroelectric devices.

FACET will provide a non-contact means of coupling in intense, femtosecond electric fields in order to definitively study the ferroelectric switching process. Electric fields larger than the coercive field will be easily generated and coupled into a variety of samples. We will be able to investigate the ability of samples to repetitively switch by using synchronized electrical pulses coupled in through an electrode structure that reset the sample after each electron bunch/field excitation pulse. An electrode structure will also enable us to partially bias the sample, with the THz pulse providing the final push.

In summary, this work will define the limits on which future ferroelectric devices may be expected to function, and should aid in the development of faster and more reliable devices.

4.4 Terahertz Radiation and Semiconductor Devices

The clock frequency of modern microprocessors is in the GHz range. However, the speed of amplifiers for state-of-the-art fiber optical communication approaches 100 GHz. Future devices will be smaller. As the dimensions shrink, parasitic capacitances as well as the gate length shrink, leading to even faster devices. At the same time, the thickness of the gate oxide is reduced to only a few nanometers. Applying a voltage to the gate leads to large electrical fields in the range of many 10s of megavolts per meter. Therefore, it is essential for the future of microelectronics to study materials under extreme electrical fields.

The FACET beam is a unique source of perfect magnetic and electrical field pulses in the THz range with large magnetic and electrical fields. The THz radiation from the electron beam is therefore an ideal tool to study electronic properties of materials on the femto- to pico-second time scale under extreme electrical fields. This combination makes the THz field unique to study materials for future electronic devices.

We anticipate a program of THz scattering experiments with semiconductors and insulators. The THz field will modify the electronic structure of the materials and lead to self-modulation of the THz field. In addition, time resolved laser spectroscopy using a THz pump pulse will allow us to investigate carrier generation and dynamics caused by the electrical field of the THz pulse in the time domain.

The THz field can be modified by lithographically defined micro antennas on the sample, leading to even stronger electromagnetic fields by concentrating the THz radiation to a small area. It will be extremely interesting to study the limits of electronic conduction in metals and semiconductors.

4.5 Terahertz Radiation and Chemistry

There are a vast number of economically important processes that rely on reactions at surfaces and interfaces, such as catalysis in chemical and energy production. The microscopic understanding of reactions at surfaces requires an in-depth knowledge of the dynamics of elementary processes on an ultrafast timescale. The intermediates that appear in each elementary step are present only for a short period of time and at extremely low concentrations. Therefore they are often undetectable under steady-state conditions. As a consequence, it has been extremely challenging to visualize the underlying reaction mechanism and dynamics of processes at surfaces.

One approach to the study of an ultrafast excitation is to initiate a chemical reaction and then probe the progression of the reaction. Excitation of phonons, frustrated rotational and translational motions of molecular adsorbates plays an important role in processes at surfaces that are driven by kT, *i.e.*, temperature. These mechanisms account for nearly all the processes of essential societal and economical interest. Femtosecond visible laser pulses have been used to trigger the reaction. Laser pulses heat the electrons, leading to a very high transient electronic temperature followed by the subsequent energy transfer to phonons and frustrated vibrational modes. As vibrational temperature rises, the reaction is initiated and the time evolution is followed through products released into the gas phase [13,14,15]. At the moment, there exists no direct way to pump surface reactions by exciting the motion of the nuclei of an adsorbed molecule on an ultrafast timescale.

The ultra short electron bunches in FACET open up the opportunity to develop new methods for triggering the motion of nuclei. Assuming an electron pulse width of 100 fs, broadband

radiation will be obtained with a cut-off frequencies as high as 10 THz, which matches the frustrated vibrational motions of adsorbed species on the surface. Therefore a temperature jump over an ultra short time scale is possible by exciting frustrated vibrational motions using an ultra short electron bunch. There are no other excitations that generate any large amount of charged hot carriers, making for a clean experiment.

Not only is the frequency of the pulse of major interest, but also the directional electric field. One of the important developments in the last decade has been the direct control and manipulation of atoms and molecules as exemplified by the movements of individual atoms and molecules on solid surfaces by means of scanning tunneling microscopes (STM) [16]. The manipulation is achieved through application of a strong electric field, typically >1x10^9 V/m (or >0.1 V/atom) as illustrated in Figure 4-8. We envision the use of electric field pulses with durations in the 100 fs – 1 ps range and comparable field strengths can be used to drive chemical reactions [17].

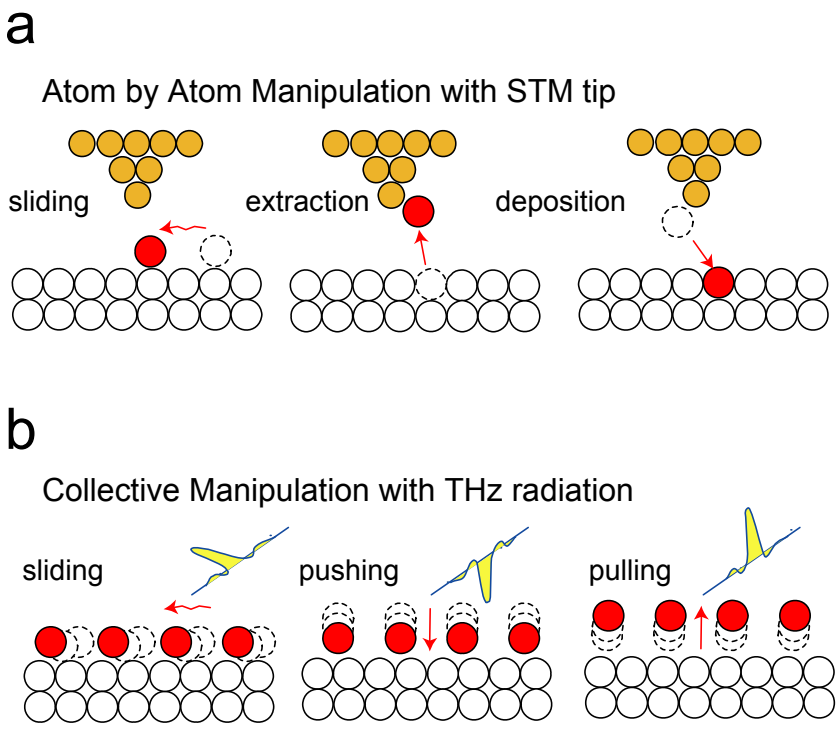

Figure 4-8. a) Atom by atom manipulation with a STM tip [15]. b) Collective manipulation with strong photon field with half cycle electric field pulse in different directions to the surface.

One experimental approach is to prepare monolayers of adsorbed molecules on single crystal metal surfaces and position the sample near an electron beam to initiate the chemical reaction. When the electron beam passes by, a strong electric field is produced close to the surface for an ultra short time period, *i.e.*, ~100 fs, resulting in exposure to broad band THz radiation. The THz temperature jump or the strong electric fields will stimulate processes on surfaces. In order to detect whether a surface reaction has occurred, the angular direction of desorbing products can be analyzed using a mass spectrometer, as shown in Figure 4-9. In the temperature jump process, the absorbed THz radiation dissipates among several degrees of freedom and we expect that the angular distribution of desorption products will show a simple

cosine distribution similar to that observed for conventional thermal desorption experiments. On the other hand, if the desorption is induced by the strong electric field, the desorbing products are expected to be strongly peaked in a direction related to the direction of the molecular motion being excited in the excitation process. Studies would initially focus on desorption of weakly bound species such as Xe adsorbed on Pt(111) and then move to more strongly adsorbed species such as CO and N_2 on Ni(100). Eventually it may be possible to investigate surface reactions involving oxidation of CO with oxygen Ru(001) and decomposition of formate to CO and hydrogen on Cu(110). FACET will therefore provide a unique tool for studying surface processes over a wide range of reactions that are of primary societal and economic interest.

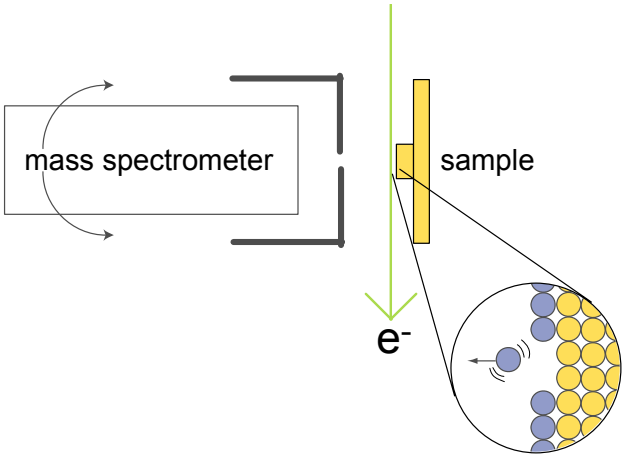

Figure 4-9. Possible experimental setup for using THz radiation or strong E-fields from the FACET beams to induce desorption and reactive desorption products. The products are then analyzed with a mass spectrometer.

THz radiation may also be used to turn on and off electrochemical reactions. Fuel cells are used to produce electricity, in a process where a proton produced from hydrogen is electrochemically combusted on the surface of a catalyst that is immersed in an electrolyte solution. There is an ionic layer formed in the electrolyte solution near the catalyst surface, denoted the electrochemical double layer. This double layer is essentially a capacitor, with an extremely strong E-field inside the electrochemical double layer of the order of 1 GV/m [18]. The ultra short electric field pulse from FACET, with comparable field strength, provides a mean to change the electron affinity in the electrochemical double layer over very short time durations. The electron affinity change will result in a variation of the electron transfer rates across the interface and can turn on and off the electrochemical reaction. A demonstration that THz radiation can stimulate the electrochemical process would be possible by studying the oxidation of Pt electrode covered with CO in an acid solution. The reaction yield of THz radiation stimulated process would be evaluated by comparing the electrochemical oxidation current of samples with and without THz irradiation. Once again, the unique properties of the FACET beams would be crucial to this area of research.

4.6 References

[1] J. Stöhr and H. C. Siegmann, "Magnetism: From Fundamentals to Nanoscale Dynamics", Springer Series in Solid-State Sciences **152**, (Springer, New York, 2006).

[2] D.J. Hilton et al., Optics Lett. **29,** 1805 2004: "Terahertz emission via ultrashort excitation of magnetic metal films".

[3] E. Baurepaire *et al.*, Appl. Phys. Lett. **84**, 3465, 2004: "Coherent terahertz emission from ferromagnetic films excited by femtosecond laser pulses".

[4] J.B. Héroux *et al.*, Phys.Stat.Sol.(c) **3**, 4271 (2006): "Magnetization induced terahertz radiation from GaMnAs".

[5] S. J. Gamble, Mark H. Burkhardt, W. Harrison, H. C. Siegmann, J. Stöhr, A. Kashuba, Rolf Allenspach, and Stuart S. P. Parkin, to be published.

[6] S.M. Cho, H.M. Jang, "Softening and mode crossing of the lowest-frequency A1 (transverse-optical) phonon in single-crystal $PbTiO_3$", Appl. Phys. Lett., **76**, 3014 (2000).

[7] G. Shirane, J.D. Axe, J. Harada, J.P Remeika, "Soft ferroelectric modes in Lead Titanate", Phys. Rev. B **2**, 155 (1970).

[8] T.P. Dougherty, G.P. Wiederrecht, K.A. Nelson, M.H. Garrett, H.P. Jensen and C. Warde, "Femtosecond resolution of soft mode dynamics in structural phase transitions", Science **258**, 770 (1992).

[9] J. Li, B. Nagaraj, H. Liang, W. Cao, Chi. H. Lee, and R. Ramesh, "Ultrafast polarization switching in thin-film ferroelectrics", Appl. Phys. Lett., **84**, 1174, (2004).

[10] T. Tybell et al.; "Domain Wall Creep in Epitaxial Ferroelectric $Pb(Zr_{0.2}Ti_{0.8})O_3$ Thin Films;" Phys. Rev. Lett. **89**, 097601 (2002). P. Paruch *et al.*; "Nanoscale studies of domain wall motion in epitaxial ferroelectric thin films;" arXiv:cond-mat/0411178.

[11] S. Ducharme et al.; "Intrinsic Ferroelectric Coercive Field;" Phys. Rev. Lett. **84**, 175 (2000).

[12] Simon R. Phillpot, Marcelo Sepliarsky, S. K. Streiffer, Marcelo G. Stachiotti, and Ricardo L. Migoni; "$KNbO_3/KTaO_3$ Solid Solutions and Superlattices by Molecular-Dynamics Simulation;" AIP Conference Proceedings; no. 626, p. 160-8 (2002).

[13] F.-J. Kao, D. G. Busch, D. Gomes da Costa and W. Ho, Phys. Rev. Lett. **70**, (1993) 4098.

[14] M. Bonn, S. Funk, Ch. Hess, D. N. Denzler, C. Stampfl, M. Scheffler, M. Wolf and G. Ertl Science, **285** (1999) 1042.

[15] K. Onda, B. Li, J. Zhao, K.D. Jordan, J. Yang, and H. Petek, Science, **308** (2005) 1154.

[16] J.A. Stroscio and D.M. Eigler, Science **254**, 1319 (1991).

[17] H. Ogasawara, D. Nordlund, A. Nilsson, SLAC-PUB-11503 (2005).

[18] J.O'M. Bockris and S.U.M. Khan, Quantum Electrochemistry, Plenum Press, New York (1979).

5 Technical Description

5.1 Modes of Operation

The FACET proposal consists of modifications to linac beam delivery systems to two experimental areas at SLAC. The overall site layout is shown schematically in Figure 1-1 with the modified areas highlighted. A new beam focusing system, designated the Accelerator Science Facility (ASF), will be installed in Sector 20 of the linac housing to support experiments requiring tightly focused and compressed beams of electrons or positrons. The bunch compressor in Sector 10 of the linac will be modified to compress positron bunches as well as electron bunches. The NIT transport line, which was built to deliver electrons from Sector 10 to the PEP-II high energy ring, will be extended into the Beam Switch Yard (BSY) and coupled to the existing A-line to allow electrons to be transported on to End Station A. This transport line extension, which will bypass the last third of the linac, is designated the Electron Bypass Line (EBL).

5.1.1 Electrons to Sector 20

The linac accelerator facility was modified and upgraded in the 1980's to generate and accelerate beams of electrons and positrons for the SLC program at repetition rates up to 120 pulses per second. This facility has been in nearly continuous use to provide short intense bunches of electrons and positrons for PEP-II, as well as for FFTB and ESA programs. A few years ago, a compressor chicane system was added in Sector 10 to provide a method for compressing electron bunches to unprecedented short longitudinal extent with corresponding high peak current to support new research programs in the FFTB facility.

The proposed Sector 20 focusing system will take full advantage of the linear accelerator facility and all these improvements. Pulse repetition rates up to a maximum of 120 pulses per second, can be accommodated with the existing control and timing systems. For most applications, 30 pulses per second is likely to be the most cost effective mode.

The linac systems up to the Sector 20 experimental area will operate independently of any LCLS activities, and experimenters will be able to enter the linac housing in this area while the LCLS is operating.

5.1.2 Positrons to Sector 20

FACET/ASF can be used to deliver either electrons or positrons to the proposed new experimental area in Sector 20. The production of positrons involves first accelerating an electron beam to Sector 19, where it is directed to a target to produce positrons. The positrons are then returned to the South Damping Ring (SDR), where they are stored until the next linac pulse.

The existing pulse compression chicane in Sector 10 only works with electrons. This is a consequence of the geometry of the chicane, which only allows beams of one charge to pass. To produce a compressed positron bunch requires that the chicane be made symmetric, allowing both electrons and positrons to pass through.

Switching the Sector 20 system between electrons and positrons will require reversing the polarities of some of the magnets, a procedure likely to take about a day or two to complete. This will not be practical as a routine quick-switch operation; however, switching polarities can be done whenever the research program requires the opposite charge, and the work required to switch polarities can be done outside the linac housing without interfering with any other running

accelerator program. With the magnet polarities reversed, a positron beam can be focused and delivered to experiments in Sector 20, and the beam parameters will be virtually identical to those that can be achieved with electrons.

The mode of operation likely to be most reliable and economical will involve pulsing the linac at 30 times per second, with 15 pulses accelerating electrons to the production target, interleaved with 15 pulses per second of positrons delivered to the users. Faster rates are possible, including a maximum possible rate of 120 pulses of positrons per second, accelerated on the same linac cycles as 120 pulses of electrons used to make more positrons.

5.1.3 Electrons to End Station A

The proposed modification and extension of the PEP-II injection bypass line (EBL) will provide the means to transport electrons with energies up to 12 GeV from the extraction point in Sector 10 to the BSY, where they can be directed into the A-line system to ESA. The existing connection from the main linac through the BSY to the A-line will be preserved, thereby providing the capability to deliver the LCLS electron beam to ESA as well. Pulse repetition rates up to 120 pulses per second will be possible, although, as for Sector 20 operation, 30 pulses per second is likely to be most economical for most applications.

The existing linac damping rings greatly reduce the transverse emittance of the beams, but these damping rings were designed to process beam pulses that occupy a single s-band RF bucket. Trains of bunches occupying every fourth s-band bucket are possible in principle, up to a maximum length corresponding to the damping ring circumference, minus the rise and fall times of the injection and extraction kickers. Longer trains of bunches are not possible with the damping rings. However, when the linac has operated in the straight-through mode without the damping rings, bunch trains in excess of 350 nsec have been achieved. Long pulses of this kind will be available to experimenters when needed, as well as the usual single-bucket pulses.

The extraction magnet in Sector 10 is a pulsed device, which means that the ESA beam could be interleaved on alternating pulses with an electron beam to Sector 20. In this way, experimental programs in both areas could take data simultaneously.

The bypass line from Sector 10 to ESA passes through the Sector 20 area above and to the south of the linac axis. Because of radiation safety considerations, no one will be allowed to enter the linac tunnel when this beam is operating. Therefore, any access to the experimental equipment in Sector 20 will require that the ESA beam be turned off first. Engineered features of the personnel protection system (PPS) will enforce this requirement.

5.2 Sector 20 Final Focus Technical Description

The ASF facility consists of a bunch compressor, a final focusing section, an experimental area, a beam dump, a shield wall, and above-ground facilities for users and data acquisition equipment. The experimental area lies in Sector 20 of the linac tunnel, upstream of the point where the LCLS injector joins the linac.

An overview map of the SLAC site is shown in Figure 1-1 with the components of the ASF at Sectors 10 and 20. The Sector 20 area is expanded in Figure 5-1 to show the paved areas on both sides of the Klystron Gallery and proposed locations for associated above-ground experimental counting house and Klystron Gallery electronics area. The position of the focal point in the linac tunnel below is also indicated for orientation.

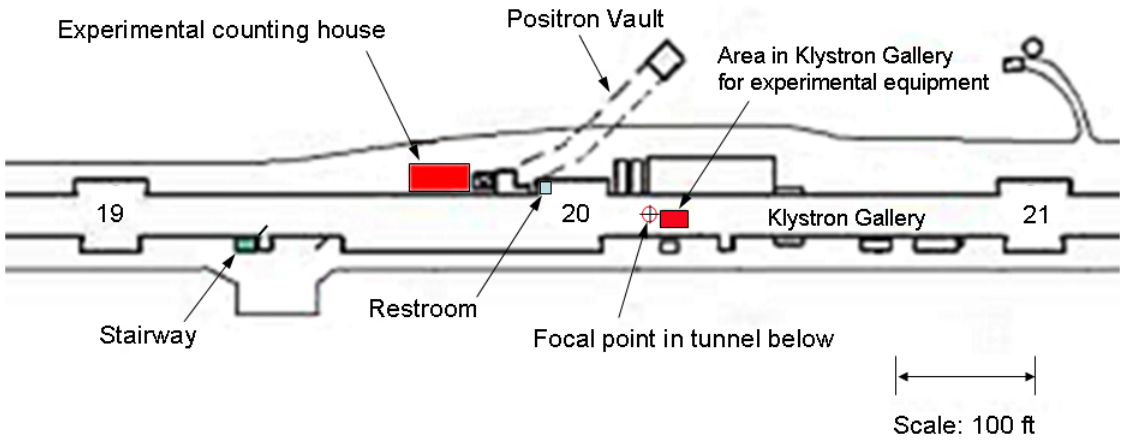

Figure 5-1. ASF region in the Klystron Gallery. The linac tunnel is approximately 25 feet underground below the Klystron Gallery and will be easily accessible through a new stairway to be installed in the Sector 19 equipment shaft (shown in green). The large red rectangle indicates the location of a building to house experimenters. The smaller red rectangle indicates an area in the Klystron Gallery for an enclosed room to house experimental equipment that must be near the focal point but accessible when the beam is on.

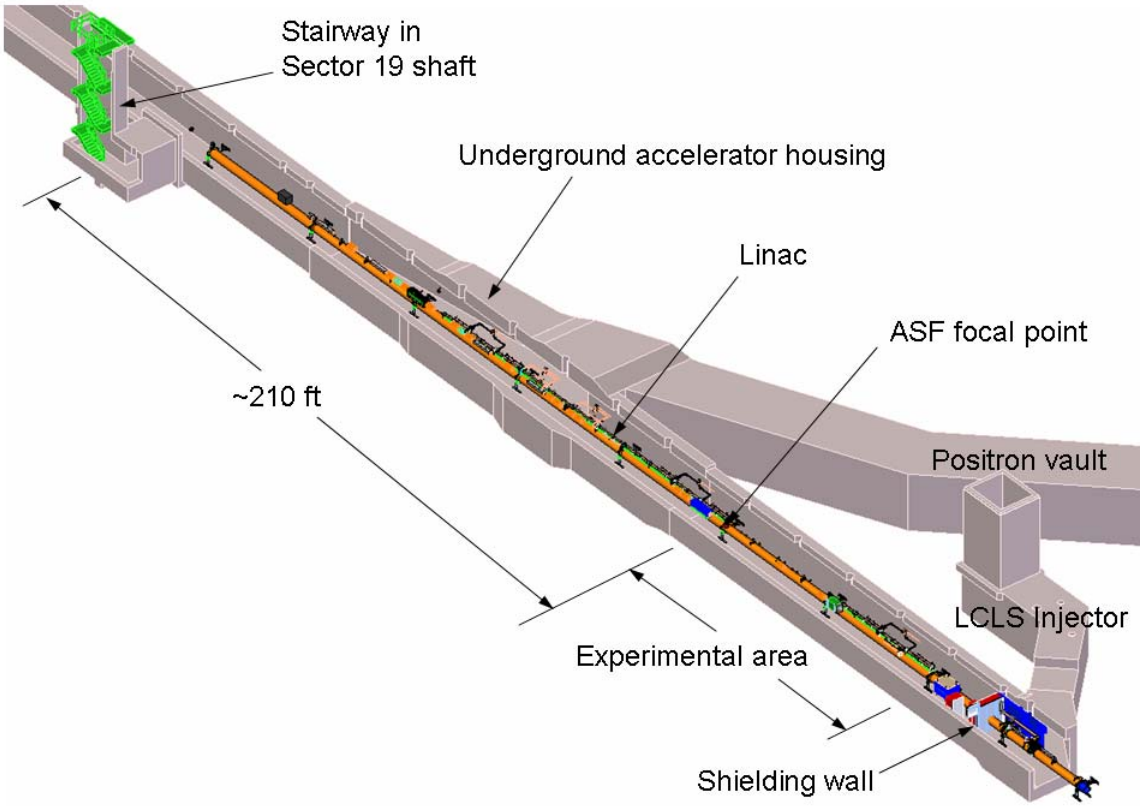

Figure 5-2. Cutaway view of the underground linac tunnel in the Sector 20 ASF final focus region showing the proposed staircase at the upper left and the LCLS injector vault in the lower right.

A cutaway drawing of the linac tunnel in this region is shown in Figure 5-2. A new entrance stairway is shown in the upper left corner of the figure, and the injector vault of the LCLS system is shown in the lower right. Personnel will walk about 210 feet down the linac tunnel from the bottom of the access stairs to the final focus area for the ASF beams.

Cross-sectional views of the linac housing upstream of the final focus and at the position of the ASF focal point are shown in Figures 5-3 and 5-4. The ASF beam is offset approximately 60 cm to the south of the nominal linac trajectory, placing it near the center of the tunnel. The existing light pipe is part of the linac alignment system and will be left in place for this purpose, although the accelerator and its associated support structure and waveguides will be removed in the area of the focal point. Also shown are two quadrupole magnets on the overhead bypass lines used to transport beams of electrons and positrons to PEP-II. The electron bypass line will be used to transport electrons to ESA.

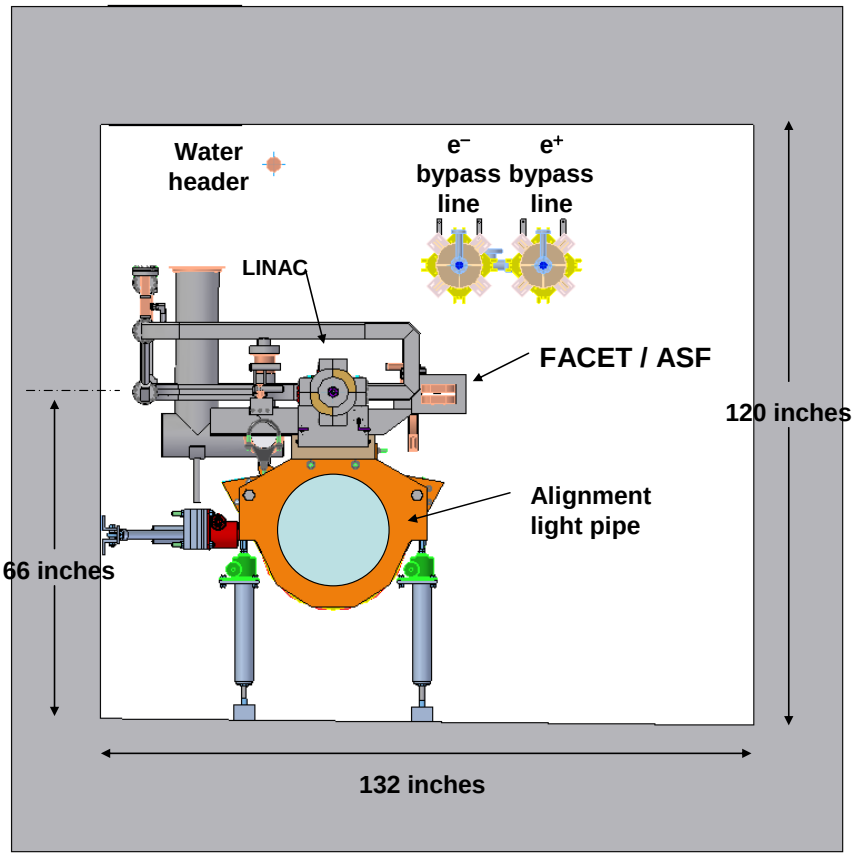

Figure 5-3. Tunnel cross section upstream of the ASF final-focus region. The linac and its support structures are shown above the alignment light pipe and the e^- and e^+ bypass lines that transport electrons and positrons to the PEP-II HER and LER rings.

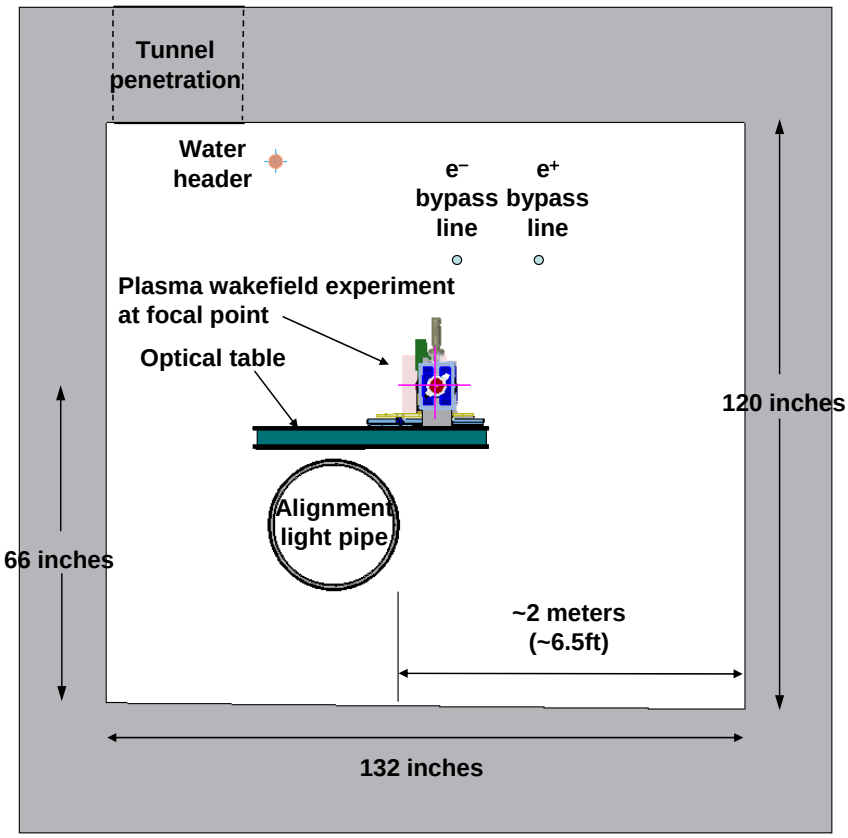

Figure 5-4. Tunnel cross section at the position of the ASF final focus. For illustration of the size of the experimental area, a four-foot wide optical table is shown which serves as a mounting platform for a lithium oven, centered on the ASF beam position, for the plasma wakefield acceleration experiment.

The linac beam trajectory, the light pipe, and the electron and positron bypass lines to PEP-II are visible in Figure 5-5, a photograph taken in the linac housing near the proposed ASF focal point. Penetrations extending up to the Klystron Gallery above are located at twenty foot intervals along the tunnel, providing convenient access for pipes, conduits, and cables. Existing cable trays visible in the upper right corner of the photograph can accommodate the anticipated experimenter requirements.

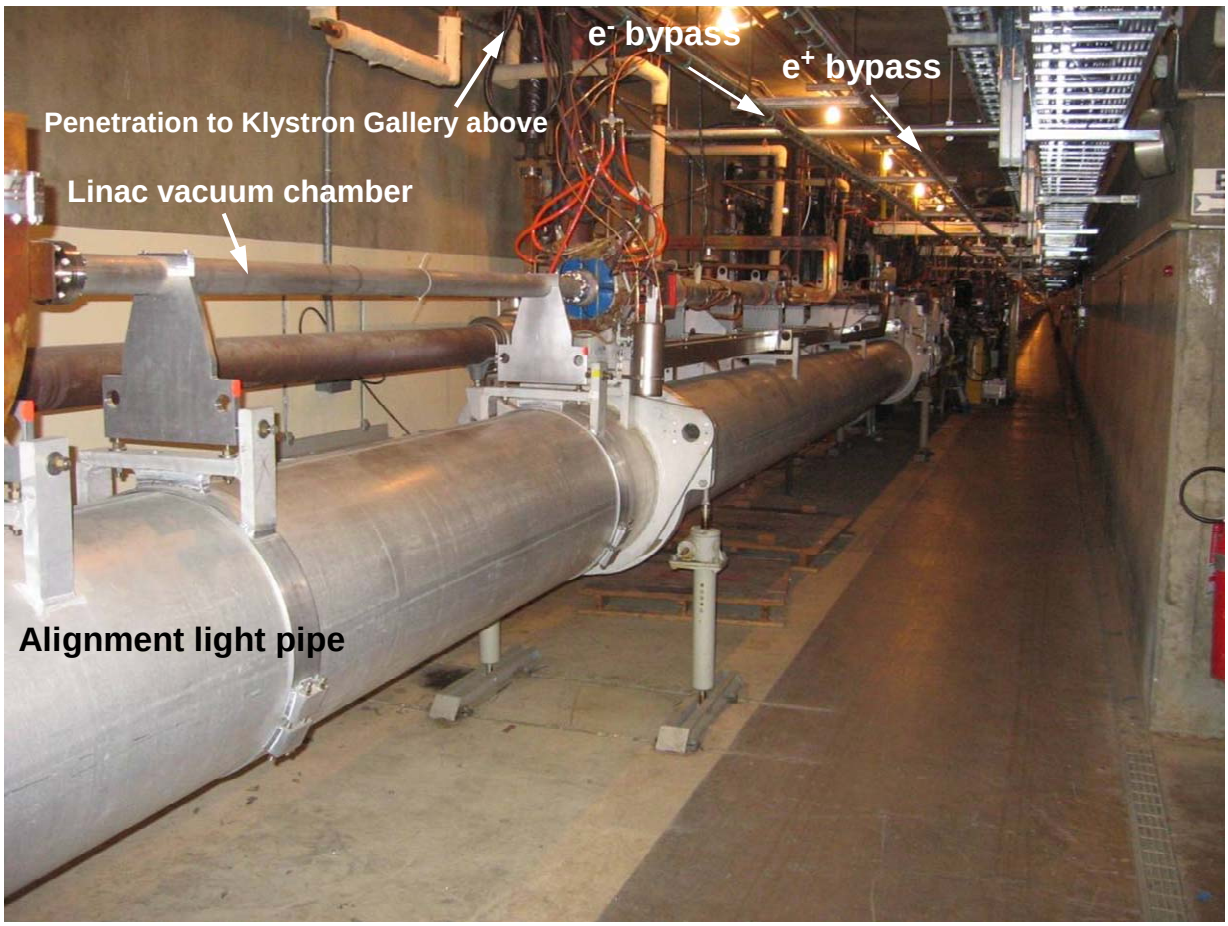

Figure 5-5. Sector 20 ASF region in the linac tunnel. The linac beam passes through the vacuum pipe directly above the large laser alignment pipe. The electron and positron transport lines (labeled NIT and SIT) are visible overhead on either side of the row of light bulbs, and a convenient cable tray runs along the upper right.

5.2.1 Sector 20 Final Focus Design

The new FACET/ASF lattice will be installed in Sector 20 beginning after quadrupole QLI20-201. A schematic plan view of the magnet layout is shown in Figure 5-6, while Figure 5-3 provides a cross-sectional view of the linac tunnel with existing components and the new ASF beamline. The lattice consists of the dogleg section, the FF section, and the experiment section with a beam dump. Four horizontal bend magnets in the dogleg section deflect the FACET beam 55.6 cm from the linac axis into a parallel beamline with the FF and experiment sections. The beam interaction point (IP) is located 2 m downstream of the last FF quadrupole.

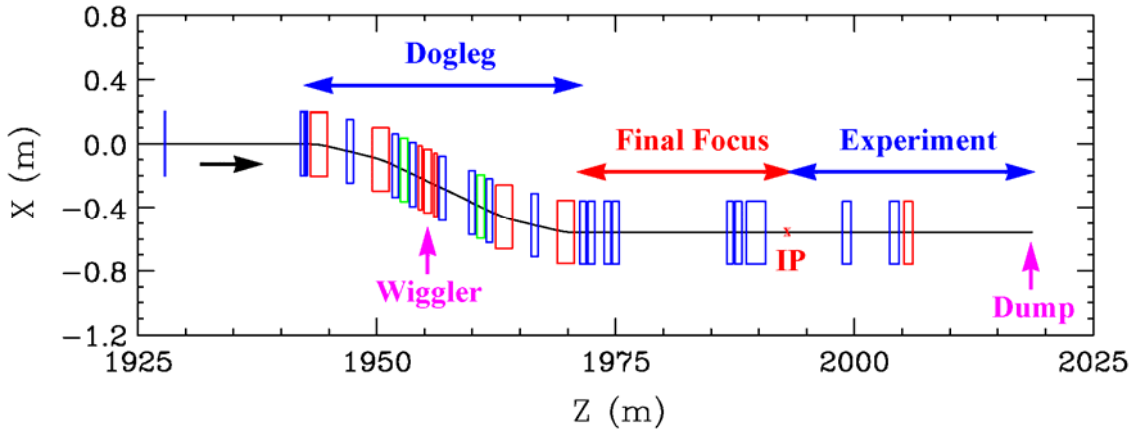

Figure 5-6. Horizontal layout of the ASF magnets in Sector 20, where quadrupoles are shown in blue, bends and wiggler in red, and sextupoles in green

The beta functions and dispersion are shown in Figure 5-7. The symmetric quadrupole arrangement in the dogleg section is designed to cancel the first-order dispersion generated in the four bends and to create the linear matrix transformation term R_{56} = 4 mm necessary for the final stage of the bunch length compression. Additionally, two sextupoles with opposite strengths cancel the second-order dispersion, as shown in Figure 5-8. The sextupoles also reduce the unwanted quadratic bunch-length term T_{566} from 44 mm to 9.5 mm. A wiggler section consisting of three vertical chicane bends is included near the dogleg center to generate a pattern of synchrotron radiation suitable for measuring the beam energy without interfering with the primary program.

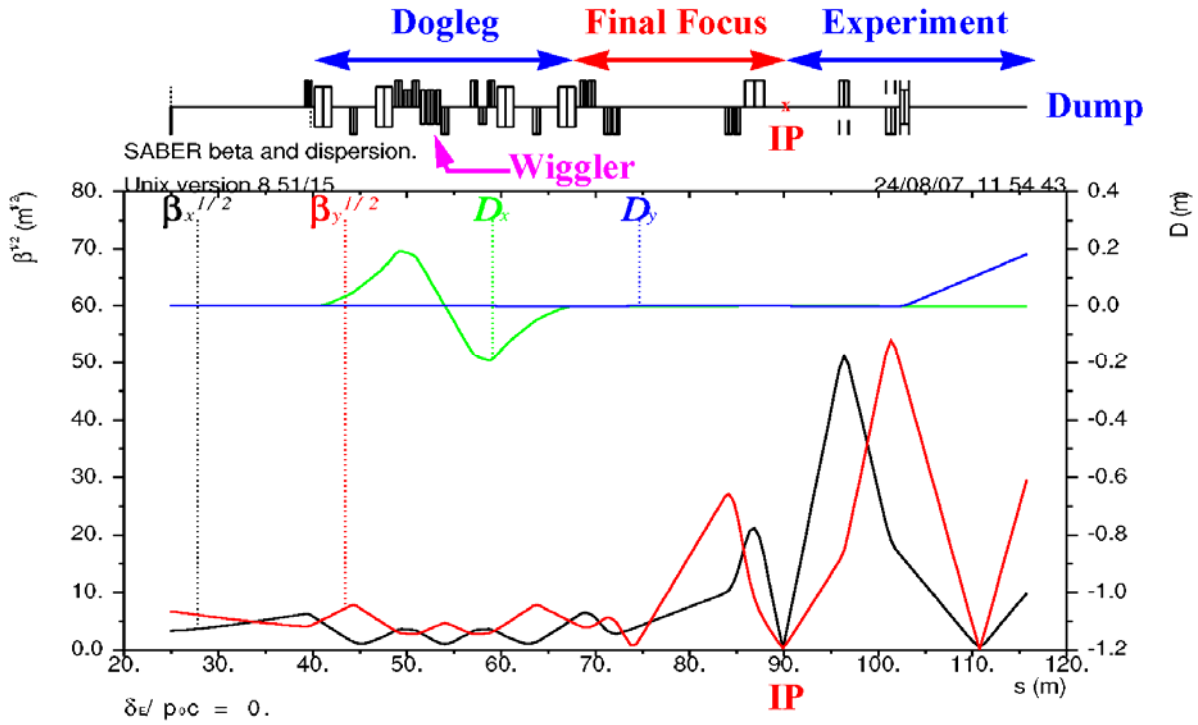

Figure 5-7. ASF beta functions and dispersion in linac Sector 20.

The final focus section consists of two quadrupole doublets which focus the beam to a small round spot at the IP with $\beta_x^* = 1.5$ cm, $\beta_y^* = 15$ cm, and zero dispersion. For a 25 GeV beam with normalized emittance of $\gamma\varepsilon_x = 50$ μm and $\gamma\varepsilon_y = 5$ μm, the first-order IP beam size is $\sigma_x = \sigma_y = 3.9$ μm. This is well below the 10 μm specification and allows for beam size growth due to the non-linear optics effects, machine errors and some variation of beam parameters. Figure 5-12 and 5-13 show calculated beam distributions with all these effects included.

The optical configuration in the experiment section consists of a quadrupole doublet located 6 m after the IP, followed by a vertical bend magnet. The quadrupoles focus the extracted beam to a second focal point, and the bend magnet deflects the beam to the dump.

The bunch length compression mechanism results in a large energy spread. This energy spread causes beam size growth due to energy dependent focusing in the quadrupoles, dispersion in the bends, and second-order aberrations in the sextupoles. Tracking simulations were used to compute the chromatic beam size growth at the IP as a function of a generic flat energy spread, as shown in Figure 5-9. A simulated 25 GeV beam with Gaussian x-y spread and normalized emittance of $\gamma\varepsilon_x = 50$ μm, $\gamma\varepsilon_y = 5$ μm was tracked through the ideal optics using the DIMAD code. Synchrotron radiation (SR) will have a very small effect on the beam size growth and energy loss (0.012%). As Figure 5-9 shows, the rms beam size increases with energy spread, but remains below 10 μm for up to ±1.6% of flat ΔE/E spread when the sextupoles are turned on. If the sextupoles are off, then the horizontal size grows faster with increasing energy spread, due to the uncorrected second-order dispersion.

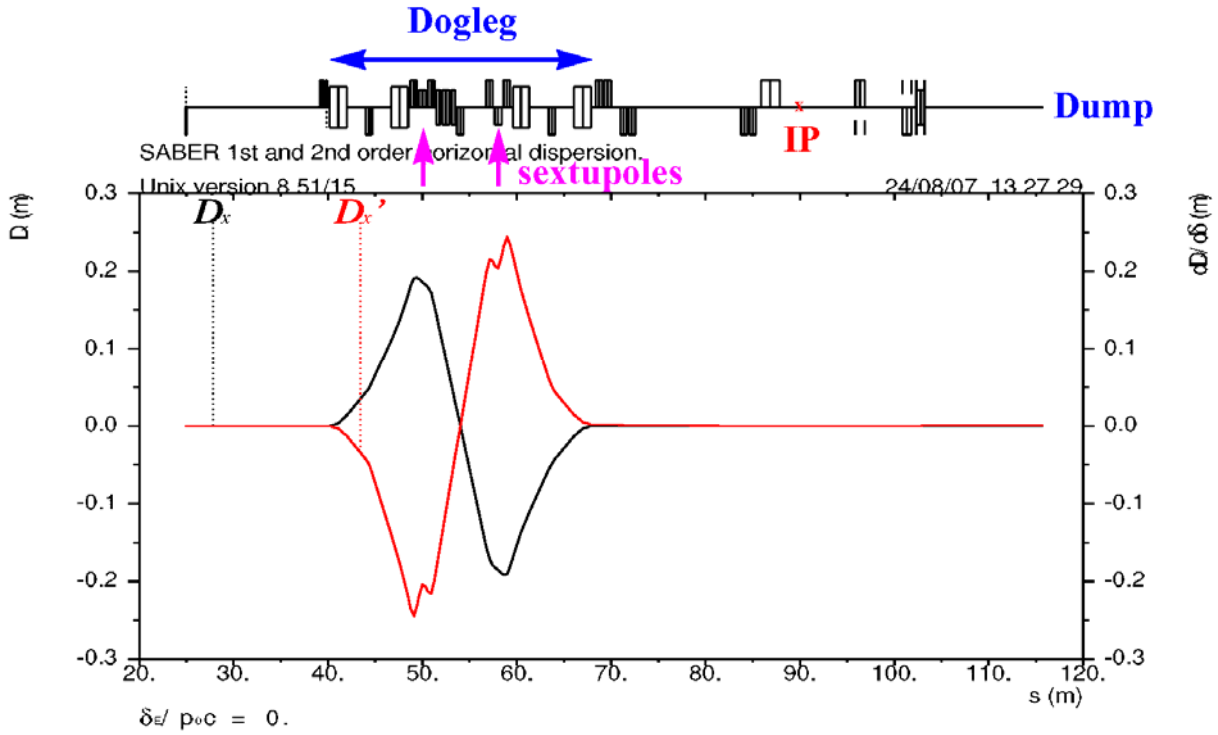

Figure 5-8. 1st and 2nd order horizontal dispersion in the ASF.

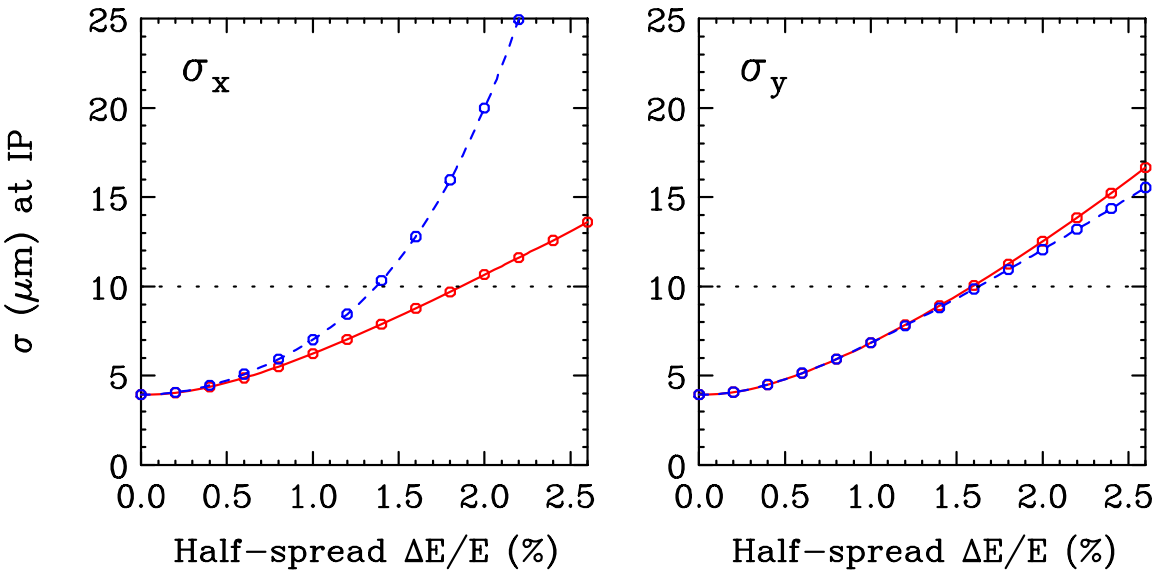

Figure 5-9. Horizontal (left) and vertical (right) rms beam size at the IP as a function of half-width of a flat energy spread, including the effects of synchrotron radiation for sextupoles turned on (red) and off (blue dash).

The bunch length is compressed in three steps, starting in the RTL transfer line from the damping ring to the linac, and followed by the compressor chicane in Sector 10, where R_{56} is not zero. The final compression is achieved in the Sector 20 dogleg with the optimum value of R_{56} = 4 mm after tuning the RF phases in the linac cavities. The RF phase settings were optimized using the LiTrack simulation code. Figure 5-10 shows the LiTrack energy and longitudinal bunch spread, and the longitudinal phase space at the IP for the shortest bunch with a Gaussian fit length of σ_z = 15.5 μm.

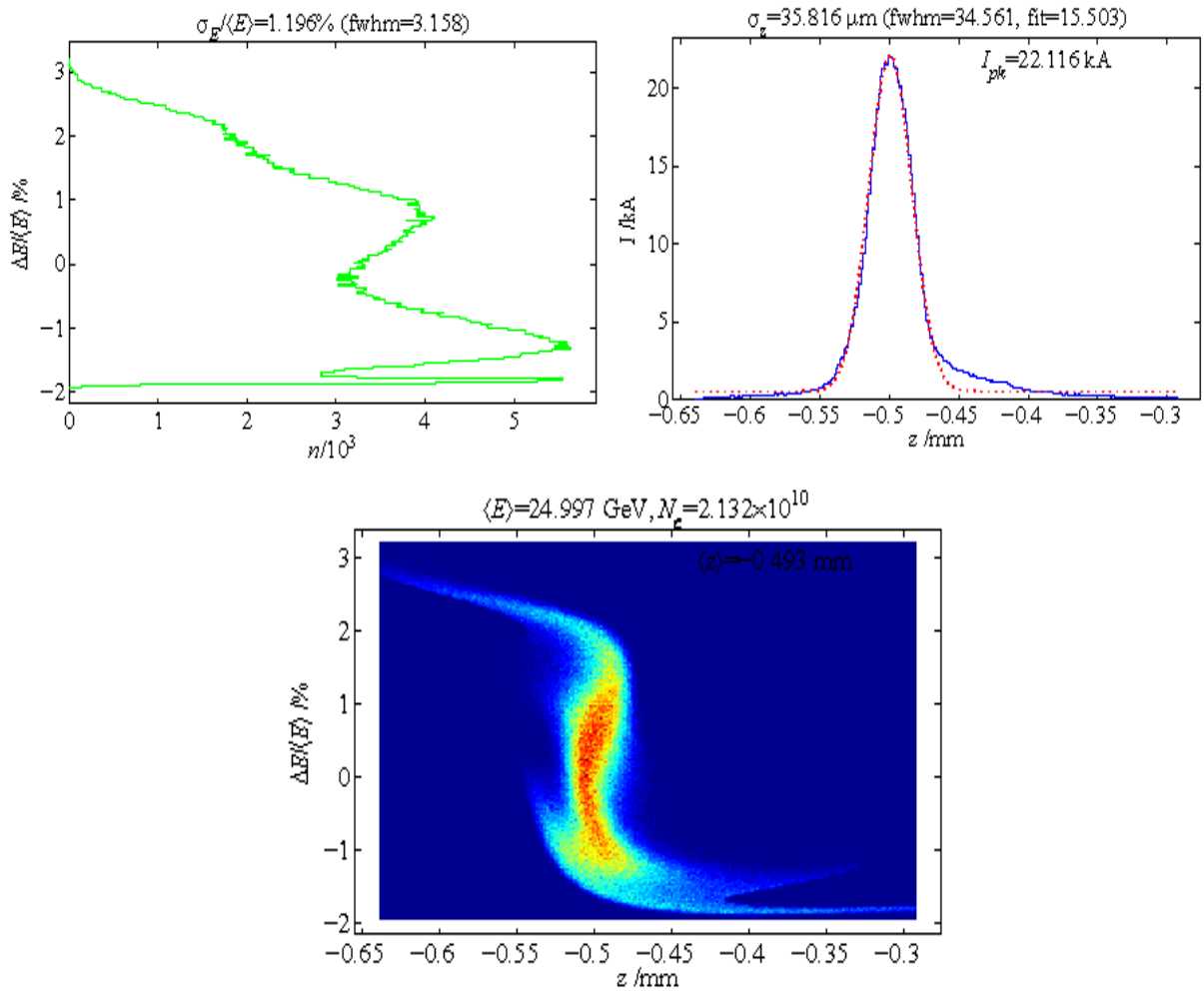

Figure 5-10. Energy spread (top left), longitudinal bunch profile with a Gaussian fit, and longitudinal phase space (bottom) at the IP for the short bunch optimized by LiTrack.

LiTrack simulates only the longitudinal bunch size and uses the global parameters (R_{56}, RF phase, voltage, wakefield, etc.) without detailed optics tracking. To confirm the LiTrack results, the exact element-by-element tracking was performed with the DIMAD code. A 25 GeV beam of 10^4 electrons with longitudinal phase space optimized by LiTrack and initial Gaussian x-y spread was tracked from Sector 19 to the IP without magnet errors. As Figure 5-11 shows, the resultant x-y beam spot has the desired round shape without long tails, and the longitudinal phase space agrees well with the LiTrack prediction.

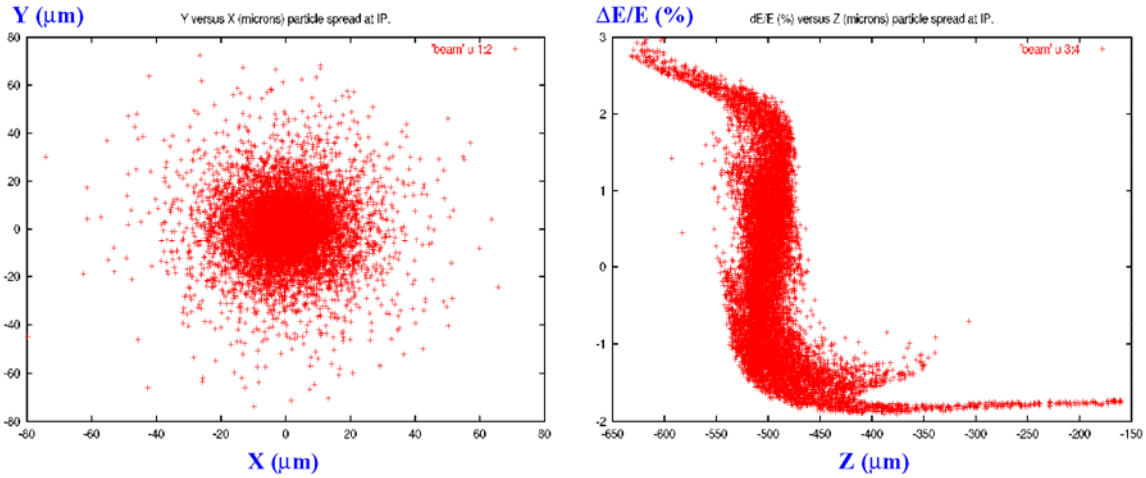

Figure 5-11. X-Y particle spread (left) and longitudinal phase space (right) at the IP for the short bunch in DIMAD tracking.

The longitudinal bunch profile at the IP and the energy spread in the DIMAD tracking, shown in Figure 5-12, agree reasonably well with the LiTrack result, although much lower statistics were used in DIMAD. This may be one reason that the 16.5 μm Gaussian bunch length obtained in DIMAD is slightly longer than in LiTrack.

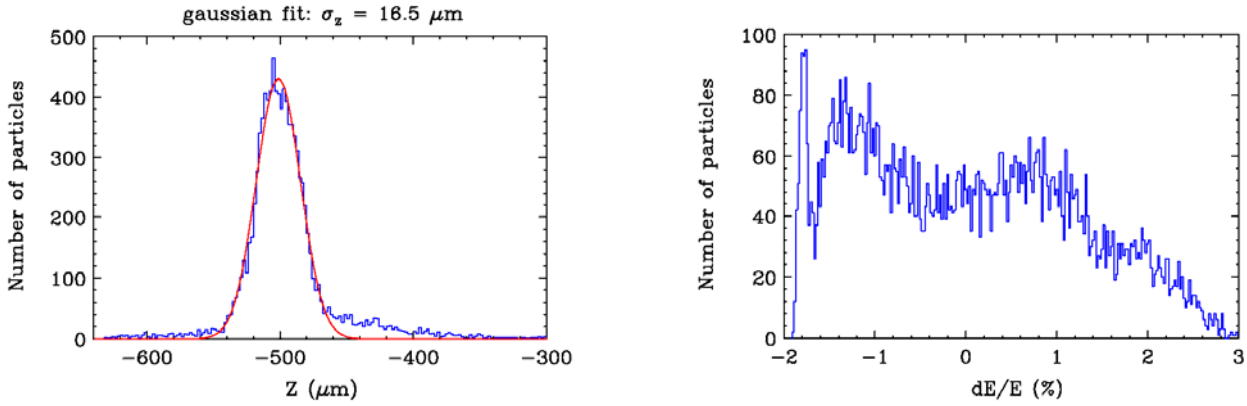

Figure 5-12. Longitudinal beam profile with a Gaussian fit (left) and energy spread (right) at the IP for the short bunch in DIMAD tracking.

The horizontal and vertical beam profiles at the IP for DIMAD tracking are shown in Figure 5-13. Gaussian fits yield the rms beam sizes of σ_x = 7.9 μm and σ_y = 8.7 μm. This beam size satisfies the 10 μm specification, even though the large energy spread, ΔE/E from -2% to +3%, in the compressed bunch leads to chromatic effects that significantly enlarge the beam. The chromatic beam size growth could be reduced if desired by adjusting the beam compression parameters for a lower energy spread but a greater bunch length.

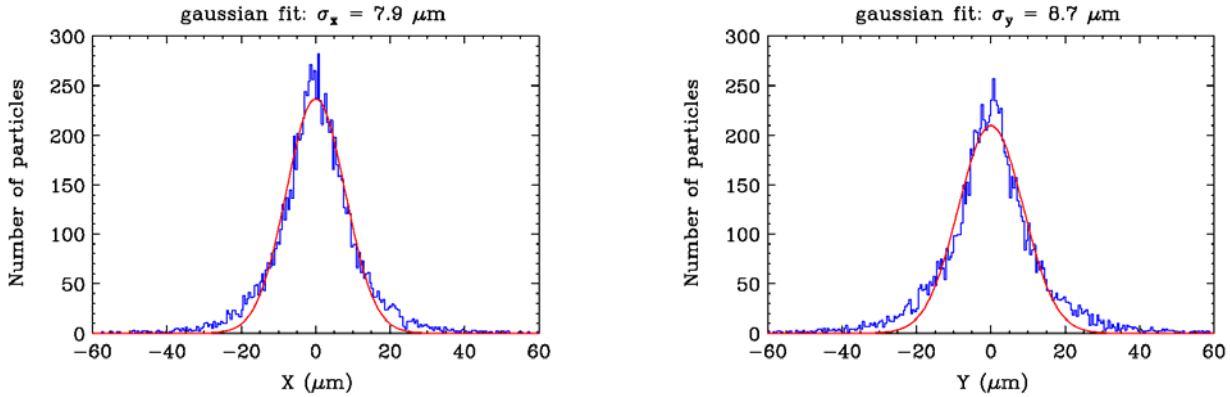

Figure 5-13. Horizontal (left) and vertical (right) beam profile at the IP with a Gaussian fit (line) for the short bunch in DIMAD tracking.

5.2.2 Sector 20 Final Focus Magnets

The Sector 20 optical configuration was designed to be built using 26 existing magnets salvaged from the SLC final focus and from the FFTB. Parameters of the quadrupoles, sextupoles and bending magnets needed for the Sector 20 system are listed in Tables 5-1, 5-2, and 5-3. The dogleg geometry was designed to use four existing bending magnets, BDL1 through BDL4, powered in series with a single power supply, even though the salvaged magnets are of two different lengths.

Table 5-1. Parameters of Sector 20 quadrupoles

Quadrupole Name	L (m)	B'L (kG) at 25 GeV	R (mm) to Pole	Number of Magnets	SLAC Magnet
Q190901T	0.107	-62.91	13.8	1	QE (existing)
Q200201T	0.107	69.44	13.8	1	QE (existing)
QDL0	0.408	114.50	20.6	1	1.625Q16
QDL1, 7	0.69	-203.85	20.6	2	1.625Q27.3
QDL2, 3, 5, 6	0.69	225.82	20.6	4	1.625Q27.3
QDL4	0.69	-255.52	20.6	1	1.625Q27.3
QFF1A, B	0.69	193.84	20.6	2	1.625Q27.3
QFF2A, B	0.69	-308.88	20.6	2	1.625Q27.3
QFF3A, B	0.69	-202.84	20.6	2	1.625Q27.3
QFF4	2.026	612.17	26.0	1	QC2
QS1	0.973	249.23	27.0	1	QP3A
QS2	0.973	-214.69	27.0	1	QP3B

Table 5-2. Parameters of Sector 20 sextupoles

Sextupole Name	L (m)	B''L (kG/m) at 25 GeV	R (mm) to Pole	Number of Magnets	SLAC Magnet
SXDL1	0.741	4569.2	20.6	1	1.625S29.2
SXDL2	0.741	-4569.2	20.6	1	1.625S29.2

Table 5-3. Parameters of Sector 20 bending magnets

Bend Name	L (m)	BL (kGm) at 25 GeV	Half-Gap (mm)	Number of Magnets	SLAC Magnet
BDL1, 4	1.812	12.197	6.35	2	2D71.3
BDL2, 3	1.739	11.705	6.35	2	2D68.5
B5D36	0.915	11.670	30.0	1	5D36

The four bend magnets needed for the dogleg section will be salvaged from the SLC final focus area.

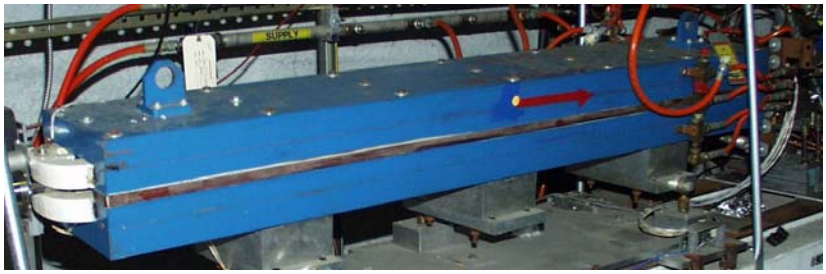

Thirteen of the quadrupole magnets will be salvaged from the SLC final focus system and refurbished for use in Sector 20. Each is supported by a fully adjustable mover base mechanism.

The last quadrupole before the IP is much stronger than the others. A magnet ideally suited for this application has been preserved from the FFTB and will be used directly in Sector 20 with a support base made from a salvaged SLC base.

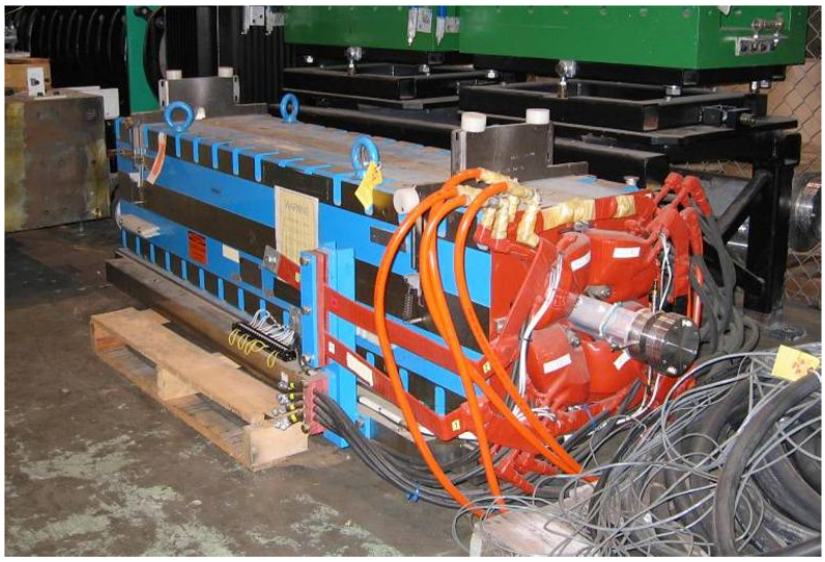

Two other large quadrupoles preserved from the FFTB are well suited for the two positions needed downstream of the IP.

Two sextupole magnets needed for the dogleg section will be salvaged from the SLC final focus chromatic correction section.

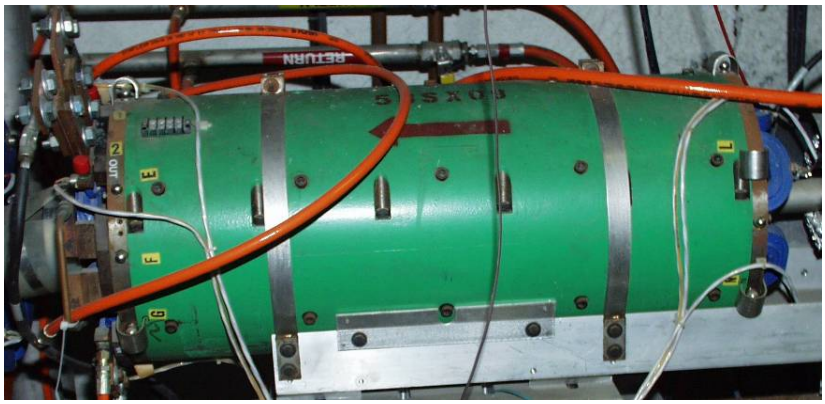

The first few magnets in Sector 20 will be mounted on the existing linac support girder using standard SLAC mechanical designs and refurbished SLC support movers. Eighteen magnets and most of the beam line instrumentation will be supported on refurbished SLC mover bases mounted on pier base supports similar to those used in the SLC final focus system, or other existing support hardware with appropriate modifications. The pier base supports will have additional braces connected to the tunnel wall where judged necessary for seismic considerations.

FFTB Support

SLC Support

A variety of magnet movers are available in decommissioned systems at SLAC and can be refurbished for use in Sector 20.

5.2.3 Sector 20 Final Focus Power Supplies

The magnets in this area will be powered by DC power supplies located in the Klystron Gallery above. A 12’ x 20’ area between klystron stations 20-6 and 20-7 presently occupied by a storage enclosure can be cleared to provide an ideal location for the power supplies. Ample 480 VAC power will be available from the K-10 substation, which is scheduled to be upgraded in October 2008 as part of the LCLS project. Table 5-4 lists the field strengths at 25 GeV and corresponding power supply requirements for the Sector 20 FACET magnets. The control system components and interface modules will be salvaged from the SLC and FFTB.

Table 5-4. Sector 20 magnet power supply requirements

S (m)	Name	Angle	B'L/Br	B"L/Br	Integ. Field	Name	Data @ 25 GeV			
		(μrad)	(1/m)	(1/m2)	(kG-m)		Amp	Ω	V	kW
24.9545	Q190901T	0.	0.0377		-62.86	QE4	123	0.109	13	1.64
25.0079	Q190901T	0.	0.0377							
39.3674	QDL0	0.	0.0695		115.81	1.625Q16	154	0.089	14	2.09
39.5712	QDL0	0.	0.0695							
39.8246	Q200201T	0.	0.0417		69.44	QE4	136	0.109	15	2.01
39.8780	Q200201T	0.	0.0417							
41.0840	BDL1A	7.17			11.95	2D71.3	170	0.056	10	1.63
41.9900	BDL1B	7.17								
44.3382	QDL1	0.	0.1222		-203.70	1.625Q27.3	-159	0.151	24	3.81
44.6833	QDL1	0.	0.1222							
47.2495	BDL2A	7.17			11.95	2D68.5	177	0.054	10	1.71
48.4620	BDL2B	7.17								
49.1070	QDL2	0.	0.1361		226.82	1.625Q27.3	177	0.151	27	4.72
49.4520	QDL2	0.	0.1361							
50.0225	SXDL1	0.		2.7980	4664.76	Type A Modific.	29	0.114	3	0.09
50.3930	SXDL1	0.		2.7980						
50.9380	QDL3	0.	0.1361		226.82	1.625Q	177	0.151	27	4.72
51.2830	QDL3	0.	0.1361							
54.0280	QDL4	0.	0.1539		-256.56	1.625Q27.3	200	0.151	30	6.04
54.3730	QDL4	0.	0.1539							
57.1180	QDL5	0.	0.1361		226.82	1.625Q27.3	177	0.151	27	4.72
57.4630	QDL5	0.	0.1361							
58.0335	SXDL2	0.		2.7980	4664.76	Type A Modific.	29	0.114	3	0.09
58.4040	SXDL2	0.		2.7980						
58.9490	QDL6	0.	0.1361		226.82	1.625Q27.3	177	0.151	27	4.72
59.2940	QDL6	0.	0.1361							
60.4635	BDL3A	7.17			11.95	2D68.5	177	0.054	10	1.71
61.3330	BDL3B	7.17								
63.7178	QDL7	0.	0.1222		203.70	1.625Q27.3	159	0.151	24	3.81
64.0628	QDL7	0.	0.1222							
66.9720	BDL4A	-7.17			11.95	2D71.3	170	0.056	10	1.63

S (m)	Name	Angle	B'L/Br	B"L/Br	Integ. Field	Name	Data @ 25 GeV			
		(μrad)	(1/m)	(1/m2)	(kG-m)		Amp	Ω	V	kW
67.8780	BDL4B	-7.17								
68.7230	QFF1A	0.	0.1167		194.51	1.625Q27.3	152	0.151	23	3.47
69.0680	QFF1A	0.	0.1167							
69.6130	QFF1B	0.	0.1167		194.51	1.625Q27.3	152	0.151	23	3.47
69.9580	QFF1B	0.	0.1167							
71.3030	QFF2A	0.	0.1853		308.86	1.625Q27.3	241	0.151	36	8.76
71.6480	QFF2A	0.	0.1853							
72.1930	QFF2B	0.	0.1853		308.86	1.625Q27.3	241	0.151	36	8.76
72.5380	QFF2B	0.	-0.1853							
84.1170	QFF3A	0.	0.1217		202.84	1.625Q27.3	158	0.151	24	3.78
84.4620	QFF3A	0.	0.1217							
85.0070	QFF3B	0.	0.1217		-202.85	1.625Q27.3	158	0.151	24	3.78
85.3520	QFF3B	0.	0.1217							
86.8650	QFF4	0.	0.3672		612.17	QC2	300	0.193	58	17.40
87.8780	QFF4	0.	0.3672							
96.3780	QS1	0.	0.1492		248.82	QP3A	292	0.084	25	7.21
96.8780	QS1	0.	0.1492							
101.3780	QS2	0.	0.1285		-428.59	QP3B	503	0.084	43	21.39
101.8780	QS2	0.	0.1285							
102.8360	B5D36_1	7.00			11.670	2D33.1	358	0.03	11	3.97
103.2930	B5D36_2	7.00								

5.2.4 Sector 20 Final Focus Vacuum System

Most of the vacuum system for the Sector 20 system will be assembled with existing magnet and component chambers and will be baked and processed for high-vacuum use. The average beam current is very low and no high-power vacuum chambers are needed. Spool sections salvaged from the FFTB will be modified to fill most of the gaps, with some new adapter flanges, bellows, and tees added. Bend chambers in the dogleg section will be polished and overcoated with copper to mitigate resistive wall effects that could degrade the bunch parameters. A special Y-chamber will be fabricated and installed downstream of the dump magnet to accommodate separated particle beam and photon beam trajectories. Collimators and ion chambers will be installed at a few critical locations to protect downstream components from any unexpected beam loss.

Most of the mechanical supports for the vacuum components will be salvaged from the FFTB or SLC final focus areas or copied from designs from those areas. Vacuum valves will be added near the beginning of Sector 20 and at each end of the experimental area. The existing fast valve at the west end of Sector 20 will be active to protect the linac from any sudden loss of vacuum in the experiment area. Pump power supplies and gauge controllers will be easily accessible in racks in the Klystron Gallery above Sector 20.

The original Sector 20 accelerator pumping system will remain in place and remain active. This will preserve the vacuum integrity of the portions of the original linac remaining in Sector 20, and will be ready, if necessary, to restore the original linac configuration. A set of discrete 55L ion pumps distributed along the beam line will ensure a vacuum level of about 10^{-6} torr.

5.2.5 Sector 20 Final Focus Instrumentation and Controls

The Sector 20 final focus instrumentation is shown in Figure 5-14. A suite of existing beam position monitors, profile monitors, wire scanners, beam loss monitors, and other specialized diagnostic devices will be installed along the beam line to monitor and control the beam and protect the machine hardware from excessive beam loss.

The controls for FACET will build on the fully tested and mature systems developed for the SLC and PEP-II facilities. All the necessary CAMAC modules and associated crates and interface electronics exist at SLAC and will be reused. The software tools and utilities needed to operate these devices all exist and have been maintained. FACET will require new entries in the control system database and a few new software control panel files, but these are well understood and easily implemented. Some costs will be incurred in moving, reconnecting, and testing interface chassis and control modules, but these are relatively small costs for this project.

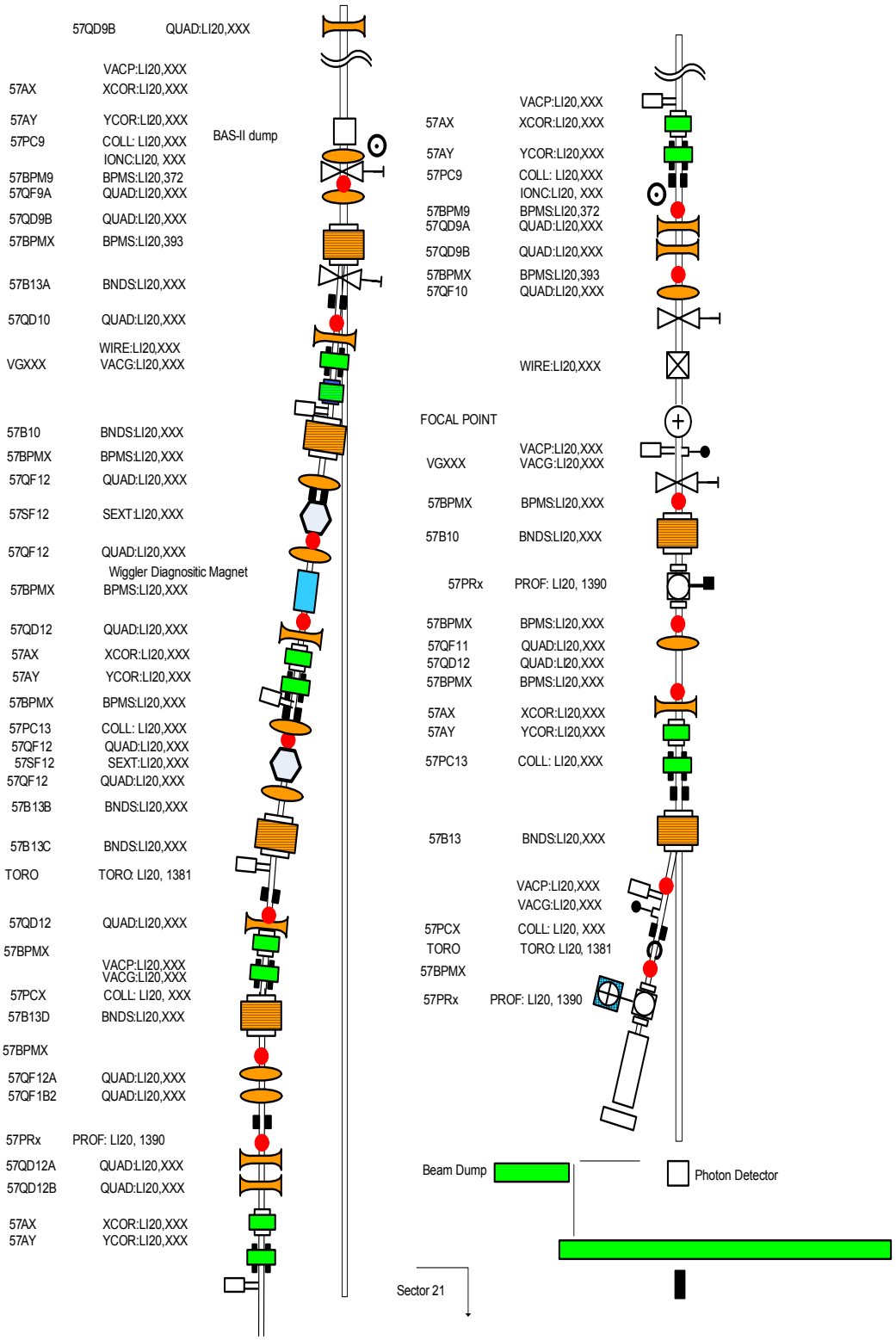

Figure 5-14. Sector 20 instrumentation.

5.2.6 Sector 20 Final Focus Experimental Area

The space available for experimental equipment starts at a vacuum valve immediately following the last final focus quadrupole before the focal point. The nominal focal point will be 2 m downstream of this quadrupole, and the beam dump will be another 23 m downstream of this point. This drift distance will accommodate a wide variety of experimental arrangements to suit the needs of users and will include a magnetic dump line spectrometer for the outgoing beam. A cross-sectional view of this section of beam line is provided in Figure 5-4.

The Klystron Gallery above the Sector 20 tunnel will house the power supplies for the focusing magnets and the electronics for the instrumentation and control system. The Klystron Gallery also has space in this area for any experimental equipment that must be near to the focal point but be continuously accessible to the experimenters when the beam is on. Existing penetrations at twenty-foot intervals provide paths for direct connections between apparatus in the Klystron Gallery and apparatus in the tunnel directly below.

Figure 5-15 is a conceptual layout of an advanced acceleration experiment involving a plasma oven set up on an optical table at the focal point. With this table in place, experimental apparatus can quickly be installed, aligned, and reconfigured as needed. Also shown are two magnets downstream of the focal point that will be used for measuring the energy of the outgoing beam and forming an image of the focal point at the second focus in the dump line. The optical table and plasma oven are also shown in the tunnel cross section view in Figure 5-4.

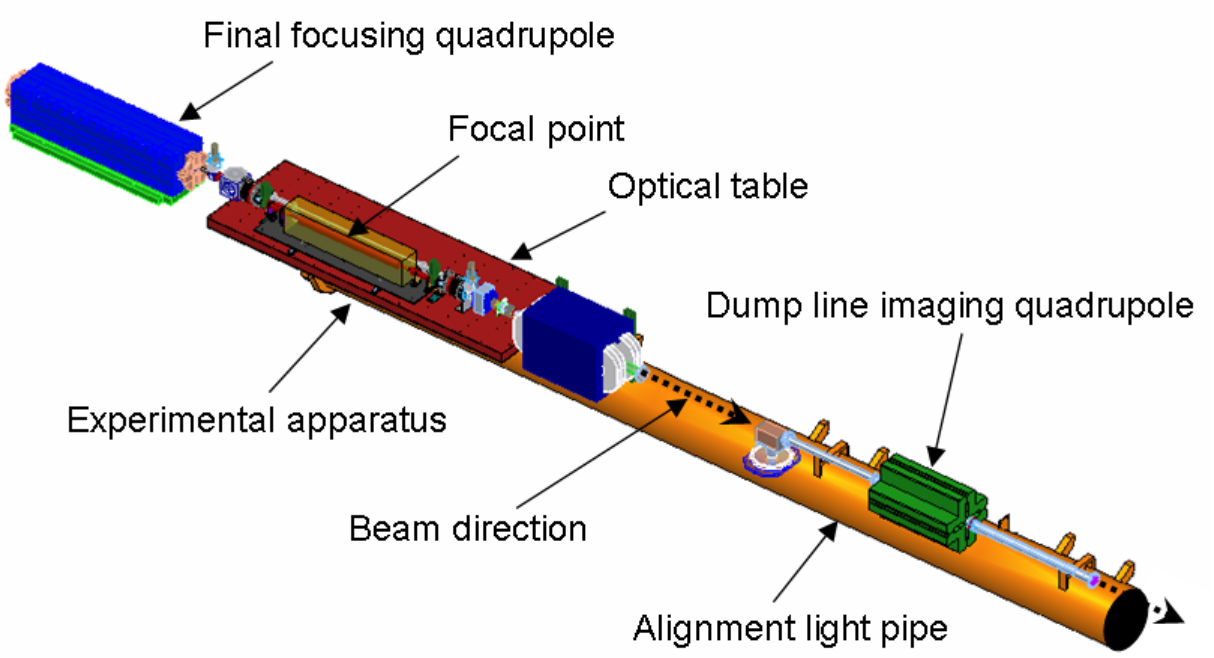

Figure 5-15. Proposed arrangement of experimental apparatus for a plasma wakefield experiment. A lithium plasma oven is shown on a general-purpose optical table, followed by magnetic spectrometer apparatus in the outgoing dump line.

5.2.7 Sector 20 Final Focus Beam Dump

The beam dump will consist of an air cooled beam dump module surrounded by steel shielding. It will be supported by a structure similar to the structure that supports the Sector 10 compressor magnets. Shielding around the dump will be constructed from a stack of steel plates clamped together using threaded rods. The beam dump module will be copper, cooled through conduction to the surrounding steel. The system will include a burn through monitor system designed to shut down the linac in the event of a dump failure. The dump will be designed to allow the addition of a water-cooling system if an experiment requires a particularly high average beam power.

5.2.8 Sector 20 Final Focus Shielding Wall

A shielding wall will be constructed in the linac tunnel between the dump and the LCLS injector area. The wall will consist of two overlapping but separated sections with a passageway between the two areas. A personnel protection system (PPS) controlled gate will limit travel between the areas during LCLS operation. The walls will be constructed by stacking concrete shielding blocks in the tunnel, with special pieces to fit around the alignment light pipe and various cable penetrations. In addition, a movable shielding plug assembly will be incorporated into the laser alignment pipe below the linac support girder to allow for the use of this alignment system when needed. The plug assembly will be copied from a similar unit near the west end of the accelerator, which is shown in Figure 5-16.

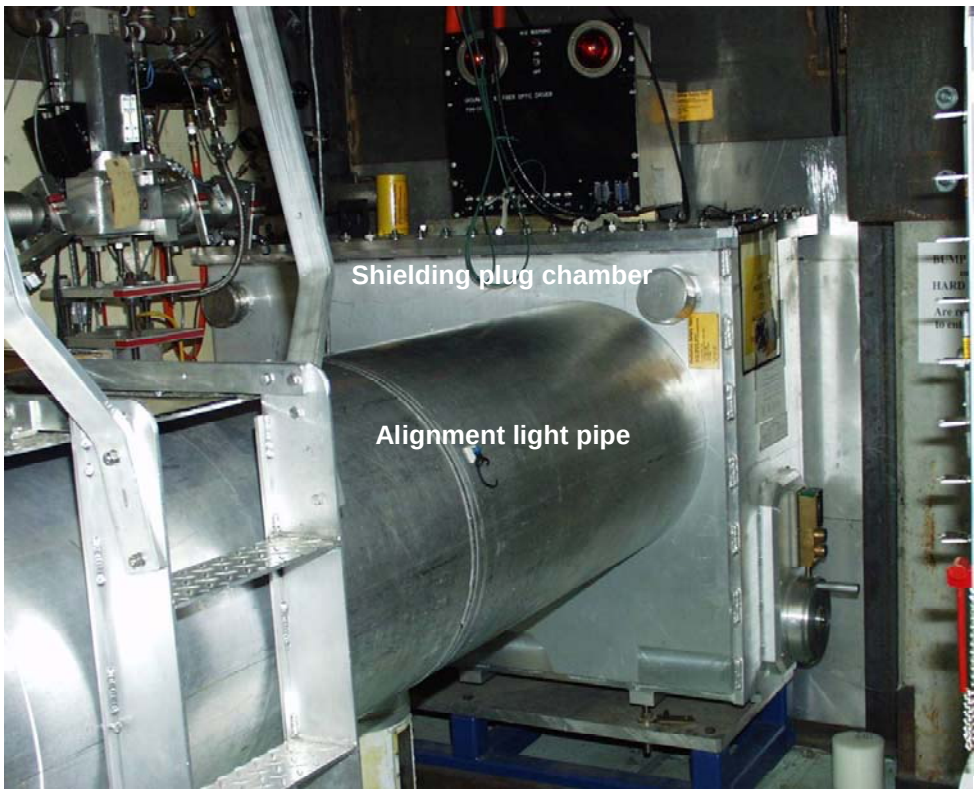

Figure 5-16. Movable radiation shielding plug in the alignment lightpipe near the west end of the linac. This design will be copied for the shielding wall to be installed at the end of Sector 20.

5.2.9 Sector 20 Final Focus Personnel Protection System

Each sector of the linac tunnel is accessible by way of a 35 foot ladder mounted in a vertical penetration. In addition, several sectors, including Sectors 14 and 19, have large equipment access shafts which can be used to lower large objects into the tunnel with a portable crane. The Sector 19 access shaft is visible behind the yellow fence in Figure 5-17. Figure 5-18 is a photograph looking down the shaft while equipment is being raised from the linac to the surface on a pallet. As part of this proposal, a stairway will be constructed in the Sector 19 shaft to facilitate easy personnel access to the tunnel near the ASF experimental setup area. A similar stairway was installed in an identical shaft in Sector 24 to provide access to LCLS components in the last third of the linac and this has worked out very well. A new entrance door will be installed at the top of the Sector 19 stairway and equipped with standard PPS provisions to allow user access under controlled conditions. The PPS-controlled entrance door at Sector 24 is shown in Figure 5-19, along with the associated status display lights, key bank, and telephone. The stairway leading to the tunnel below is shown in Figure 5-20. The new PPS features and stairway proposed for Sector 19 will be identical to the arrangement in Sector 24. Personnel will walk about 210 feet down the linac tunnel from the foot of the access stairway to the ASF experimental area.

Figure 5-17. Equipment access shaft in Sector 19 along the south road of the Klystron Gallery. A pallet of equipment is being lifted out of the shaft with a portable crane. Identical access shafts exist at five-sector intervals along the Klystron Gallery.

Figure 5-18. Pallet of equipment being raised through the equipment shaft in Sector 19 near the ASF focusing system. Identical shafts exist at five-sector intervals along the linac.

With a stairway installed in the Sector 19 shaft, the nearest equipment shaft to the ASF experimental area will be in Sector 14. This shaft will remain available for lowering large or heavy objects into the linac tunnel. Equipment lowered into Sector 14 can be easily moved on carts to Sector 20, a distance of about 2000 feet. Moving equipment in this way is standard practice in the linac tunnel.

The PPS system for the linac tunnel as currently configured requires that the entire tunnel be vacated and locked as a condition for turning on power to the klystrons. This system will be modified to separate the linac tunnel into two functionally independent zones in such a way that persons will be able to enter the linac tunnel in Sector 20 or any sector upstream of this point while the LCLS is operating in Sector 21 and beyond. These new features will require several changes to the PPS system. An electronically locked and monitored passage will be provided in the new shielding wall to be installed between Sectors 20 and 21.

Figure 5-19. Personnel access door leading from the Klystron Gallery to the linac tunnel in Sector 24. The stairway and PPS controls will be copied in Sector 19.

The klystron stations in Sectors 19 and 20, including four klystrons needed for LCLS operation, are powered by the same variable-voltage substation, which now must be interlocked off as a condition for any tunnel entries. To overcome this limitation, individual disconnect switches will be configured in each of the klystron modulators in this sector-pair, and the PPS logic will modified to ensure that the appropriate klystrons are off to allow access to the ASF area while the LCLS is operating. This change is relatively simple, but must be done with rigorous formality including full testing and certification.

Figure 5-20. Existing stairway at Sector 24, which will be duplicated at Sector 19 for ASF users.

5.2.10 Sector 20 Final Focus Experimental Counting House

The large rectangle on the north side of the Klystron Gallery in Figure 5-1 shows the proposed location of a 20 by 40 foot building to serve as a counting house for data acquisition systems, computers or other equipment needed for conducting and monitoring ASF experiments. The Klystron Gallery also offers space for experimenter data acquisition equipment. A 12 by 25 foot room could be accommodated between klystrons 20-5 and 20-6, or between klystrons 20-6 and 20-7, above the experimental area in the linac tunnel below. Such an equipment area is indicated by the smaller red rectangle near the final focus location in Figure 5-1. Figure 5-21 showing a similar existing arrangement for the LCLS The nearest restroom for both experimental support buildings is located in the Klystron Gallery near the Sector 20 alcove. Paved parking space is available adjacent to the Klystron Gallery for experimenters who choose to bring their data acquisition equipment in a trailer or similar vehicle.

Figure 5-21. Enclosure for precision LCLS equipment in the Klystron Gallery. A structure similar to this will be constructed near klystron station 20-6. Data acquisition systems or other electronic equipment that must be near the beam could be set up here, directly above the experiment area in the linac tunnel 25 feet below.

5.2.11 Positron Compressor Technical Description

A bunch compressor system was installed in Sector 10 of the linac in 2002 and was used in conjunction with previously existing accelerator systems to compress electron bunches to less than 100 fsec as they were delivered to experimenters in the FFTB tunnel. The key components of the electron compressor system are four identical dipole magnets, which together form a magnetic chicane. Upstream of this chicane, the linac RF system is tuned to introduce a correlation between the momentum of the electrons and their longitudinal position within the bunch, such that the higher momentum electrons are shifted toward the trailing end of the bunch. As the bunch passes through the chicane, the electrons with lower momentum follow a longer path, allowing the higher momentum electrons to catch up, and resulting in a significantly shorter bunch.

This system works well for electron bunches, but cannot be used simultaneously for positrons. This lack of symmetry comes about because positrons are produced by first accelerating electrons, which must pass through the same section of the linac. The compressor system as it currently exists allows only negatively charged particles to pass. This limitation can be overcome by installing two more dipole magnets identical to the others, but on the opposite side of the linac. The support structures that were installed for the electron compressor can also support the additional hardware needed for positrons with only minor modifications. New vacuum chambers will be needed to pass the diverging and recombining beam paths of the electrons and positrons, and some additional instrumentation will be required to facilitate steering and focusing the two beams simultaneously.

5.2.12 Positron Compressor Design

The positron compressor is a mirror-image of the electron compressor, which has been used successfully to support several experiments over the past five years. This proven design can easily be extended to compress positrons as well as electrons. The only technical features that introduce new complexity will be the use of non-identical dipole magnets, powered in series, to form the four-bend chicane, and the differing transverse parameters of the electron and positron beams at the entrance to the compressor section. Any differences between the two magnet designs can be accommodated with trim windings, and optical differences between the beams can be accommodated by optimizing the optical match for the positron beam. The parameters of the electron beam used to generate positrons are not critical for this purpose.

5.2.13 Positron Compressor Layout

The compressor layout is shown schematically in Figure 5-22. A pair of new dipole magnets will serve in the first and fourth positions of both the left and right chicanes.

5.2.14 Positron Compressor Components

In this design, the existing magnets in the first and fourth positions of the chicane will be used in the second and third positions on the positron side of the new configuration to form a mirror-image of the electron side. Two new dipole magnets will then be needed to replace the first and fourth magnets, which are centered on the linac axis and bend electrons and positrons in opposite directions. The two new dipoles will require wider pole tips and vacuum chambers than the originals. Calculations have shown that such magnets can be built and still powered in series with the other dipoles. These magnets are each 1.8 m long, with a gap height of 50 mm, and a field of 1.6 T.

The support structure under the existing chicane magnets was constructed to be symmetric about the plane of the linac, in anticipation of eventual addition of two more dipoles to compress positron bunches. The new supports and other mechanical devices needed for the compressor system will be direct copies of existing designs.

The existing chicane power supply has insufficient voltage to power all six dipoles in series. Another power supply, salvaged from SPEAR-II, could be refurbished and relocated to Sector 10 for this application. Additional small power supplies will be needed to power trim windings on the dipoles to correct for tracking differences between the two magnet designs.

The vacuum components needed for the positron side of the compressor chicane will be mirror-image copies of the components on the electron side.

The new instrumentation for the positron compressor modification will be copies of the corresponding devices in the electron side of the chicane. Most of these devices will be salvaged from the FFTB or SLAC final focus system.

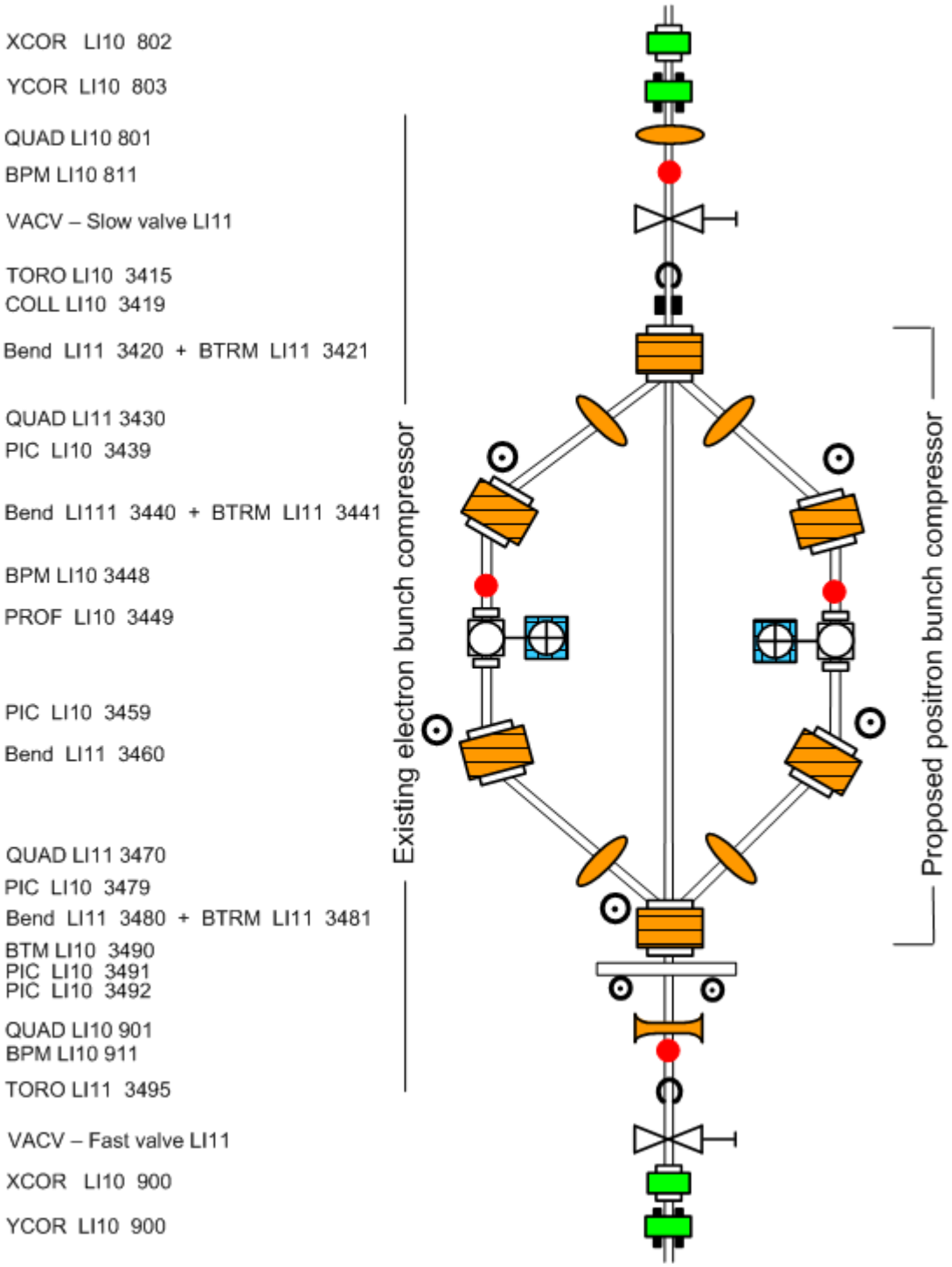

Figure 5-22. Positron compressor layout.

5.3 ESA Electron Bypass Line (EBL) Technical Description

5.3.1 EBL Design

The PEP-II HER injection bypass line will be extended to inject a beam into the A-Line leading to End Station A as shown in Figure 5-23. Conceptually, the A-Line will be extended upstream to a point where it intersects the downstream extrapolation of the bypass line. Four bend magnets and a set of quadrupoles will be installed to match the trajectories and optical functions of the two systems.

The existing 12 GeV PEP-II NIT beam line (dashed blue line), which bypasses the linac from Sector 10 through Sector 30 to supply electrons for injection into the HER ring, is perfectly suited for this continuation into the A-line. This beam line is offset on the south side of the linac by approximately the same distance as the offset (0.62 m) of the A-line at the entrance to the D-10 collimator/dump assembly on the north. Two horizontal bend magnets, referred to as BBH1 and BBH2, provide a bend of 0.25° each and are separated by the negative of the optical identity matrix to cancel the dispersion through the subsequent drift. The A-line already has dispersion matching capability to accommodate this connection. A focusing lattice consisting of two 90° FODO cells between the two magnets will provide the desired matrix transformation. The separation of the effective bending points of the two magnets is 43.2 m, and the resulting length of each FODO cell is 21.6 m. The FODO cell lattice extends upstream to provide a 2π phase advance. Two vertical bending magnets, BBV1 and BBV2, are also needed to lower the elevation of the ESA Electron Bypass Line (EBL) 0.64m to the elevation of the A-line. The optical transformation between the two magnets ensures that the vertical dispersion outside the intervening region is zero.

The linac is pitched downward by about 47 feet in its length of 10,000 feet. To compensate for this downward pitch and make the A-line perpendicular to local gravity in ESA, the entire beam line is rolled (clockwise as seen by the beam) about the linac axis by 10.4 milliradians. After a horizontal bend of 24.5° in this rolled plane, the vertical pitch is zero. While the linac and A-line have the same elevation at the point where this bend starts, the A-line is about 7 mm higher than the linac at D10. The first horizontal bend magnet, BBH1, will be about 9 mm below the elevation of the linac. Two small vertical bend magnets placed near the horizontal bending magnets will provide a total vertical deflection of 125 μ-radians. The dispersion from these two vertical bends will cancel each other.

The lattice parameters are further constrained by the requirement to match the geometry with a minimum number of bending magnets without generating dispersion. The EBL FODO cell parameters are: L_{Cell} = 21.6 m, quadrupole spacing = 10.8 m, β_{max} = 36 m, β_{min} = 6 m, $\mu_{x,y}$ = $\pi/2$, focal length = ± 7.54 m, GL = ± 53.0 kG at the nominal energy of 12.0 GeV. The position of the entire ensemble of quadrupoles can be chosen to minimize the interference with other existing component of the linac and LCLS without affecting the cancellation of dispersion. The placement of elements was adjusted in three dimensions using the Solid Edge design program to arrive at a solution that avoided any major conflicts.

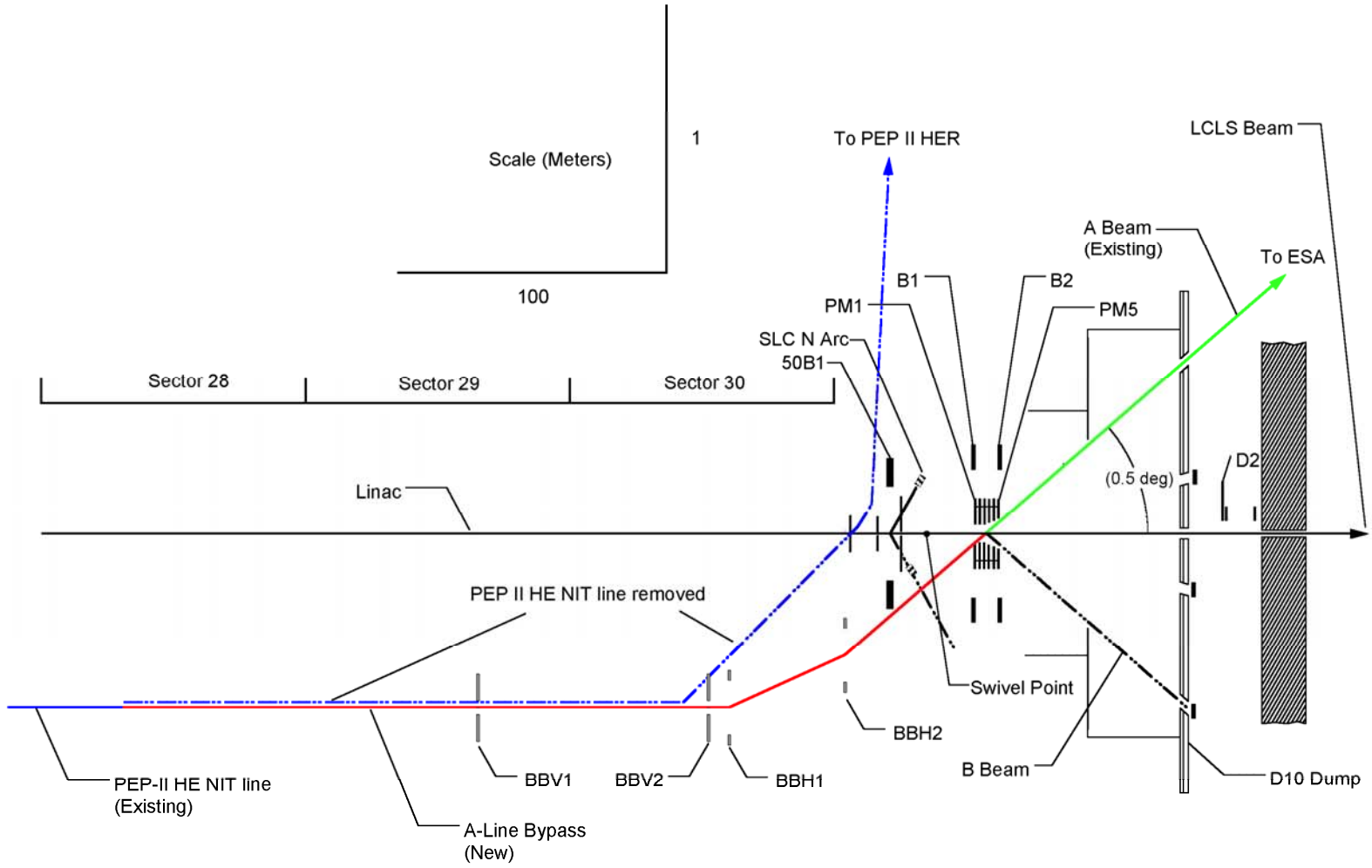

Figure 5-23. Plan view of proposed transition from NIT to EBL. *Note: Unequal horizontal and vertical scales, 100:1.*

5.3.2 EBL Optical Solution for Matching to NIT and A-Line

The linac optical match to the SLC arcs was defined at a particular point in the BSY, labeled "Swivel Point" in Figure 5-23. The beam parameters at this point have been the established starting values for setting up beams to other experiments in the past. To duplicate this optical match from the EBL to the A-line, matching quadrupoles must be provided in the EBL line. The placement of the last horizontal bend magnet BBH2 has been chosen to fit the geometry, as described earlier, and also to allow adequate transverse and longitudinal space for the necessary quadrupoles. Four independently powered quadrupoles downstream of BBH2 will provide adequate degrees of freedom to optically match the EBL lattice parameters to those of the swivel point.

The NIT beam line and new EBL lattice are coaxial and separated by a drift region of about 130 m. Four matching quadrupoles will be installed in this drift to match the NIT FODO cell parameters to the EBL parameters described above.

The EBL consists of four bending magnets, eight matching quadrupoles and fourteen lattice quadrupoles as listed in Table 5-5. Existing magnets suitable for each of these functions are also listed in Table 5-5.

Table 5-5. EBL magnets

Bends						
Element Name	**Type**	**Bend Angle (degrees)**	**BL (kG-m) at 12 GEV**	**Existing Magnet Type**	**Length (m)**	**Aperture (mm)**
BBV1, BBV2	Vertical	0.250	1.749	1.0D38.37	0.975	25.4
BBH1, BBH2	Horizontal	0.436	3.045	2.0D38.37	0.949	50.8

Quadrupoles						
Element Name	**Type**	**Focal Length (m)**	**GL (kG) at 12 GeV**	**Existing Magnet Type**	**Length (m)**	**Aperture (mm)**
QB15	QD	-52.9	7.6	2Q4	0.1	50.8
QBM01	QF	31.9	38.3	2Q20	0.5	50.8
QBM02	QD	-17.6	21.1	2Q20	0.5	50.8
QBM03	QF	11.7	14.1	2Q20	0.5	50.8
QBM04	QD	-6.7	8.1	2Q20	0.5	50.8
QBL05, 07, 09, 11, 13, 15, 17	QF	7.54	53.1	2Q20	0.5	50.8
QBL06, 08, 10, 12, 14, 16, 18	QD	-7.54	53.1	2Q20	0.45	20.6
QBM19	QD	10.6	12.7	0.813Q17.7	0.45	20.6
QBM20	QF	-7.0	8.4	0.813Q17.7	0.45	20.6
QBM21	QD	5.5	6.6	0.813Q17.7	0.45	20.6
QBM22	QF	-6.0	7.2	0.813Q17.7	0.45	20.6

Figures 5-24, 5-25, 5-26, and 5-27 illustrate the optical functions for the complete EBL system. Figures 5-24 and 5-25 show the beta and dispersion functions covering a length of 2250 meters from Sector 12 of the linac to the Beam Dump East, the termination of the A-line. The new connecting region, EBL, is between 1500 m and 1850 m. The A-line optical functions shown were used successfully a few years ago in the configuration for Experiment E-158. Figures 5-26 and 5-27 show only the new components for the proposed EBL, which match the β_{max} = 350 m, β_{min} = 59 m of the NIT to the $\beta_x = \beta_y$ = 14 m at the match point.

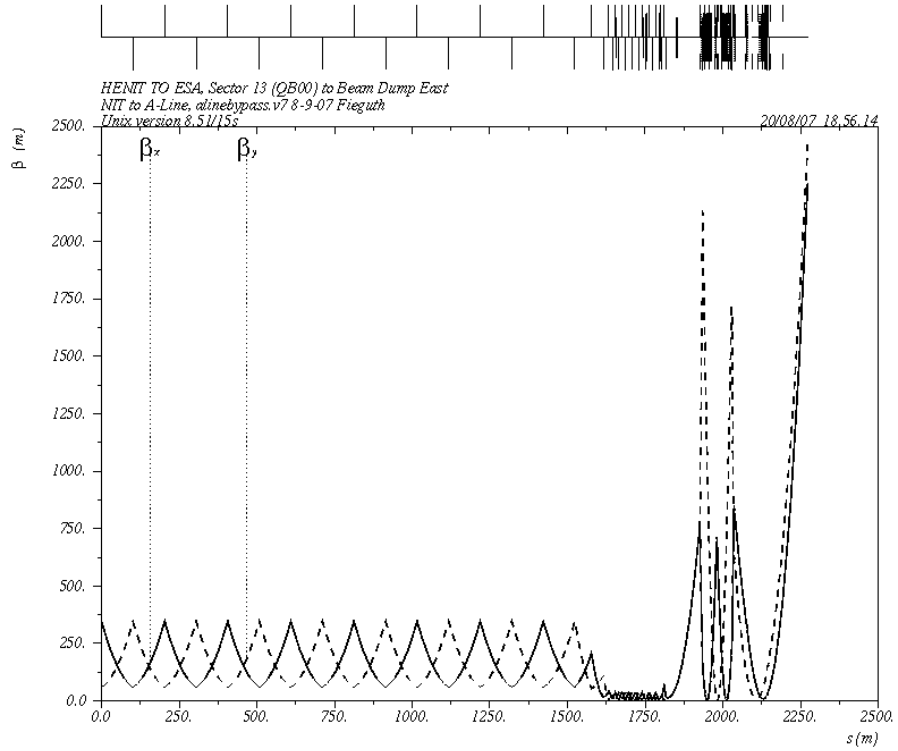

Figure 5-24. Beta functions of the EBL system, including the matching section and bends connecting the NIT lattice to the A-line, and ending at Beam Dump East.

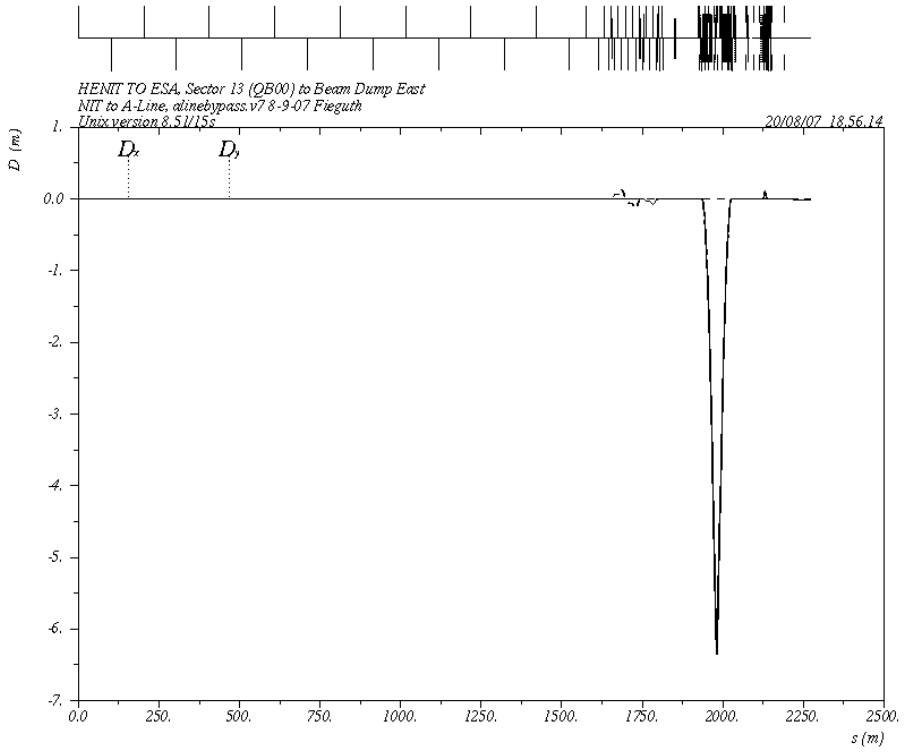

Figure 5-25. Dispersion functions of the EBL system, including the bends connecting the NIT lattice to the A-line, and ending at Beam Dump East.

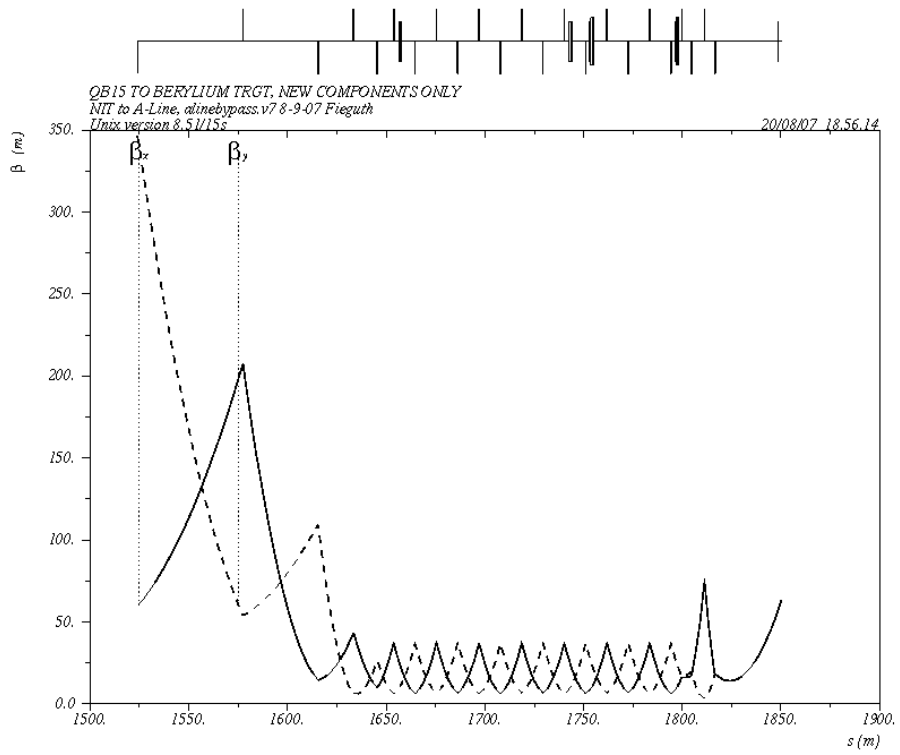

Figure 5-26. Beta functions of the proposed new section of the EBL.

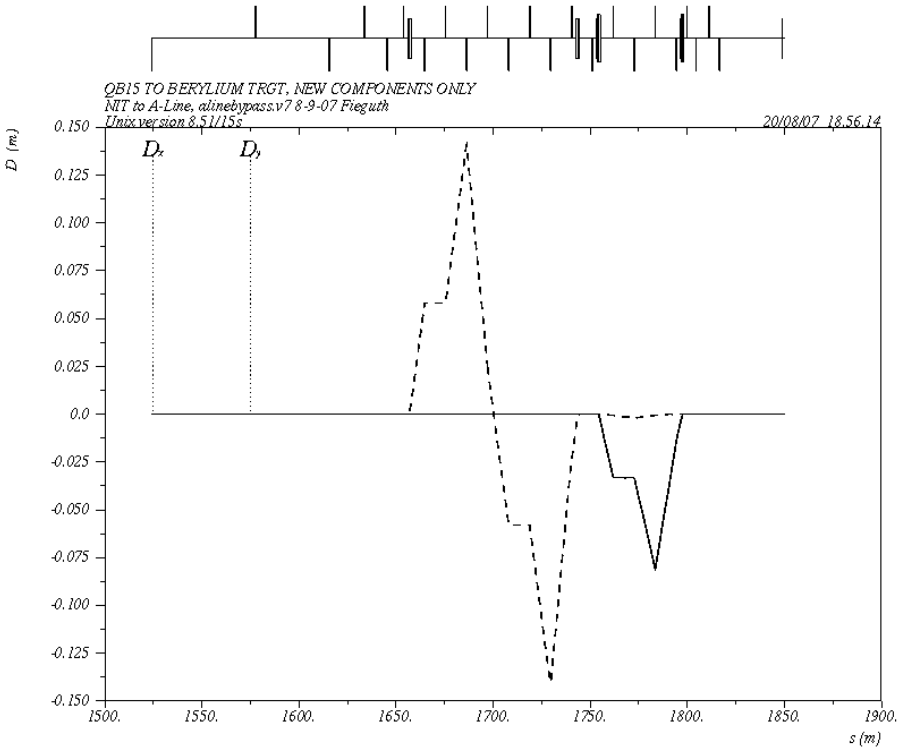

Figure 5-27. Dispersion functions of the proposed new section of the EBL.

5.3.3 Reusing Existing Components

The lattice described above is very similar in all respects to the existing lattice in the arc region of the PEP-II high energy electron injection line. The parameters of the three lattices, the PEP-II NIT line in the linac housing, the PEP-II transport arc lattice, and the proposed EBL, are listed in Table 5-6. Most components needed for the EBL, including bend magnets, quadrupoles, orbit corrector magnets, beam position monitors and their support structures, can be salvaged from other areas of the PEP-II injection transport system and relocated to new positions for the EBL. In many cases the modifications to the support structures involves only lengthening or shortening the cylindrical pedestals. PEP-II power supplies with their existing control systems can also be used, in some cases without the need for relocation; it will be only necessary to re-cable them to the new locations of the components. Vacuum pipes and some diagnostic instruments will require modification. Figures 5-28 and 5-29 show typical existing magnets, quadrupoles, beam position monitors and orbit correctors and how they may be used for the EBL. Figure 5-30 is an isometric view generated by Solid Edge showing how conflicts are avoided between EBL components and critical linac and LCLS components.

Table 5-6. FODO lattice parameters for PEP-II and the proposed EBL

Parameter	Unit	PEP-II HENIT	PEP-II Arc Lattice	Proposed EBL
L_{cell}	m	203.2	17	21.6
Quad spacing	m	101.6	8.5	10.8
β_{max}	m	350	28.5	36
β_{min}	m	59	5	6
Focal length	m	72	5.9	7.5
Phase Advance		$\pi/2$	$\pi/2$	$\pi/2$
GL	kG	4.2 at 9 GeV	51 at 9 GeV	53 at 12 GeV

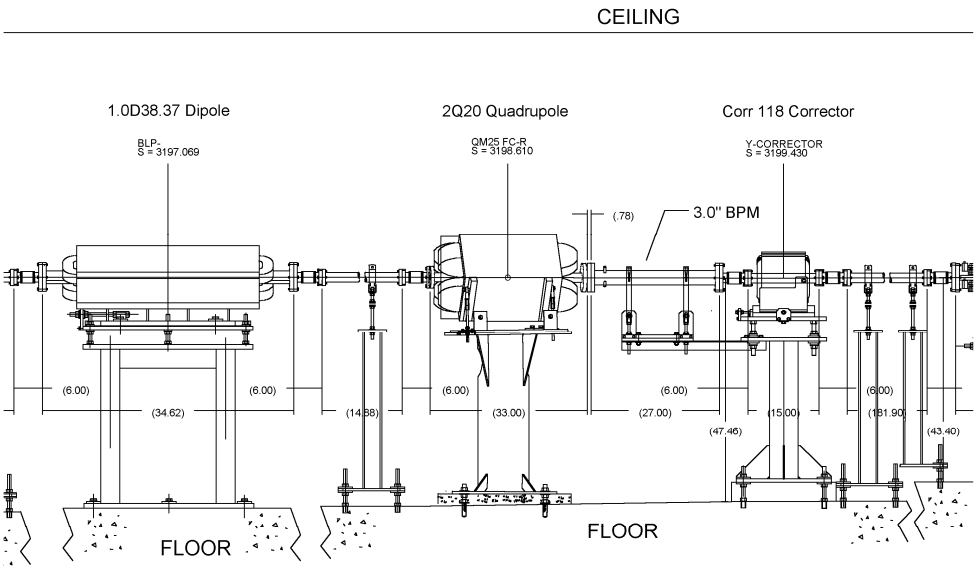

Figure 5-28. Typical PEP-II transport arc lattice components, showing a bend magnet, quadrupole, BPM, corrector magnet and supporting stands. Modification of the supports will make them suitable for use in the EBL.

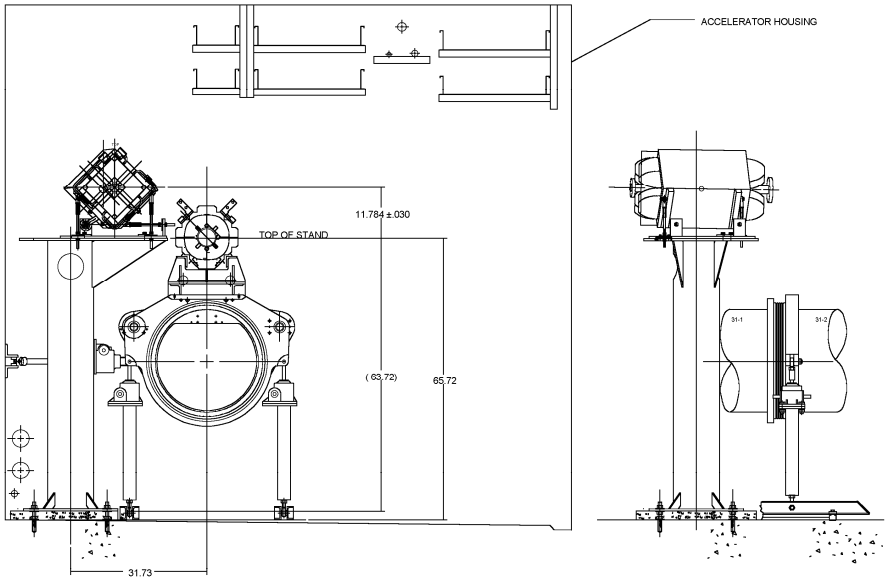

Figure 5-29. A typical tunnel cross section, looking downstream near the beginning of the PEP-II injection transport arc. The pedestals and mounting hardware will be modified and moved to the other side of the linac to support the EBL elements.

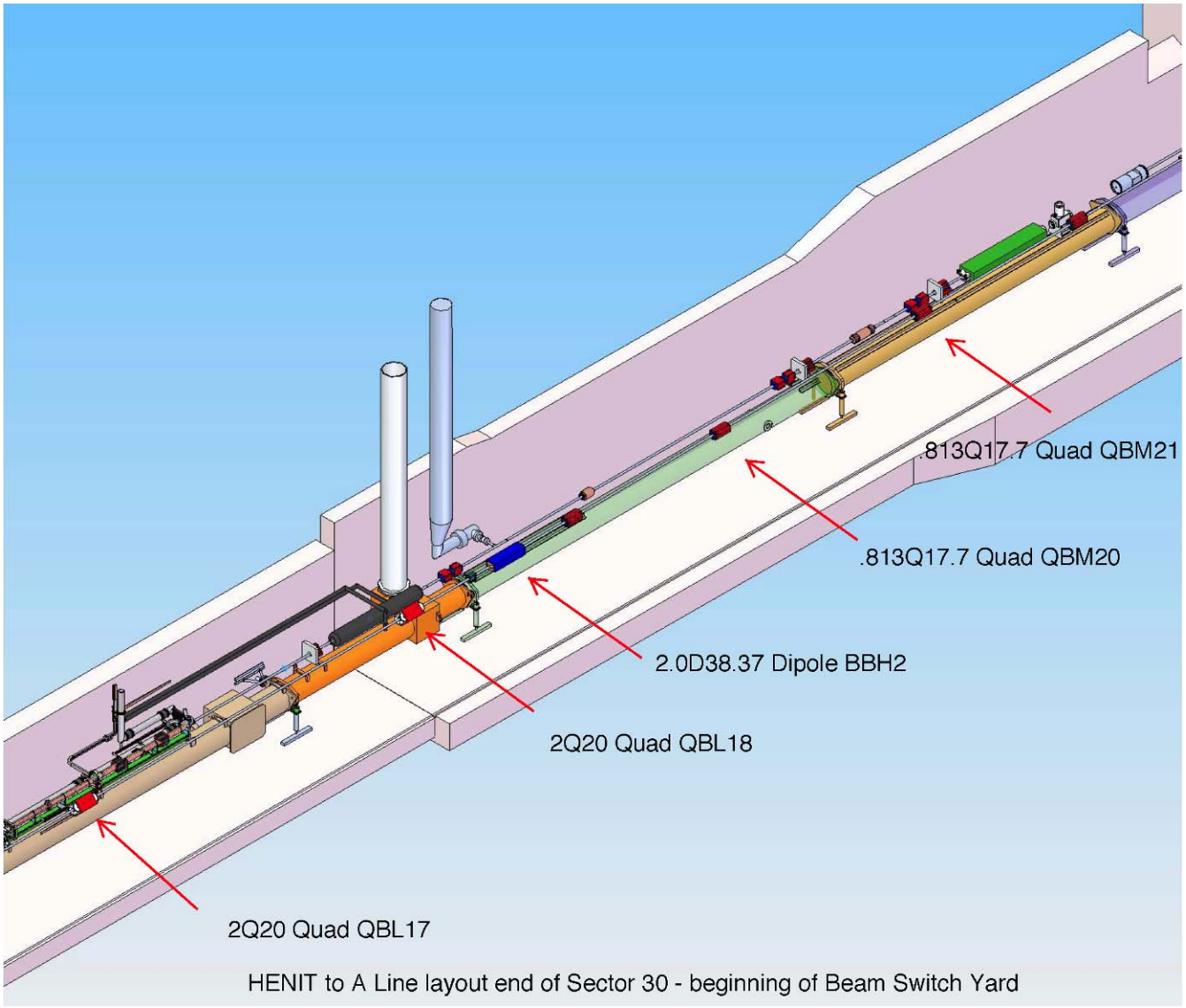

Figure 5-30. Solid Edge model of the region at the end of the linac, showing RF waveguides, vacuum manifolds, the refrigerated baffle, and critical components of both the LCLS and FACET facilities.

5.3.4 Emittance, Beam Size and Beam Stay Clear

The beams to ESA must vary in energy, intensity, and repetition rate in order to meet the various needs of the different experiments. Both damped short pulse length beams from the damping ring and long pulse beams direct from the CID injector will be available to users. Nominal values for the parameters of these two sources are compared in Table 5-7. Included in this table are the beam emittances and monochromatic and chromatic beam sizes. These rms values were used to determine the Beam Stay Clear (BSC) specifications for the vacuum chambers. In general, the maximum beam sizes are sub-millimeter, and thus the BSC specification will be easily met by the existing 50.8 mm bore quadrupoles, 50.8 mm vacuum pipes, and the 76.2 mm diameter beam position monitors from the PEP-II injection arc lattice.

Table 5-7. Typical beam parameters expected for beams transporting through NIT and EBL to ESA

						HENIT		Proposed EBL	
Source	**Beam Current (electrons)**	**Rep Rate (Hz)**	**Beam Power (kW) 12 GeV**	**Invariant Emittance (m-rad)**	**Geometric Emittance At 12 GeV (m-rad)**	**σ_{max} (mono-chromatic) (μm)**	**σ_{min} (mono-chromatic) (μm)**	**σ_{max} (mono-chromatic) (μm)**	**σ_{min} (mono-chromatic) (μm)**
Damping Ring	2×10^{10}	60	2.5	$\gamma\varepsilon_x = 5\times10^{-5}$	$\varepsilon_x = 2\times10^{-9}$	860	350	280 500*	110
				$\gamma\varepsilon_y = 0.5\times10^{-5}$	$\varepsilon_y = 2\times10^{-10}$	270	110	90 700*	40
CID Gun Long pulse	2×10^{11}	60	25	13×10^{-5}	5.5×10^{-9}	1400	570	450 830*	180

* For $(\delta p/p)_{rms} = 0.005$

5.3.5 Orbit Correctors and Beam Position Monitors

The orbit correctors and beam position monitors (BPMs) for the existing PEP-II transport arc system will be adequate for use in the EBL. In the PEP-II design, the orbit correctors are located only at quadrupoles where $\beta = \beta_{max}$. This means that X correctors are located near horizontally focusing quadrupoles and Y correctors are located near defocusing quadrupoles. Such an arrangement is shown in Figure 5-28, where a quadrupole is followed by a BPM followed by a corrector. The random walk beam offset at the last lattice quadrupole due to an alignment tolerance of δx_{rms} = 500 microns of the focusing quadrupoles is estimated to be Δx_{rms} = 5 mm. The beam offset due to the defocusing quadrupoles will be Δx_{rms} = 2 mm. A single corrector is capable of moving the beam position by about 5 mm at the following BPM. This is more than sufficient to correct for misalignments. Given these estimates, the PEP-II arc orbit corrector magnets (Type Cor 118, as shown in Figure 5-28) have strength about 2.5 times greater than required.

5.3.6 Power Supplies

The power supplies for the PEP-II transport arc magnets are located in the Klystron Gallery at Sector 30. This is an ideal location for supplying power to the EBL magnets most of which require shorter cable runs than those existing. In Tables 5-8 and 5-9 the PEP-II power supplies have been paired with appropriate EBL magnets. Noteworthy is the fact that these power supplies when so paired are mainly capable of providing current for 24 GeV. This may become important in the future if the extraction point from the linac is moved from Sector 10 to Sector 18. The controls for these power supplies are all in place and operating.

5.3.7 Beam Diagnostics and Instrumentation

An assortment of wire scanners, toroid current monitors, and protection ion chambers will be needed to monitor the beam, in addition to the BPMs described above. Figures 5-31 and 5-32 are schematic layouts of the EBL line showing a tentative placement of most components.

Table 5-8. EBL bend magnet power supplies matched to existing power supplies

Proposed Electron Bypass Line (EBL)						Existing Power Supplies		
Power Supply Name	**Element Name**	**Type**	**Existing Magnet Type**	**Required Current (Amps) at 26 GeV**	**Volts**	**Power Supply Name**	**Element Name**	**Power Supply Type (A/V)**
PSBBV	BBV1, BBV2 in series	VERT	1.0D38.37	209	23	LGPS 6155	BV1A	EMI/ESS 40/375
PSBBH	BBH1, BBH2 in series	HORZ	2.0D38.37	248	28	LGPS 6195	BV1B	EMI/ESS 40/375

Table 5-9. EBL quadrupole power supplies matched to existing power supplies

Proposed Electron Bypass Line (EBL)						Existing Power Supplies		
Power Supply Name	**Element Name**	**Type**	**Existing Magnet Type**	**Required Current (Amps) at 26 GeV**	**Volts**	**Power Supply Name**	**Element Name**	**Power Supply Type (A/V)**
PSQB15	QB15	QD	2Q4	tbd	tbd	tbd	tbd	tbd
PSQBM01	QBM01	QF	2Q20	40	5	LGPS 6320	QM25	EMI/ESS 20/125
PSQBM02	QBM02	QD	2Q20	60	7	LGPS 6330	QM26	EMI/ESS 20/125
PSQBM03	QBM03	QF	2Q20	85	10	LGPS 6340	QM27	EMI/ESS 20/125
PSQBM04	QBM04	QD	2Q20	160	18	LGPS 6310	QM24	EMI/ESS 40/250
PSBQF	QBL05, 07, 09, 11, 13, 15, 17 in series	QF	2Q20	140	110	LGPS 6120	QA08-32	EMI/ESS 100/100

Proposed Electron Bypass Line (EBL)						Existing Power Supplies		
Power Supply Name	**Element Name**	**Type**	**Existing Magnet Type**	**Required Current (Amps) at 26 GeV**	**Volts**	**Power Supply Name**	**Element Name**	**Power Supply Type (A/V)**
PSBQD	QBL06, 08, 10, 12, 14, 16, 18 in series	QD	2Q20	140	110	LGPS 6130	QA09-23	EMI/ESS 100/100
PSQBM19	QBM19	QF	.813Q17.7	38	5	LGPS 6350	QM28	EMI/ESS 20/125
PSQBM20	QBM20	QD	.813Q17.7	58	7	LGPS 6360	QM29	EMI/ESS 20/125
PSQBM21	QBM21	QF	.813Q17.7	74	9	LGPS 6370	QM30	EMI/ESS 20/125
PQBM22	QBM22	QD	.813Q17.7	68	8	LGPS 6380	QM31	EMI/ESS 20/125

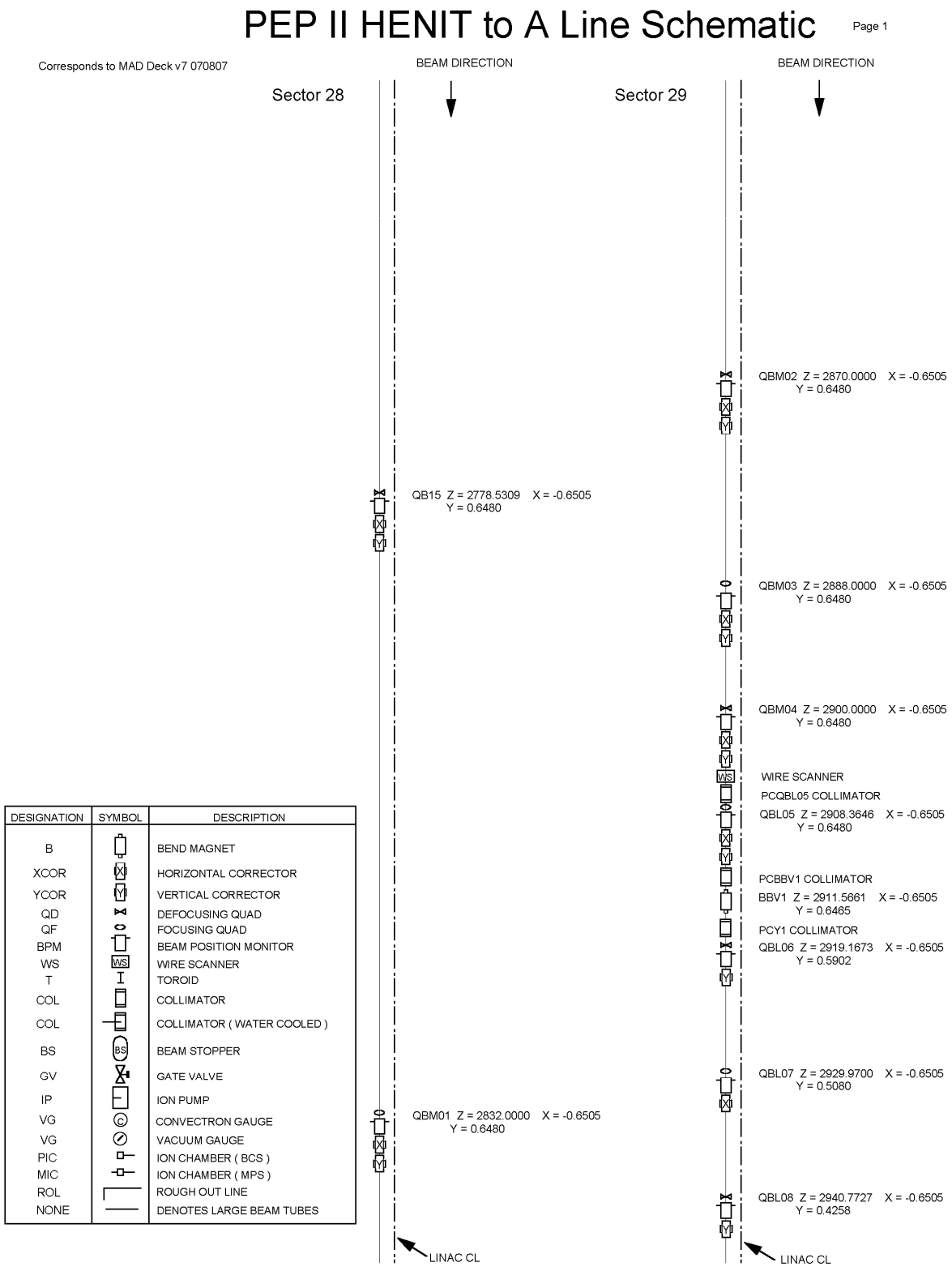

Figure 5-31. Schematic (page 1of 2) showing the locations of components starting with the last NIT quadrupole QB15, located 0.65m to the south and 0.648m above the linac accelerating waveguide.

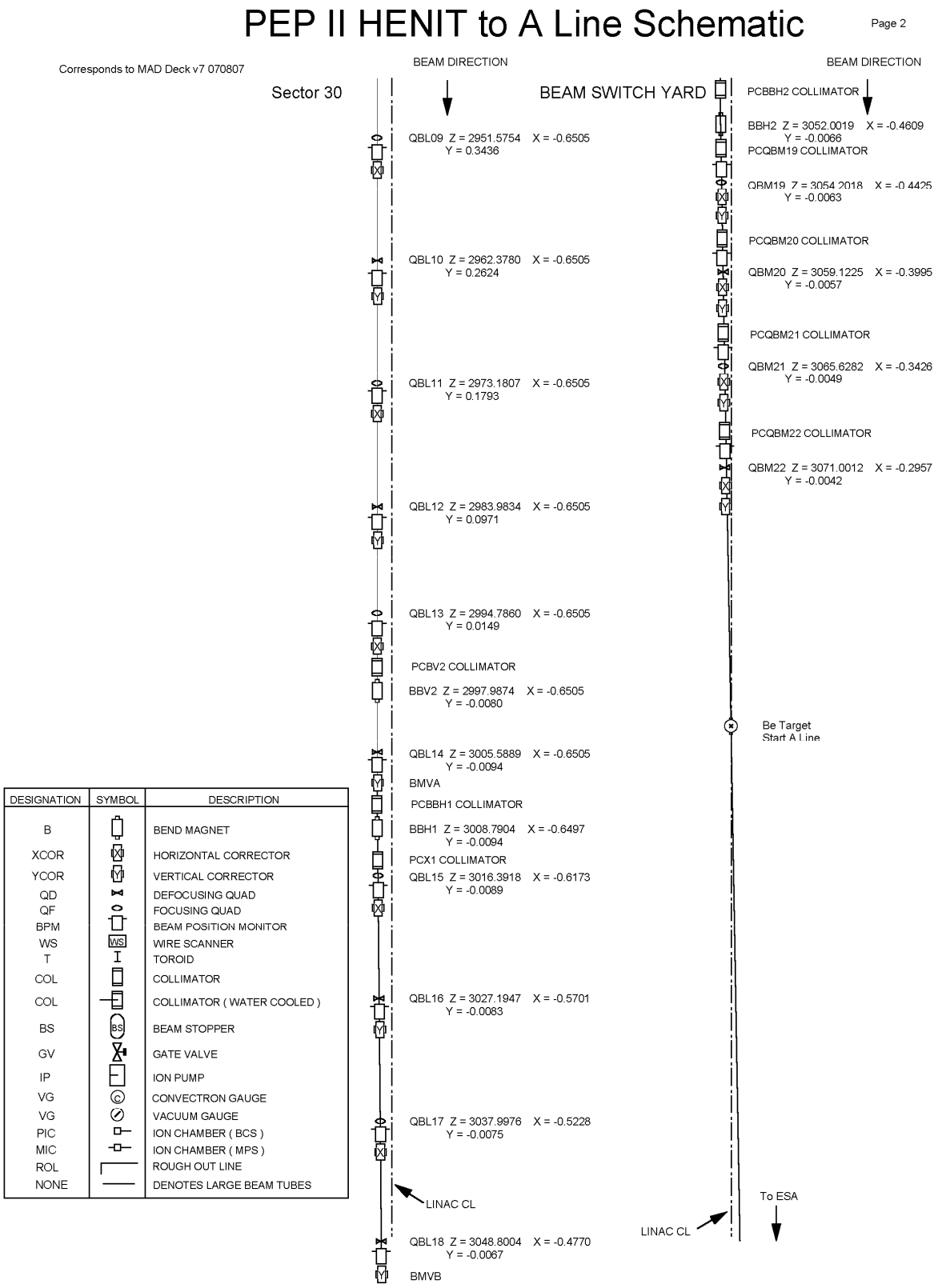

Figure 5-32. Schematic (page 2 of 2) showing the locations of components and horizontal bends used to deflect the beam across the LCLS path at the location marked “Be Target”.

5.4 ESA Facilities and Test Beams

ESA is an excellent facility for a wide variety of experiments operating in three distinct modes: i) primary beam, ii) secondary beam, and iii) beam dump. Figure 5-33 shows space allocations for these types of experiments for test beam experiments conducted in 2006-08. Additional space for experimental equipment, in particular for beam dump tests, is available in the tunnel leading to Beam Dump East. The ESA experimental hall is 60 meters in length with 15- and 50-ton overhead cranes and excellent availability of utilities, cable plant, and data acquisition. It is ideal for detector development and testing large scale prototypes or complete systems.

Dual experimental facilities in Sector 20 and in ESA enable a broad suite of experiments. Small-scale test setups can be accommodated at the ASF, while large-scale tests will be carried out in ESA. ESA can be accessed while beam is delivered to the ASF, allowing easy setup and modifications of ESA experiments. Existing pulsed magnets to extract the linac beam to ESA will allow concurrent interleaved operation of experiments at the ASF and ESA experimental areas.

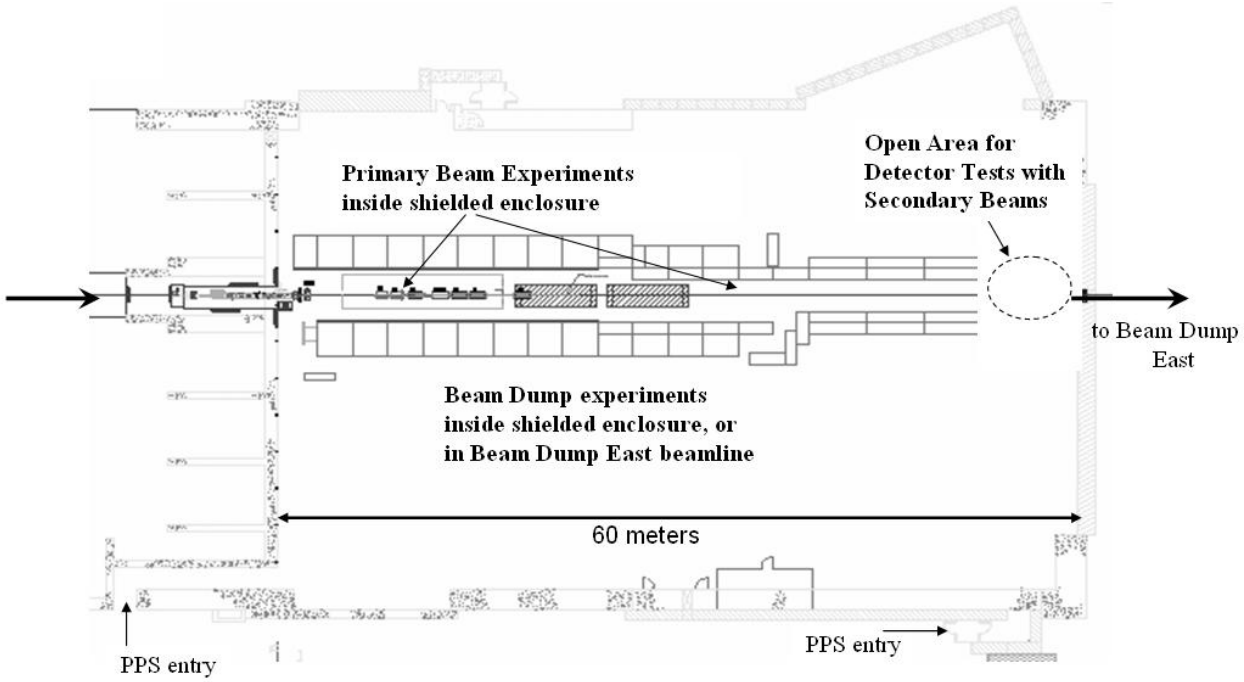

Figure 5-33. End Station A Facility configuration for test beam experiments in 2006-08, showing locations for i) primary beam experiments, ii) secondary beam tests, and iii) beam dump experiments.

Primary Beam. Characteristics for primary beam to the ASF and ESA are summarized in Tables 1-1 and 1-2. The A-line that transports beam from the new EBL line to ESA provides precise (0.1%) momentum-analyzed beams. At 12 GeV, there is only modest emittance growth in the A-line due to synchrotron radiation. This becomes larger with the energy upgrade—the invariant emittance in ESA at 28.5 GeV with present beams is roughly 300 mm-mrad horizontal, and 15 mm-mrad vertical. Very short bunches are hard to achieve in ESA because of the large R56 (=0.465m) Transport term that couples energy spread and bunch length. Modest bunch length compression is achievable, however, if the linac phase is chosen to give proper E-z correlation. A

future electron source upgrade to an RF photo-injector gun, with very small longitudinal emittance and energy spread, could enable much shorter bunches in ESA.

Low intensity primary beam. Low intensity beams from ~1 particle per bunch to full intensity (3.5×10^{10}) can be achieved by closing the A-line momentum slits.

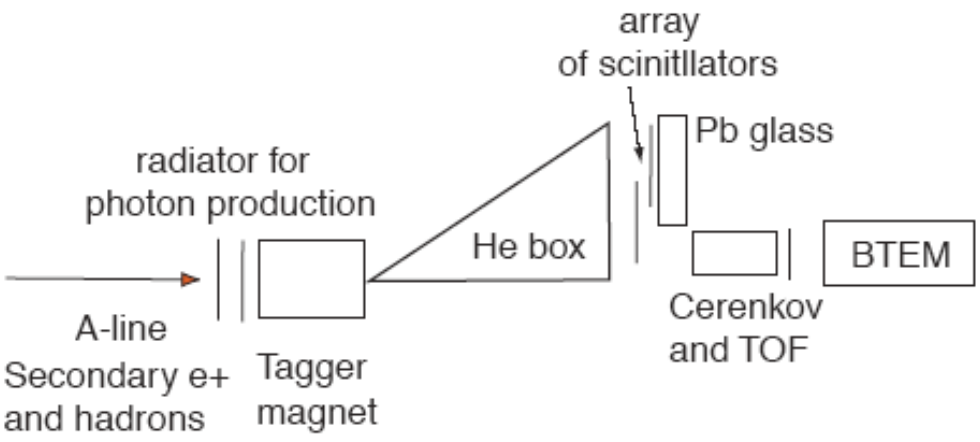

Figure 5-34. Tagged photon beam capability for ESA. The setup shown here was used for a GLAST beam test [3], which sent tagged photons to a BTEM detector module.

Secondary electrons. Secondary electron or positron beams with low intensity (0.1 up to ~1000 particles per bunch) can be produced by scraping a low intensity beam on a collimator in the EBL near Sector 20 or 30 to produce photons which are converted in a downstream vacuum valve which can be inserted into the beam. Secondary electrons or positrons are then momentum selected in the A-line. This technique was used during SLC operation in the 1990s to produce parasitic electron test beams to both the ESA and FFTB facilities [1]**.** SLAC Experiment E-146, for example, ran with such a beam in ESA to study the Landau-Pomeranchuk-Migdal interference effect in bremsstrahlung due to multiple scattering [2].

Tagged photons. A tagged photon beam can be produced in ESA as illustrated in Figure 5-34. A secondary electron (or positron/hadron) beam is momentum-selected in the A-line and is incident on a thin radiator in ESA. The scattered electron (or positron) has its energy measured in a calorimeter (Pb glass for the GLAST test), thereby tagging the photon energy.

Secondary hadrons (and electrons). The Be target currently located in the BSY will be moved to the end of the A-line to generate secondary electrons and hadrons. A schematic of the proposed configuration is shown in Figure 5-35. A 0.8-degree bend magnet (B28) will be installed to divert the primary beam onto the Be target. The primary beam will continue to a beam dump, while secondaries at a 1.5-degree production angle will be collimated and sent to ESA using a second 0.7-degree bend magnet (B29). A quadrupole doublet (Q29, Q30) will be used to focus the secondaries to the detector region in ESA, and Q38 will be used to correct for the dispersion. The acceptance will be about 6 μsr and 11% $\Delta p/p$, which is significantly larger than the current acceptance of 0.14 μsr and 2% $\Delta p/p$ for secondary particle production to the A-line from the Be target at its present location in the BSY. We will use the existing Q30 and Q38 magnets and relocate an identical magnet (previously installed as Q41) for Q29. B28 and B29

will be existing 10D37 magnets. The beam dump also exists and will be relocated to the A-line; it was previously used as ST4 in the SLC arcs and for a recent test beam experiment in ESA.

The configuration shown in Figure 5-35 will yield rates up to 10 π^+ per pulse per 1 x 10^{10} electrons incident on the Be target. Rates for K^+ and protons are factors of 10 to 50 smaller than for π^+. The particle rates can be easily adjusted down by tuning the incident beam current from the source and by adjusting the A-Line momentum slit SL10. The C37 collimator just in front of the entrance to ESA can also be used to reduce the flux and narrow the momentum acceptance if desired. C37 has 30 radiation lengths of copper followed by 30 radiation lengths of tungsten for each of 4 adjustable jaws.

Particle identification will be made by combinations of gas threshold Cherenkov counters in ESA and calorimetry. Measuring time-of-flight over the roughly 110 m between the Be target and detectors in ESA can also improve the separation of π/K/p. Long pulse operation can allow higher rates and improve the usable kaon and proton flux.

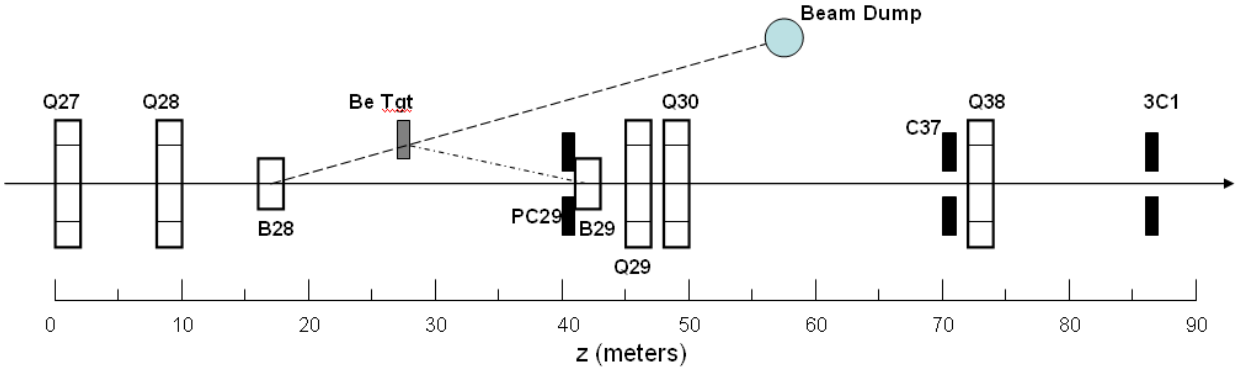

Figure 5-35. Relocated Be Target at the end of the A-line for producing secondary hadrons.

5.5 Future Opportunities

The beam parameters achievable with the FACET facility will be adequate to support the science programs outlined above. If the results from these programs lead in future directions with more stringent demands on the beams, then the facilities could be upgraded with one or more hardware improvement projects or changes in operating parameters, depending on the specific requirements. Among the possibilities are the following:

- The energy of the damping rings could be lowered, which would reduce the beam emittance. This would provide higher charge density in both electron and positron bunches. Calculations have shown that if the damping ring energies were lowered from 1.2 GeV to 0.9 GeV, a final bunch length of 13 μm could be achieved.
- A new photo injector, based on the design developed for the LCLS project, could be installed at the west end of the linac to produce very short low-emittance electron bunches without the need for the damping ring.
- Going beyond the notched beam approach of initial experiments, a capability to produce a fully independent witness bunch, in which a second bunch of electrons follows closely behind the first bunch, could be developed in conjunction with a new photo injector.
- The compressor chicane in Sector 10 could be moved upstream, which would improve the bunch compression without increasing the momentum spread.

- The energy of the beam to End Station A could be increased from 12 GeV to approximately 24 GeV by moving the extraction point from Sector 10 to Sector 18.

These future opportunities are at the proof-of-concept stage. More remains to be done to fully understand the achievable beam parameters and to prepare detailed designs and cost estimates.

5.6 References

[1] "A Method of Obtaining Parasitic e+ or e^- Beams during SLAC Linear Collider Operation", M. Cavalli-Sforza et al., SLAC-PUB-6387 (1993).

[2] SLAC E-146 publications: "An Accurate measurement of the Landau-Pomeranchuk-Migdal effect", P.L. Anthony et al. SLAC-PUB-6796, published in Phys.Rev.Lett. **75**:1949-1952 (1995), and "Measurement of dielectric suppression of Bremsstrahlung", P.L. Anthony et al. SLAC-PUB-6996, Phys.Rev.Lett. **76**:3550-3553 (1996).

[3] "Results from the Beam Test of the Engineering Model of the GLAST Large Area Telescope", E. do Couto e Silva et al., SLAC-PUB-8682, Nucl.Instrum.Meth.A **474**:19-37 (2001).

6 Project Management, Costs and Schedule

6.1 Project Execution Plan

A Project Execution Plan (PEP) is in development for the construction phase of the FACET project at SLAC, including project schedule and budget. The PEP describes how the estimates of the costs and their associated contingencies were made, the methods that will be used to control the project and identify issues as they arise in order to ensure early corrective action. The PEP also includes plans for safety, risk management, and formal procedures for system engineering, including change control. We assume the DOE Office of Science/High Energy Physics will be the sponsor of FACET.

The FACET project has already completed its conceptual engineering phase. The SLAC linac, damping rings, and positron source are able to produce the basic FACET particle beams now. Essentially all the difficult components for the facilities presently exist, including magnets and beam diagnostics. The project involves refurbishing some of the existing components and installation of the final focus, the positron compressor, and the electron bypass beam line. These installation activities have been conducted many times in the past at SLAC and the management, trained workers, safety oversight, and contractors are available to execute this relatively modest project.

Many of the components for the Sector 20 Final Focus, including magnets, vacuum equipment, diagnostic devices, electronics, and power supplies have been salvaged from the FFTB and SLC facilities and will be reused directly or refurbished as needed. Most of the components for the bypass line to End Station A can be reused from the existing NIT line when the PEP-II program ends. Other components will be acquired from outside vendors or fabricated in SLAC shops. New components to be constructed in SLAC shops will all be copies or simple extensions of proven designs from other SLAC facilities. For example, the new components for the positron compressor chicane will be similar to components that are now used to compress electrons.

6.2 Project Organization

The FACET project will be executed as a construction project within the framework of the Stanford Linear Accelerator Center, SLAC DOE Site Office, and Stanford University.

6.2.1 Project Management Team

During the construction phase of FACET there will be a project structure including a project manager, system scientists, system engineers, safety officer, quality control officer, and business management officer.

The project manager will be responsible for the overall conduct of the project and will be charged with both ensuring that both the scientific goals and management constraints on the project are met. He or she will report to the director of the Particle Physics and Astrophysics Directorate at SLAC as a PPA assistant director. The project manager will be responsible for completing the project within the budget and schedule approved by DOE and the project manager and is expected to submit status reports. He or she will control all contingency funds and will serve as the chair of the Change Control Board.

The system scientists will be the principle leaders of the scientific analyses required by the project and will be responsible for ensuring that the technical solutions adopted by the project engineers meet the scientific requirements.

The system engineers will be the chief technical leaders of the project. The system engineers will be responsible for integrating the various technical contributions into an integrated system through interface design and specification, modeling, and simulation.

6.2.2 Project Management Control

The FACET project has three phases: 1) design, 2) construction and commissioning, and 3) operations.

A Work Breakdown Structure (WBS), dictionary, cost estimate, and integrated schedule for the FACET facility have been constructed to encompass all three phases. The WBS structure has four main components: 1) Project management, 2) Sector 20 final focus, 3) Sector 10 positron compressor, 4) Bypass line extension in the Beam Switch Yard, and 5) Hadron production facility.

The project has task-based cost estimates, contingency and escalation. The costs for the FACET construction phase are associated with tasks that describe the resources and labor needed to complete the WBS elements. Task based estimates of cost and resources, along with the documented basis of estimate, were prepared by members of the subsystem teams, who consulted technical experts and outside contractors as appropriate. The guidelines used to prepare the task-based estimates were documented. The estimates were in FY2007 dollars. The project includes both schedule and financial contingency. A schedule contingency of order three months has been included in the WBS.

Contingency funds were estimated at the task level using standard risk methodology. Contingency funds are included in the total project cost estimate and will be managed at the project level. The overall project contingency at this early stage of the project is about 30%. Space does not permit the inclusion of the full WBS dictionary, schedule, budget, and basis of estimate.

The project management Office will include a task scheduler and financial accountant. These individuals will provide monthly reports for senior management to review. These reports will support the project monthly reports by summarizing successes as well as any problems or issues that arise. Corrective action will be implemented and tracked as needed.

6.2.3 Project Safety

The FACET project will follow best design and construction practices and comply fully with United States law and standards for all aspects. Furthermore, the FACET project will be subject to the SLAC safety review policies, which include formal reviews of radiation, electrical, laser, chemical, non-ionizing, and seismic hazards, as well as applicable OSHA, NEC, and NEPA considerations. The safety officer will ensure that these requirements are met by FACET. In addition, the construction activities will be subject to a formal review of applicable hoisting and rigging procedures, the Accelerator Systems Division Work Authorization Procedure, and SLAC Work Planning and Control (WPC).

6.2.4 Project Quality Control

The quality control officer will work with the project engineers, designers, contractors and shops to ensure that the technical details of FACET meet rigorous quality assurance at all phases of the project. These technical groups will be responsible for preparing the Quality Management Plan for FACET. The quality assurance plan will include configuration control procedures, inspection methods, inventory control, acceptance test plans, and calibration procedures. The system engineers will have the additional responsibility of ensuring that the subsystem engineering teams utilize project standard version control and change-tracking tools and processes throughout development, integration, and test.

6.2.5 Project Staffing

Experienced staff needed to carry out FACET will be available at SLAC in FY2009, FY2010, and FY2011. PEP-II is turning off in September 2008, freeing support engineers and physicists. In addition, the LCLS construction project is starting to ramp down freeing technical support for FACET construction. We believe it will be possible to staff the FACET construction project to a large degree from these sources.

6.3 Construction Schedule

The installation of FACET components could extend over a three year period, depending on availability of funding and compatibility with other accelerator programs. Beams will be deliverable to experiments between installation downtimes throughout this period, with performance and functionality improvements as new features are commissioned. The installation and commissioning will proceed as shown in Table 6-1 and Figure 6-1, assuming the proposed funding profile. This schedule was developed to be compatible with the anticipated LCLS construction and operating plans, but this schedule may vary as the LCLS construction and commissioning progresses. We also make a set of assumptions about critical decision milestones that define the onset of project approval and funding. The project completion is defined by a CD-4 milestone that is broken into CD-4a, defined as the completion of the Sector 20 final focus, and CD-4b, defined as completion of the full project. This division of the project completion milestone is meant to allow early operation of the Sector 20 facility for advanced accelerator R&D with electrons.

Table 6-1. Installation and commissioning

Fall 2008	Installation of shielding wall in linac tunnel between Sectors 20 and 21. This allows tunnel installation work to proceed in Sector 20 while the LCLS injector and other downstream systems operate in 2009.
January through September 2009	Installation of Sector 20 magnets and vacuum systems while LCLS commissioning activities proceed in downstream sectors.
Fall 2009	Removal of existing components of the PEP-II injection transport systems in the BSY, as needed for FACET. Modifications to the Common Line vacuum system in the BSY.
FY 2010	First operation of Sector 20 final focus with electrons. Installation of positron compressor system in Sector 10.
Fall 2010	Installation of the bypass line in the BSY and Hadron Production Facility.
FY 2011	All FACET systems fully operational, independent of LCLS operations.

The proposed construction schedule is illustrated in Figures 6-1a-d.

ID	WBS	Task Name
1	**1.1**	**Project management**
2	1.1.1	Technical management
3	1.1.2	Safety oversight
4	1.1.3	Financial planner
5	**1.2**	**Sector 20 Final Focus Region**
6	**1.2.1**	**Magnets**
7	1.2.1.1	Remove existing components
8	1.2.1.2	Reburbish
9	**1.2.2**	**Supports**
10	1.2.2.1	Design
11	1.2.2.2	Fabricate
12	**1.2.3**	**Plumping and facilities**
13	1.2.3.1	Design
14	1.2.3.2	Fabricate
15	**1.2.4**	**Power supplies and cables**
16	1.2.4.1	Design supplies
17	1.2.4.2	Refurbish & move supplies
18	1.2.4.3	Design cables
19	1.2.4.4	Procure cables
20	**1.2.5**	**Vacuum systems**
21	1.2.5.1	Design
22	1.2.5.2	Fabricate
23	**1.2.6**	**Controls and instruments**
24	1.2.6.1	Design
25	1.2.6.2	Fabricate
26	**1.2.7**	**Alignment and installation**
27	1.2.7.1	Install magnets and supports
28	1.2.7.2	Install vacuum
29	1.2.7.3	Install plumbing and utilities
30	1.2.7.4	Install controls and instrumentation
31	1.2.7.5	Sector 20 Final Focus complete
32	**1.2.8**	**Shield wall and PPS**
33	1.2.8.1	Design shield wall
34	1.2.8.2	Identify & stage shield wall blocks
35	1.2.8.3	Install shield wall
36	1.2.8.4	Design optical coupler
37	1.2.8.5	Fabricate optical coupler
38	1.2.8.6	Install optical coupler
39	1.2.8.7	Design PPS system
40	1.2.8.8	Fabricate PPS components
41	1.2.8.9	Install PPS system
42	1.2.8.10	Test PPS system
139	**1.6**	**Project planning and constraints**
146	1.6.7	Fall 2008 LCLS down period
147	1.6.8	Fall 2009 LCLS down period
148	1.6.9	Fall 2010 LCLS down period

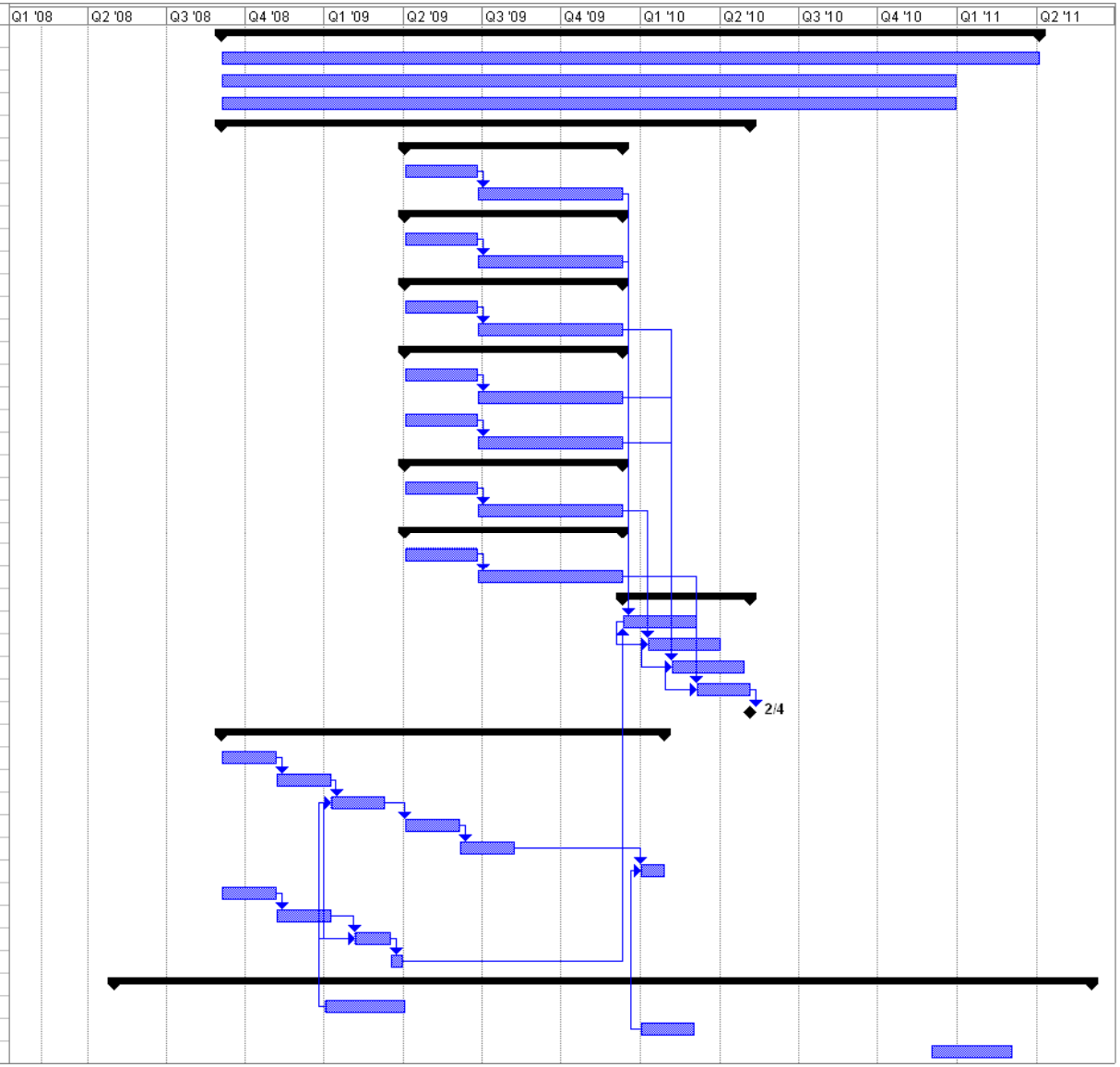

Figure 6-1a. Timeline for proposed FACET Sector 20 construction schedule, matching proposed funding profile and constraints from requirements for beamline access during LCLS down periods. LCLS down periods are subject to change.

ID	WBS	Task Name
43	**1.3**	**Positron Bunch Compressor**
44	**1.3.1**	**Magnets**
45	1.3.1.1	Design new magnets
46	1.3.1.2	Procure new magnets
47	**1.3.2**	**Supports**
48	1.3.2.1	Design
49	1.3.2.2	Fabricate
50	**1.3.3**	**Plumbing and facilities**
51	1.3.3.1	Design
52	1.3.3.2	Fabricate
53	**1.3.4**	**Power supplies and cables**
54	1.3.4.1	Design supplies
55	1.3.4.2	Refurbish & move supplies
56	1.3.4.3	Design cables
57	1.3.4.4	Procure cables
58	**1.3.5**	**Vacuum systems**
59	1.3.5.1	Design
60	1.3.5.2	Fabricate
61	**1.3.6**	**Controls and instruments**
62	1.3.6.1	Design
63	1.3.6.2	Fabricate
64	**1.3.7**	**Alignment and installation**
65	1.3.7.1	Install magnets and supports
66	1.3.7.2	Install vacuum
67	1.3.7.3	Install plumbing and utilities
68	1.3.7.4	Install controls and instrumentation
69	1.3.7.5	Positron Bunch Compressor complete
139	**1.6**	**Project planning and constraints**
146	1.6.7	Fall 2008 LCLS down period
147	1.6.8	Fall 2009 LCLS down period
148	1.6.9	Fall 2010 LCLS down period

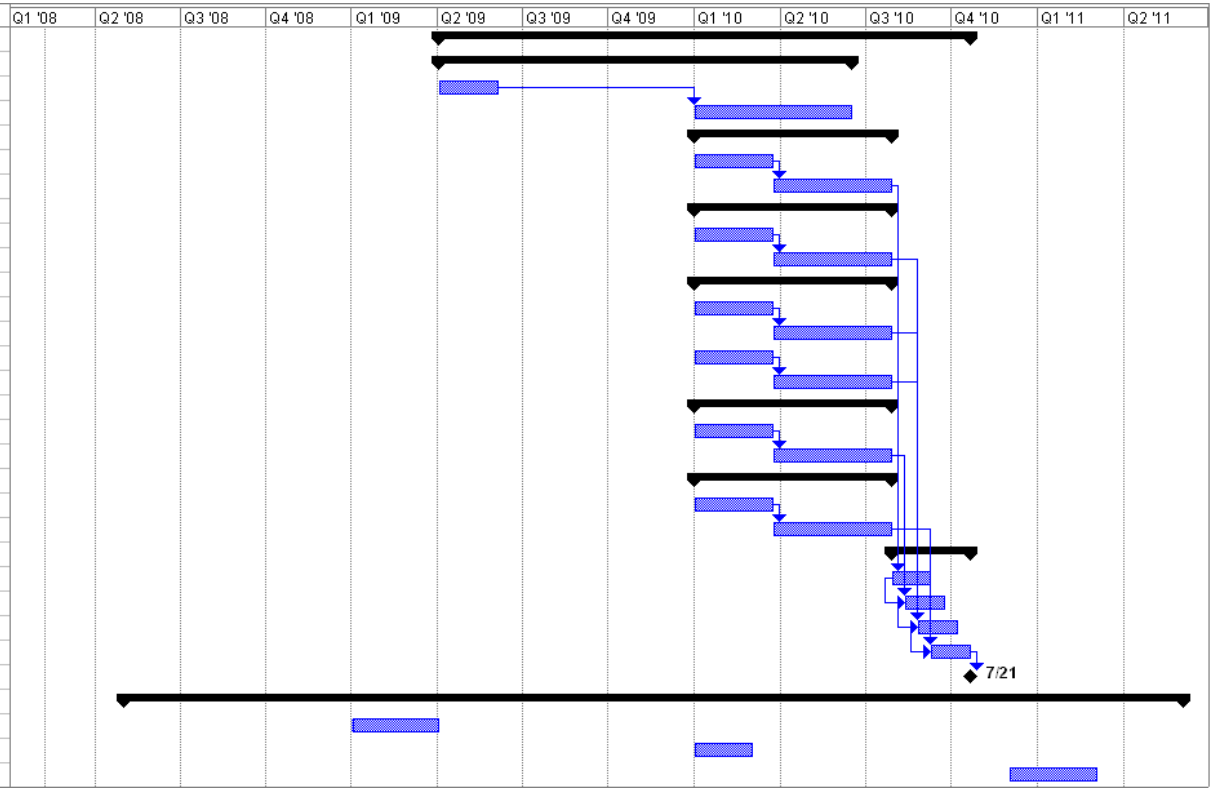

Figure 6-1b. Timeline for proposed FACET positron compressor construction schedule, matching proposed funding profile and constraints from requirements for beamline access during LCLS down periods. LCLS down periods are subject to change.

ID	WBS	Task Name
70	**1.4**	**Bypass and ESA Injection Line**
71	**1.4.1**	**Magnets**
72	1.4.1.1	Design
73	1.4.1.2	Remove existing components
74	1.4.1.3	Refurbish
75	**1.4.2**	**Supports**
76	1.4.2.1	Design
77	1.4.2.2	Remove existing supports
78	1.4.2.3	Modify supports
79	**1.4.3**	**Plumbing and facilities**
80	1.4.3.1	Design
81	1.4.3.2	Fabricate
82	**1.4.4**	**Power supplies and cables**
83	1.4.4.1	Design supplies
84	1.4.4.2	Refurbish supplies
85	1.4.4.3	Design cables
86	1.4.4.4	Procure cables
87	**1.4.5**	**Vacuum system**
88	1.4.5.1	Design
89	1.4.5.2	Fabricate
90	**1.4.6**	**Controls and instruments**
91	1.4.6.1	Design
92	1.4.6.2	Frabciate
93	**1.4.7**	**Alignment and installation**
94	1.4.7.1	Install magnets and supports
95	1.4.7.2	Install vacuum
96	1.4.7.3	Install plumbing and utilities
97	1.4.7.4	Install controls and instrumentation
98	1.4.7.5	Bypass and ESA Injection Line complete
99	**1.4.8**	**ESA PPS system**
100	1.4.8.1	Design
101	1.4.8.2	Frabricate components
102	1.4.8.3	Install
103	1.4.8.4	Test
139	**1.6**	**Project planning and constraints**
146	1.6.7	Fall 2008 LCLS down period
147	1.6.8	Fall 2009 LCLS down period
148	1.6.9	Fall 2010 LCLS down period

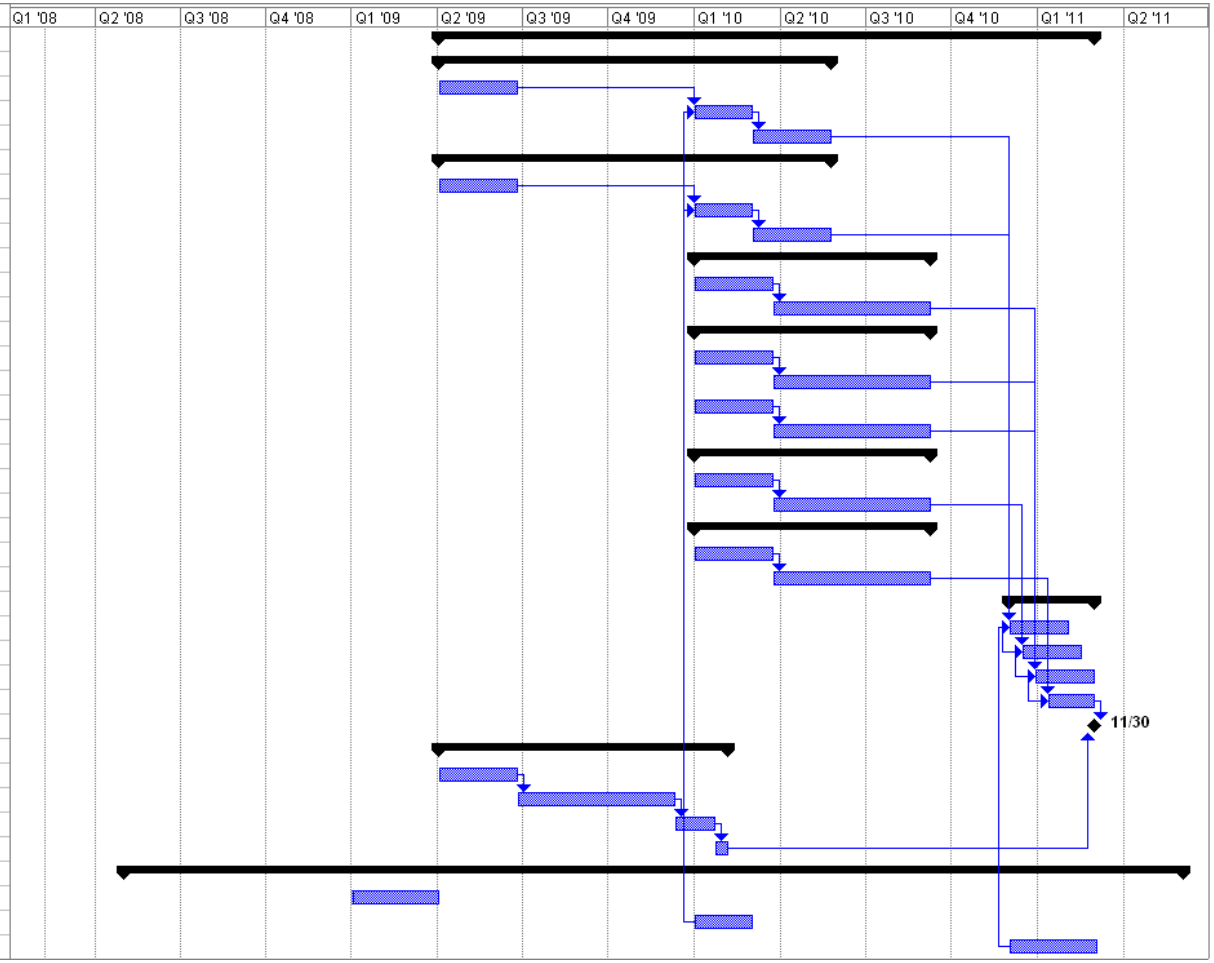

Figure 6-1c. Timeline for proposed FACET EBL construction schedule, matching proposed funding profile and constraints from requirements for beamline access during LCLS down periods. LCLS down periods are subject to change.

ID	WBS	Task Name
104	**1.5**	**Hadron Production Facility**
105	**1.5.1**	**Magnets**
106	1.5.1.1	Remove existing components
107	1.5.1.2	Refurbish
108	**1.5.2**	**Supports**
109	1.5.2.1	Remove existing supports
110	1.5.2.2	Modify supports
111	**1.5.3**	**Plumbing and facilities**
112	1.5.3.1	Design
113	1.5.3.2	Fabricate
114	**1.5.4**	**Power supplies and cables**
115	1.5.4.1	Design cables
116	1.5.4.2	Procure cables
117	**1.5.5**	**Vacuum system**
118	1.5.5.1	Design
119	1.5.5.2	Fabricate
120	**1.5.6**	**Controls and instrumentation**
121	1.5.6.1	Design
122	1.5.6.2	Fabricate
123	**1.5.7**	**Alignment and installation**
124	1.5.7.1	Install magnets and supports
125	1.5.7.2	Install vacuum
126	1.5.7.3	Install plumbing and utilities
127	1.5.7.4	Install controls and instrumentation
128	**1.5.8**	**Be target, collimators, and dump**
129	1.5.8.1	Design target
130	1.5.8.2	Fabricate target
131	1.5.8.3	Install target
132	1.5.8.4	Design collimators
133	1.5.8.5	Fabricate collimators
134	1.5.8.6	Install collimators
135	1.5.8.7	Design dump
136	1.5.8.8	Fabricate dump
137	1.5.8.9	Install dump
138	1.5.8.10	Hadron Production Facility complete
139	**1.6**	**Project planning and constraints**
146	1.6.7	Fall 2008 LCLS down period
147	1.6.8	Fall 2009 LCLS down period
148	1.6.9	Fall 2010 LCLS down period

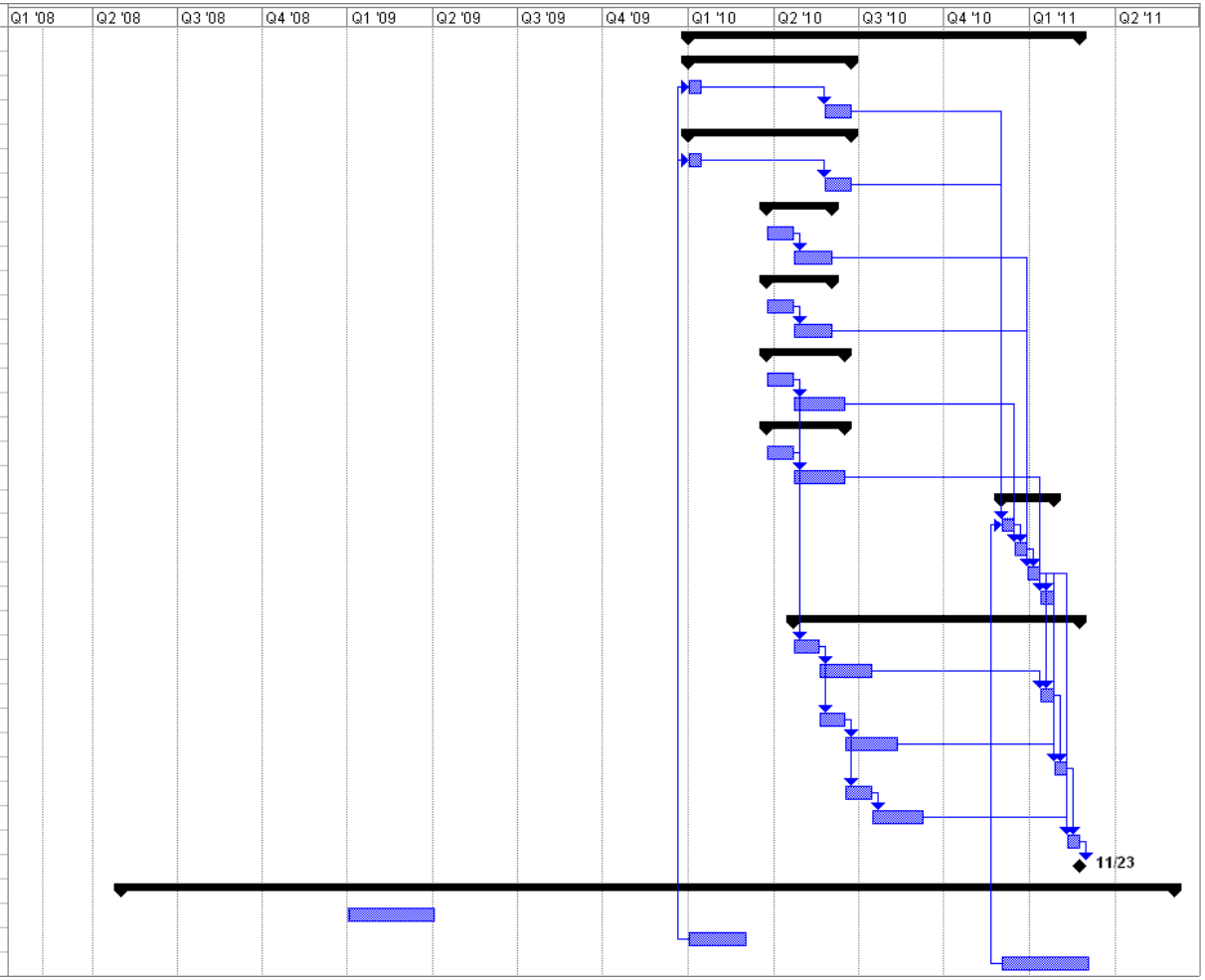

Figure 6-1d. Timeline for proposed FACET Hadron Production Facility construction schedule, matching proposed funding profile and constraints from requirements for beamline access during LCLS down periods. LCLS down periods are subject to change.

ID	WBS	Task Name
139	**1.6**	**Project planning and constraints**
140	1.6.1	CD-0
141	1.6.2	CD-1
142	1.6.3	CD-2
143	1.6.4	CD-3
144	1.6.5	CD-4A
145	1.6.6	CD-4B
146	1.6.7	Fall 2008 LCLS down period
147	1.6.8	Fall 2009 LCLS down period
148	1.6.9	Fall 2010 LCLS down period
149	1.6.10	FY2009 funding
150	1.6.11	FY2010 funding

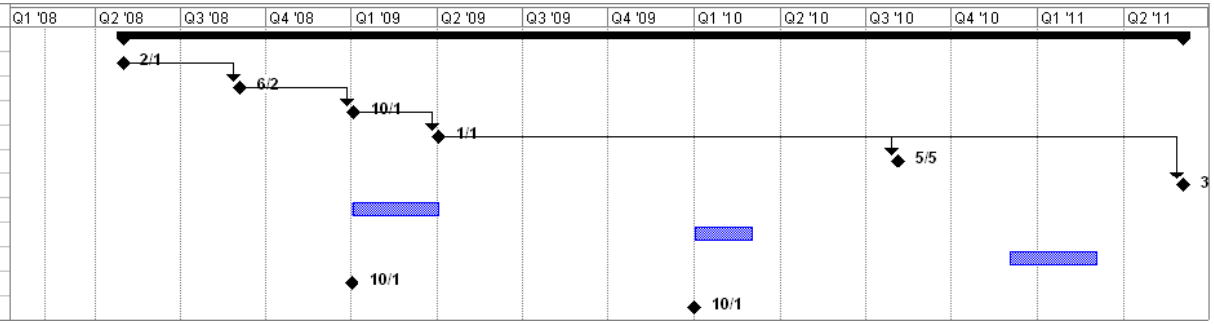

Figure 6-1e. Assumed timeline for critical decision milestones for the FACET project. LCLS down periods are subject to change.

6.4 Estimated Construction Costs

Tables 6-2 and 6-3 summarize the FACET budget estimates for each of the three major areas of the project and the projected construction costs distributed by quarter and fiscal year. The methodology for producing these cost estimates was based on ground-up engineering exercises. All necessary components were identified, and the resulting counts were listed in a spread sheet. The costs for M&S and labor hours associated with each category of components or tasks were estimated and recorded, and the sums were tallied to arrive at the total cost estimates.

The major categories of components and tasks in this project include magnet removal and refurbishment, support removal and modification, vacuum chamber refurbishment and/or construction, cooling water distribution and interlocks, personnel protection system changes, power supplies, AC power distribution, power cables, shield wall construction, controls, instrumentation, installation, and alignment. Many of the components will be salvaged from either the SLC final focus system or the FFTB and most of the remainder will be salvaged from PEP-II after it is shut down at the end of September 2008. The engineering and detailed design of the new systems will proceed very efficiently, because the core beam parameters, the tunnel layout, and the dimensions and specifications of nearly all the components are already known.

Costs for the three accelerator areas were estimated separately. The labor requirements and M&S estimates were based on historical trends for similar projects and activities at SLAC. The SLAC labor rates are up to date as of August 2007, and the overhead burden was added separately for M&S and for labor. Finally, a 30% contingency was added to all tasks.

Year	Month	LCLS	FACET Shield Wall	FACET S-20 ASF	FACET e+ compressor	FACET EBL to ESA	FACET Hadron Production Facility
FY09	Oct	Down	Construct				
FY09	Nov	Down	Construct				
FY09	Dec	Down	Construct				
FY09	Jan	Run		Construct			
FY09	Feb	Run		Construct			
FY09	Mar	Run		Construct			
FY09	Apr	Run		Construct			
FY09	May	Run		Construct			
FY09	Jun	Run		Construct			
FY09	Jul	Run		Construct			
FY09	Aug	Run		Construct			
FY09	Sept	Run		Construct			
FY10	Oct	Down		Construct	Construct	Construct	Construct
FY10	Nov	Down		Construct	Construct	Construct	Construct
FY10	Dec	Run		Construct	Construct	Construct	Construct
FY10	Jan	Run		Construct	Construct	Construct	Construct
FY10	Feb	Run		Construct	Construct	Construct	Construct
FY10	Mar	Run		Down	Construct	Construct	Construct
FY10	Apr	Run		Run	Construct	Construct	Construct
FY10	May	Run		Run	Construct	Construct	Construct
FY10	Jun	Run		Down	Construct	Construct	Construct
FY10	Jul	Down		Down	Construct	Construct	Construct
FY10	Aug	Down		Down	Down	Construct	Construct
FY10	Sept	Down		Down	Down	Construct	Construct
FY11	Oct	Down		Down	Down	Construct	Construct
FY11	Nov	Down		Down	Down	Construct	Construct
FY11	Dec	Run		Run	Run	Run	Run
FY11	Jan	Run		Run	Run	Run	Run
FY11	Feb	Run		Down	Down	Down	Down
FY11	Mar	Run		Down	Down	Down	Down
FY11	Apr	Run		Run	Run	Run	Run
FY11	May	Run		Run	Run	Run	Run
FY11	Jun	Run		Down	Down	Down	Down
FY11	Jul	Down		Down	Down	Down	Down
FY11	Aug	Down		Down	Down	Down	Down
FY11	Sept	Down		Down	Down	Down	Down
FY12	Oct	Down		Down	Down	Down	Down
FY12	Nov	Run		Run	Run	Run	Run
FY12	Dec	Run		Run	Run	Run	Run

Figure 6-2. Overview of proposed FACET construction and initial operation schedule.

Table 6-2. FACET budget statement

WBS		M&S (k$)	EDI (k$)	Indirects (k$)	Contingency (k$)	Total (k$)
1	**Overall FACET Project**	**7481**	**2256**	**2834**	**2947**	**15518**
1.1	**Project Management**	**174**	**970**	**395**	**435**	**1974**
1.1.1	Technical management	78	410	167	185	840
1.1.2	Safety management	38	280	114	114	554
1.1.3	Financial management	58	280	114	114	580
1.2	**Sector 20 ASF Region**	**4486**	**595**	**461**	**1561**	**7103**
1.2.1	Magnets	337	45	35	117	534
1.2.2	Supports	634	85	66	221	1006
1.2.3	Plumbing and facilities	456	60	46	159	721
1.2.4	Power supplies and cables	319	43	33	111	506
1.2.5	Vacuum system	816	107	83	284	1290
1.2.6	Controls and instruments	275	37	28	96	436
1.2.7	Alignment and installation	954	126	99	332	1511
1.2.8	User counting room	81	12	8	28	129
1.2.9	Shield wall and PPS	614	80	63	213	970
1.3	**Positron Bunch Compressor**	**947**	**156**	**111**	**342**	**1556**
1.3.1	Magnets	378	39	35	127	579
1.3.2	Supports	83	14	10	30	137
1.3.3	Plumbing and facilities	38	2	3	12	55
1.3.4	Power supplies and cables	62	20	12	26	120
1.3.5	Vacuum system	268	65	39	105	477
1.3.6	Controls and instruments	59	10	7	22	98
1.3.7	Alignment and installation	59	6	5	20	90
1.4	**Bypass to A-Line Transport Line**	**2710**	**384**	**288**	**954**	**4336**
1.4.1	Magnets	92	31	17	40	180
1.4.2	Supports	346	45	35	120	546
1.4.3	Plumbing and facilities	141	18	14	49	222
1.4.4	Power supplies and cables	233	33	25	82	373
1.4.5	Vacuum system	502	65	51	174	792
1.4.6	Controls and instruments	196	41	26	74	337
1.4.7	Alignment and installation	963	119	96	332	1510
1.4.8	ESA PPS System	237	32	24	83	376

WBS		M&S (k$)	EDI (k$)	Indirects (k$)	Contingency (k$)	Total (k$)
1.5	**ESA Hadron Production Facility**	**312**	**72**	**44**	**121**	**549**
1.5.1	Magnets	13	6	3	6	28
1.5.2	Supports	17	6	3	7	33
1.5.3	Plumbing and facilities	45	9	6	17	77
1.5.4	Power supplies and cables	77	15	10	29	131
1.5.5	Vacuum system	24	7	4	10	45
1.5.6	Controls and instruments	32	7	4	12	55
1.5.7	Alignment and installation	62	12	8	23	105
1.5.8	Be target, collimators, and dump	42	10	6	17	75

Table 6-3. FACET yearly costs for construction

Fiscal Year	Quarter	Project Management (k$)	Sector 20 ASF (k$)	e+ Bunch Compressor (k$)	EBL (k$)	Hadron Prod. Facility (k$)	Totals (k$)
FY2009	Q1	50	200	0	100	0	350
FY2009	Q2	100	1600	20	50	0	1770
FY2009	Q3	250	1900	20	50	0	2220
FY2009	Q4	400	2200	60	200	0	2860
FY2009 total	All year	800	5900	100	400	0	7200
FY2010	Q1	350	580	500	800	10	2240
FY2010	Q2	350	480	500	800	20	2150
FY2010	Q3	300	100	300	800	50	1550
FY2010	Q4	174	43	156	700	100	1173
FY2010 total	All year	1174	1203	1456	3100	180	7113
FY2011	Q1	0	0	0	650	300	950
FY2011	Q2	0	0	0	186	69	255
FY2011	Q3	0	0	0	0	0	0
FY2011	Q4	0	0	0	0	0	0
FY2011 total	All year	0	0	0	836	369	1205
Overall total		1974	7103	1556	4336	549	15518

6.5 Estimated Operating Costs

SLAC is in the midst of a three year transition from on-site accelerator based programs focused primarily on high energy particle physics to programs focused primarily on photon sciences. It is anticipated that by FY2009, most of the costs for operating and maintaining the accelerator facilities will by funded through the DOE Office of Basic Energy Sciences, although the incremental cost of operating FACET for high energy physics programs will be funded through the Office of High Energy Physics. The underlying assumption is that OS-BES will support the maintenance of the entire linac, including Sectors 1-20, as recommended by the DOE review of the transition plan in fall 2006. The incremental operating costs for OS-HEP would cover the additional personnel, M&S, and power for operating the linac, final focus, and transfer lines of the FACET facility.

The costs for operating FACET are shown in Table 6-4 for three different scenarios: simultaneous operations of both Sector 20 and ESA, operation of Sector 20 only, and operation of ESA only. The sum of operating costs for Sector 20 and ESA separately is more than for the simultaneous mode, where power and labor costs can be shared and exploitation of the two facilities will be optimal. The costs for the experimental programs in Sector 20 and in ESA are not included in Table 6-4. Estimates for operating costs are in FY2007 dollars and can be extrapolated to then-year dollars as needed.

It is anticipated that the FACET-related operations costs to run the Sector 20 final focus region and the bypass line to ESA will be about 1.5 M$ per month for a four month run. While some costs, such as electric power, scale with the length of the running period, other costs, such as personnel, do not. Therefore, the table lists the estimated operating costs for six, eight, and ten month running periods as well. These numbers include the overall incremental costs to run positrons to Sector 20 and electrons to ESA.

6.6 Management of the FACET Scientific Program

FACET is a user facility designed to support the national program in advanced accelerator science and ILC instrumentation and detector development. As has been the case for other beam-related user facilities at SLAC, we anticipate that there will be broad demand for beam time from these communities, and a wide variety of other HEP applications. FACET may also prove attractive for a broader scientific audience.

The SLAC Experimental Physics Advisory Committee (EPAC) has been in existence since the founding of SLAC more that 45 years ago. This committee has reviewed proposals for experiments for HEP and provided recommendations to the laboratory director. The EPAC typically met once or twice each year, depending on the number of proposals under discussion. With advice from the EPAC and other inputs, the laboratory director made choices about which experiments are funded and carried out. This process was also used for the accelerator experimental program in the FFTB and ESA in the past and has worked well.

We propose to adapt the EPAC for the purpose of managing the scientific program at FACET. Its membership will be adjusted to obtain an appropriate balance of expertise in advanced accelerator science and HEP. Reflecting the current institutional organization, the reconstituted EPAC will advise the director of the Particle Physics and Astrophysics Directorate on the priorities for experiments to be mounted at FACET and on the future development of this facility.

Table 6-4. Estimated FACET operating costs

FACET Operating Costs for Sector 20 ASF & ESA					
Cost Item	**Funding Source**	**4 Month Run (k$)**	**6 Month Run (k$)**	**8 Month Run (k$)**	**10 Month Run (k$)**
Sector 0-20 Linac Maintenance	BES	8386	8386	8386	8386
Sector 0-20 Linac Maintenance Power	BES	3338	3338	3338	3338
Linac Sector 0-20 Operations Power	HEP	1075	1612	2150	2687
FACET Sector 0-20 + A-Line Operations Labor	HEP	3704	4688	5671	6655
FACET Sector 0-20 + A-Line Operations M&S	HEP	950	1130	1310	1490
FF, Bypass line and A-Line Operations Power	HEP	281	422	562	702
Sub-total HEP	HEP	6010	7852	9693	11534
FACET Operating for Sector 20 ASF Only					
Cost Item	**Funding Source**	**4 Month Run (k$)**	**6 Month Run (k$)**	**8 Month Run (k$)**	**10 Month Run (k$)**
Sector 0-20 Linac Maintenance	BES	8386	8386	8386	8386
Sector 0-20 Linac Maintenance Power	BES	3338	3338	3338	3338
Linac Sector 0-20 Operations Power	HEP	1075	1612	2150	2687
FACET Sector 0-20 + A-Line Operations Labor	HEP	3304	4188	5071	5955
FACET Sector 0-20 + A-Line Operations M&S	HEP	850	1010	1170	1330
FF, Bypass line and A-Line Operations Power	HEP	140	211	281	351
Sub-total HEP	HEP	5369	7021	8672	10323
FACET Operating for ESA Only					
Cost Item	**Funding Source**	**4 Month Run (k$)**	**6 Month Run (k$)**	**8 Month Run (k$)**	**10 Month Run (k$)**
Sector 0-20 Linac Maintenance	BES	8386	8386	8386	8386
Sector 0-20 Linac Maintenance Power	BES	3338	3338	3338	3338
Linac Sector 0-20 Operations Power	HEP	538	806	1075	1344
FACET Sector 0-20 + A-Line Operations Labor	HEP	2469	3125	3780	4436
FACET Sector 0-20 + A-Line Operations M&S	HEP	633	753	873	993
FF, Bypass line and A-Line Operations Power	HEP	140	211	281	351
Sub-total HEP	HEP	3780	4895	6009	7124

Appendix A. Publications from the Advanced Accelerator Program

Peer-Reviewed Publications from E157/E162/E164/E164X/E167

1) M. J. Hogan *et al, "*E-157: A 1.4 Meter-Long Plasma Wakefield Acceleration Experiment Using a 30 GeV Electron Beam from the Stanford Linear Accelerator Center Linac", Physics of Plasmas **7**, 2241 (2000).
2) P. Muggli *et al,* "Collective Refraction of a Beam of Electrons at a Plasma-Gas Interface", Nature **411**, 43 (3 May 2001).
3) P. Catravas *et al,* "Measurements of Radiation Near an Atomic Spectral Line from the Interaction of a 30 GeV Electron Beam and a Long Plasma", Physical Review E **64** 046502 (2001).
4) P. Muggli *et al*, "Collective Refraction of a Beam of Electrons at a Plasma-Gas Interface", Physical Review Special Topics - Accelerators and Beams **4**, 091301 (2001).
5) S. Lee *et al*, "Energy Doubler for a Linear Collider", Physical Review Special Topics - Accelerators and Beams **5**, 011001 (2002).
6) Shouqin Wang *et al,* "X-Ray Emission from Betatron Motion in a Plasma Wiggler", Physical Review Letters **88**, 135004 (2002).
7) C. E. Clayton *et al,* "Transverse Envelope Dynamics of a 28.5 GeV Electron Beam in a Long Plasma", Physical Review Letters **88**, 154801 (2002).
8) C. Joshi *et al,* "High Energy Density Plasma Science with an Ultra-Relativistic Electron Beam", Physics of Plasmas **9**, 1845 (2002).
9) C. O'Connell *et al*, "Dynamic Focusing of an Electron Beam through a Long Plasma", Physical Review Special Topics – Accelerators and Beams **5**, 121301 (2002).
10) M. J. Hogan *et al*, "Ultrarelativistic-Positron-Beam Transport through Meter-Scale Plasmas", Physical Review Letters **90**, 205002 (2003).
11) B. Blue *et al*, "Plasma Wakefield Acceleration of an Intense Positron Beam", Physical Review Letters **90**, 214801 (2003).
12) C. Joshi and T. Katsouleas, "Plasma Accelerators at the Energy Frontier and on Tabletops", Physics Today, 47 (June 2003).
13) P. Muggli *et al*, "Meter-Scale Plasma-Wakefield Accelerator Driven by a Matched Electron Beam", Physical Review Letters **93**, 014802 (2004).
14) R. Maeda *et al*, "On the Possibility of a Multi-Bunch Afterburner for Linear Colliders", Physical Review Special Topics – Accelerators and Beams **7**, 111301 (2004).
15) M. J. Hogan *et al*, "Multi-GeV Energy Gain in a Plasma-Wakefield Accelerator", Physical Review Letters **95**, 054802 (2005).
16) C.L. O'Connell *et al*, "Plasma Production via Field Ionization", Physical Review Special Topics – Accelerators and Beams **9**, 101301 (2006).
17) D. K. Johnson *et al*, "Positron Production by X-Rays Emitted by Betatron Motion in a Plasma Wiggler", to be published in Physical Review Letters **97**, 175003 (2006).
18) R. Ischebeck *et al*, "Beam-Driven Plasma Wakefield Acceleration at SLAC", submitted to Physics of Plasmas.

19) Ian Blumenfeld *et al*, "Energy Doubling of 42 GeV Electrons in a Meter Scale Plasma Wakefield Accelerator", Nature **445,** 741-744 (2007).

20) E. Oz *et al*, "Ionization Induced Electron Trapping in Ultra-relativistic Plasma Wakes", Physical Review Letters **98**, 084801 (2007).

Related Peer-Reviewed Simulation Papers

1) S. Lee *et al,* "Simulations of a Meter-Long Plasma Wakefield Accelerator", Physical Review E **61**, 7014 (2000).

2) R. G. Hemker *et al, "*Dynamic Effects in Plasma Wakefield Excitation", Physical Review Special Topics – Accelerators and Beams **3**, 061301 (2000).

3) S. Lee *et al*, "Plasma-Wakefield Acceleration of a Positron Beam", Physical Review E **64**, 045501(R) (2001).

4) E. S. Dodd *et al*, "Hosing and Sloshing of Short-Pulse GeV-Class Wakefield Drivers", Physical Review Letters **88**, 125001 (2002).

5) S. Deng *et al*, "Plasma Wakefield Acceleration in Self-ionized Gas or Plasmas", Physical Review E **68**, 047401 (2003).

6) R. Maeda *et al*, "Possibility of a Multibunch Plasma Afterburner for Linear Colliders", Physical Review Special Topics – Accelerators and Beams **7**, 111301 (2004).

7) S. Deng *et al*, "Hose Instability and Wake Generation by an Intense Electron Beam in a Self-ionized Gas", Physical Review Letters **96,** 045001 (2006).

9) W. Lu *et al,* "Nonlinear Theory for Relativistic Plasma Wakefields in the Blowout Regime", Physical Review Letters **96**, 165002 (2007).

Student Theses

1) Brent E. Blue, M.S. UCLA, "Hosing Instability of the Drive Electron Beam in the E-157 Plasma-Wakefield Acceleration Experiment at the Stanford Linear Accelerator" December 2000.

2) Seung Lee, Ph.D. USC, "Non-linear Plasma Wakefield Acceleration: Models and Experiments" May 2002.

3) Sho Wang, Ph.D. UCLA, "X-ray Synchrotron Radiation in a Plasma Wiggler" June 2002.

4) Brent E. Blue, Ph.D. UCLA, "Plasma Wakefield Acceleration of an Intense Positron Beam" January 2003.

5) Wei Lu, M.S. UCLA, "Some Results on Linear and Nonlinear Plasma Wake Excitation : Theory and Simulation Verification".

6) Chenkun Huang, M.S. UCLA, "Development of a Novel PIC code for Studying Beam-Plasma Interactions".

7) Caolionn O'Connell, Ph.D. Stanford, "Field Ionization of Neutral Lithium Vapor using a 28.5 GeV Electron Beam" 2005.

8) Chengkun Huang, Ph.D. UCLA "Quasistatic Modeling of Beam-Plasma and Laser-Plasma Interactions" 2005.

9) Devon Johnson, Ph.D. UCLA, "Positron Production in a Plasma Wakefield Accelerator" 2006.

10) Chris Barnes, Ph.D. Stanford, "Phase Space Determination in the FFTB and Investigation of Hosing Effects" 2006.

11) Suzhi Deng, Ph. D. USC, "Models and Physics of Plasma Wakefield Accelerators in Beam-ionized Gases" 2006.

12) Wei Lu, Ph.D. UCLA, "Nonlinear Plasma Wakefield Theory and Optimal Scaling for Laser Wakefield Acceleration in the Blowout Regime" 2006.

13) Erdem Oz, Ph.D. USC, "Physics of Particle Trapping in Ultrarelativistic Plasma Wakes" 2007.

Student Theses in Preparation

1) Miaomiao Zhou, Ph.D. UCLA, "Accelerating Ultra-short Electron/Positron Bunches in Field Ionization Produced Plasmas".